

Micronization of Polyethylene Wax in an Extrusion Process using Supercritical Carbon Dioxide

by

Nowrin Raihan Abedin

A thesis
presented to the University of Waterloo
in fulfillment of the
thesis requirement for the degree of
Master of Applied Science
in
Chemical Engineering

Waterloo, Ontario, Canada, 2011

© Nowrin Raihan Abedin 2011

AUTHOR'S DECLARATION

I hereby declare that I am the sole author of this thesis. This is a true copy of the thesis, including any required final revisions, as accepted by my examiners.

I understand that my thesis may be made electronically available to the public.

Nowrin R. Abedin

ABSTRACT

Supercritical fluid technology is a well documented and emergent technology used in many industries today for the formation of micro- and nano- particles. The use of supercritical fluids allows synthesis of various types of particles since their properties can be varied with temperature or pressure, which sequentially can control the physical and chemical properties of the particles produced. Several different processes designed to generate powders and composites using supercritical fluids have been proposed in the past 20 years which can be used to synthesize materials with high performance specifications and unique functionality. In this research work, an extrusion micronization process using supercritical fluid has been proposed. This powder production technique could be a promising alternative to conventional techniques in terms of improvement in product quality as it provides a better control over particle size, morphology and particle size distribution, without degradation or contamination of the product. In addition, as extrusion is globally used for polymer production and processing, particle production by extrusion will allow production and processing in a single process step, eliminating the need for secondary particle production methods.

The micronization process designed and described in this thesis involves a twin screw extruder equipped with a converging die and a high resistance spraying nozzle for particle production. A special CO₂ injection device and polymer collection chamber was designed for CO₂ supply and powder collection. To ensure complete dissolution of CO₂ into the polymer matrix, stable injection of CO₂, pressure generation and constant spray of micronized polymer particles, a special screw configuration was carefully designed for the extrusion process. The feasibility and the performance of this process have been demonstrated by experimental studies

performed with low molecular weight polyethylene wax. Carbon dioxide at supercritical conditions was used as a solvent for processing the polymer.

The generated polyethylene particles from the polyethylene wax/carbon dioxide solution system were analyzed and studied using an optical microscope, scanning electron microscope, capillary rheometer and differential scanning calorimeter. A detailed study on the effects of the processing parameters, such as temperature, pressure, flow rate and supercritical fluid on properties of polyethylene particle produced was carried out. The particle size data collected using an optical microscope indicate a significant impact of temperature and CO₂ content on particle size. The obtained size data were utilized to generate particle size distribution plots and studied to analyze the effect of the processing variables. It was found that particle size distribution is affected by processing temperature and CO₂ content. Studies of the SEM images reveal that the morphology of particles can be controlled by varying processing variables like temperature, polymer feed rate and CO₂ content.

The particles generated during this study indicate that particle production in an extrusion process using supercritical carbon dioxide is achievable and appears to be a promising alternative to conventional polymer particle production methods such as grinding, milling and other supercritical fluid-based precipitation methods. To validate and generalize the applicability of this process, micronization of other polymeric material should be performed. Commercialization of this technology will further require predictability and consistency of the characteristics of the product, for which a detailed understanding of the influence of all relevant process variables is necessary. In addition, development of theoretical models will further assist in the scale-up and commercialization of this supercritical fluid assisted micronization technology in the near future.

ACKNOWLEDGEMENTS

I would like to express my sincerest gratitude to my supervisor, Dr. Costas Tzoganakis. Without his assistance, guidance and supervision this thesis would not be possible. Besides all the knowledge on polymer processing, I am grateful for his support and understanding during my father's illness. I consider myself to be very fortunate to have met and studied under such a distinguished mentor.

I would like to thank Dr. Alexander Penlidis and Dr. Neil McManus, my thesis committee members, for accepting to be readers of my thesis, and for all their help and guidance. I would also like to acknowledge my colleagues, especially Dr. Shuihan Zhu, for all their valuable assistance throughout my graduate research. Further, I would like to acknowledge the financial support and assistance provided by Ingenia Polymers, the industrial partner.

I would like to dedicate this thesis to my family for all their love and support throughout my life.

TABLE OF CONTENTS

AUTHOR'S DECLARATION	ii
ABSTRACT	iii
ACKNOWLEDGEMENTS	v
DEDICATION	vi
LIST OF FIGURES	x
LIST OF TABLES	xiii
LIST OF ABBREVIATIONS	xv
CHAPTER 1: INTRODUCTION AND OBJECTIVE	1
1.1 INTRODUCTION.....	1
1.2 RESEARCH OBJECTIVE.....	3
CHAPTER 2: LITERATURE REVIEW	5
2.1 INTRODUCTION.....	5
2.2 POLYMER.....	6
2.2.1 Polyethylene Wax.....	6
2.3 SUPERCRITICAL FLUID.....	8
2.3.1 Supercritical Fluid.....	8
2.3.2 Carbon Dioxide as a Supercritical Fluid	10
2.4 APPLICATION OF SUPERCRITICAL FLUIDS FOR PARTICLE PRODUCTION.....	11
2.4.1 Supercritical Fluid as a Solvent Processes (RESS, RESOLV)	11
2.4.2 Supercritical Fluid as an Antisolvent Processes (GAS, SAS, SEDS).....	13
2.4.3 Particles from Gas-Saturated Solution (PGSS, DELOS).....	15
2.4.4 Carbon Dioxide assisted Spray Drying (SAA, CAN-BD).....	16
2.4.5 Selection of Methods for Particle Production.....	17
2.5 EXTRUSION IN PARTICLE PRODUCTION	17
2.6 POLYMER/ SUPERCRITICAL FLUID SOLUTION.....	20
2.6.1 Solubility.....	21
2.6.2 Viscosity.....	26
2.7 EFFECT OF PROCESS VARIABLES ON MICRONIZATION.....	30
2.7.1 Effect of Pressure and Temperature	31
2.7.2 Effect of Molecular Weight.....	32
2.7.3 Effect of Spraying Nozzle Diameter.....	33

2.7.4	Effect of CO ₂ Content	34
2.7.5	Effect of Solidification Time.....	35
CHAPTER 3: EXPERIMENTAL		36
3.1	INTRODUCTION.....	36
3.2	MATERIALS.....	36
3.2.1	Polyethylene Wax.....	36
3.2.2	Supercritical Carbon Dioxide.....	37
3.3	EQUIPMENT	38
3.3.1	Leistritz LSM 30.34 Twin-Screw Extruder.....	38
3.3.2	ISCO Positive Displacement Pump	40
3.3.3	SCF Injection Device	41
3.3.4	Spraying Nozzle.....	44
3.3.5	OPTO22 Data Acquisition System.....	45
3.3.6	Polymer Collection Chamber Design.....	45
3.3.7	Design of Twin-screw Configuration	47
3.4	EXTRUDER OPERATION AND SAMPLE COLLECTION PROCEDURE	50
3.5	CHARACTERIZATION.....	51
3.5.1	Capillary Rheometer.....	51
3.5.2	DSC.....	52
3.5.3	Microscopy	52
3.5.4	SEM.....	53
3.6	PRELIMINARY EXPERIMENTS.....	54
3.6.1	Effect of Polymer Feed Rate.....	54
3.6.2	Effect of Screw Speed	55
3.6.3	Effect of CO ₂ Feed Rate.....	55
3.6.4	Effect of Nozzle Diameter.....	56
CHAPTER 4: MICRONIZATION OF POLYETHYLENE WAX		57
4.1	INTRODUCTION.....	57
4.2	EXPERIMENTAL DESIGN.....	59
4.2.1	Design of Experiments.....	59
4.3	RESULTS AD DISCUSSION.....	60
4.3.1	Particle Size.....	62
4.3.2	Particle Size Distribution	70

4.3.3	Morphology	76
4.3.4	Melting Point and Glass Transition Temperature.....	85
CHAPTER 5: CONCLUSIONS AND RECOMMENDATIONS.....		89
5.1	CONCLUSIONS.....	89
5.2	RECOMMENDATIONS	91
REFERENCES		93
Appendix A: Formulas for Mean Particle Size Calculation		103
Appendix B: Data for Particle Size Calculation.....		104
Appendix C: Data for Particle Size Distribution Plots.....		107
Appendix D: Viscosity Data for PE Wax and Micronized PE Wax.....		110
Appendix E: Optical Microscope Images.....		112
Appendix F: SEM Images.....		118
Appendix G: LABVIEW Program for Data Acquisition		124

LIST OF FIGURES

Figure 2.1: Structure of Polyethylene Molecule.....	6
Figure 2.2: Phase Diagram of a Pure Compound.....	10
Figure 2.3: Schematic Representation of RESS Process	12
Figure 2.4: Schematic Representation of: a) GAS Process, and b) SAS Process	14
Figure 2.5: Schematic Representation of PGSS process.....	15
Figure 2.6: Typical Extrusion Process.....	18
Figure 2.7: Morphology Change of a Polymer-Gas System in an Extrusion Particle Production Process Using Supercritical Fluid Solution	19
Figure 2.8: Solubility of CO ₂ in Different Polymer Melts at 473.15 K Under Different Saturation Pressure.....	24
Figure 2.9: Solubility of CO ₂ in PP Polymer Melts at Different Temperature with and without Swelling Degree Correction.	25
Figure 3.1: Shear viscosity of Polyethylene Wax at Various Temperatures	37
Figure 3.2: Schematic of the extrusion system.....	39
Figure 3.3: The CO ₂ Injection Device for Twin-Screw Extruder.....	42
Figure 3.4: The Barrel Cross Section of a Twin-Screw Extruder Showing the Injection Location.....	43
Figure 3.5: Schematic of Spraying Nozzle Used.....	44
Figure 3.6: Micronized Polymer Collection Chamber	46
Figure 3.7: Schematic of the Twin-Screw Configuration.....	49
Figure 4.1: SEM Images of Particles Produced at CO ₂ Feed Rate of 25 ml/min, Screw Speed of 50 rpm, and Nozzle Temperature at 200 ^o C.....	61
Figure 4.2: SEM Images of Particle Produced at Different Polymer Feed Rate	67
Figure 4.3: Normalized Particle Size Distributions at Different Polymer Feed Rates.....	71
Figure 4.4: Normalized Particle Size Distribution at Lower Nozzle Temperatures.....	73
Figure 4.5: Normalized Particle Size Distribution at Higher Nozzle Temperatures	74
Figure 4.6: Normalized Particle Size Distribution at Different CO ₂ Feed Rate	75
Figure 4.7: SEM Images of Particle Produced at Different Nozzle Temperatures at a	77
Figure 4.8: SEM Images of Particle Produced at Different Nozzle Temperatures at a	78
Figure 4.9: SEM Images of Particle Produced at Different Polymer Feed Rate at Nozzle Temperatures 160 ^o C (CO ₂ Feed Rate = 25 ml/min, Screw Speed = 50 rpm).....	80

Figure 4.10: SEM Images of Particles Produced at Different Polymer Feed Rate at Nozzle Temperatures 180 ^o C (CO ₂ Feed Rate = 25 ml/min, Screw Speed = 50 rpm).....	81
Figure 4.11: SEM Images of Particles Produced at Different CO ₂ Feed Rate at 500X Magnification (Polymer Feed Rate= 55 g/min, Screw Speed = 50 rpm, Nozzle Temperature = 140 ^o C).....	83
Figure 4.12: SEM Images of Particles Produced at Different CO ₂ Feed Rate at 100X Magnification (Polymer Feed Rate= 55 g/min, Screw Speed = 50 rpm, Nozzle Temperature = 140 ^o C).....	84
Figure 4.13: DSC of Micronized and Unprocessed Polyethylene Wax at Various Nozzle Temperatures and Two Different Polymeric Feed Rates (CO ₂ Feed Rate = 25 ml/min, Screw Speed = 50 rpm).....	86
Figure 4.14: DSC of Micronized and Unprocessed Polyethylene Wax	87
Figure 0.1: Optical Microscope Image of Particles Produced at Polymer Feed Rate =13 g/min and Nozzle Temperature =140 ^o C.....	112
Figure 0.2: Optical Microscope Image of Particles Produced at Polymer Feed Rate =13 g/min and Nozzle Temperature =160 ^o C.....	112
Figure 0.3: Optical Microscope Image of Particles Produced at Polymer Feed Rate =13 g/min and Nozzle Temperature =180 ^o C.....	113
Figure 0.4: Optical Microscope Image of Particles Produced at Polymer Feed Rate =13 g/min and Nozzle Temperature =200 ^o C.....	113
Figure 0.5: Optical Microscope Image of Particles Produced at Polymer Feed Rate =26 g/min and Nozzle Temperature =140 ^o C.....	114
Figure 0.6: Optical Microscope Image of Particles Produced at Polymer Feed Rate =26 g/min and Nozzle Temperature =160 ^o C.....	114
Figure 0.7: Optical Microscope Image of Particles Produced at Polymer Feed Rate =26 g/min and Nozzle Temperature =180 ^o C.....	115
Figure 0.8: Optical Microscope Image of Particles Produced at Polymer Feed Rate =26 g/min and Nozzle Temperature =200 ^o C.....	115
Figure 0.9: Optical Microscope Image of Particles Produced at CO ₂ Feed Rate of 35 ml/min	116
Figure 0.10: Optical Microscope Image of Particles Produced at CO ₂ Feed Rate of 45 ml/min	116
Figure 0.11: Optical Microscope Image of Particles Produced at CO ₂ Feed Rate of 55 ml/min	117

Figure 0.12: SEM Images of Particles Produced at Polymer Feed Rate= 13 g/min, CO ₂ Feed Rate =25 ml/min, Screw Speed =50 rpm, and Nozzle Temperature= 140 ⁰ C.....	118
Figure 0.13: SEM Images of Particles Produced at Polymer Feed Rate= 13 g/min, CO ₂ Feed Rate= 25 ml/min, Screw Speed =50 rpm, and Nozzle Temperature =160 ⁰ C.....	118
Figure 0.14: SEM Images of Particles Produced at Polymer Feed Rate= 13 g/min, CO ₂ Feed Rate =25 ml/min, Screw Speed =50 rpm, and Nozzle Temperature =180 ⁰ C.....	119
Figure 0.15: SEM Images of Particles Produced at Polymer Feed Rate= 13 g/min, CO ₂ Feed Rate =25 ml/min, Screw Speed =50 rpm, and Nozzle Temperature =200 ⁰ C.....	119
Figure 0.16: SEM Images of Particles Produced at Polymer Feed Rate= 26 g/min, CO ₂ Feed Rate =25 ml/min, Screw Speed =50 rpm, and Nozzle Temperature =140 ⁰ C.....	120
Figure 0.17: SEM Images of Particles Produced at Polymer Feed Rate= 26 g/min, CO ₂ Feed Rate =25 ml/min, Screw Speed =50 rpm, and Nozzle Temperature =160 ⁰ C.....	120
Figure 0.18: SEM Images of Particles Produced at Polymer Feed Rate= 26 g/min, CO ₂ Feed Rate =25 ml/min, Screw Speed =50 rpm, and Nozzle Temperature =180 ⁰ C.....	121
Figure 0.19: SEM Images of Particles Produced at Polymer Feed Rate =26 g/min, CO ₂ Feed Rate =25 ml/min, Screw Speed =50 rpm, and Nozzle Temperature =200 ⁰ C.....	121
Figure 0.20: SEM Images of Particles Produced at Polymer Feed Rate =52 g/min, CO ₂ Feed Rate =35 ml/min, Screw Speed =50 rpm, and Nozzle Temperature =200 ⁰ C.....	122
Figure 0.21: SEM Images of Particles Produced at Polymer Feed Rate =52 g/min, CO ₂ Feed Rate =45 ml/min, Screw Speed =50 rpm, and Nozzle Temperature =200 ⁰	122
Figure 0.22: SEM Images of Particles Produced at Polymer Feed Rate =52 g/min, CO ₂ Feed Rate =55 ml/min, Screw Speed =50 rpm, and Nozzle Temperature =200 ⁰	123

LIST OF TABLES

Table 2.1: Characteristic Properties of PE Wax	7
Table 2.2: Critical Temperature and Critical Pressures of Some Common Substances	9
Table 2.3: Physical Properties of Gas, Liquid and SCF	9
Table 3.1: Positive Displacement Pump Specifications	40
Table 4.1: Mean Particle Diameter at Different Polymer Feed Rates and Nozzle Temperatures (CO ₂ feed rate =25 ml/min, screw speed= 50 rpm)	64
Table 4.2: Mean Particle Diameter at Different CO ₂ Feed Rates for a Constant Polymer Feed Rate of 52 g/min (Screw Speed = 55 rpm and Nozzle Temperature = 140 ⁰ C).....	68
Table 4.3: ANOVA Table	69
Table 4.4: Effect of Micronization on Melting Point Temperature of Polyethylene Wax.....	88
Table 0.1: Definition of Mean Particle Diameters.....	103
Table 0.2: Diameters of Polyethylene Wax Particles Produced at a Constant Polymer Feed Rate of 13 g/min and Different Nozzle Temperatures Measured via an Optical Microscope (Screw Speed=50 rpm, CO ₂ Feed Rate =25 ml/min).....	104
Table 0.3: Diameters of Polyethylene Wax Particles Produced at a Constant Polymer Feed Rate of 26 g/min and Different Nozzle Temperatures Measured via an Optical Microscope (Screw Speed=50 rpm, CO ₂ Feed Rate =25 ml/min).....	105
Table 0.4: Diameters of Polyethylene Wax Particles Produced at Different CO ₂ Feed Rate Obtained via Optical Microscopic Measurements (Screw Speed=50 rpm, Polymer Feed Rate =52 g/min, Nozzle Temperature= 140 ⁰ C)	106
Table 0.5: Frequency and Normalized Frequency of Particle Diameters of Polyethylene Wax Particles Produced at 15 g/min Polymer Feed Rate (Screw Speed=50 rpm, CO ₂ Feed Rate =25 ml/min)	107
Table 0.6: Frequency and Normalized Frequency of Particle Diameters of Polyethylene Wax Particles Produced at 26 g/min Polymer Feed Rate (Screw Speed=50 rpm, CO ₂ Feed Rate =25 ml/min)	108
Table 0.7: Frequency and Normalized Frequency of Particle Diameters of Polyethylene Wax Particles Produced at Different CO ₂ Feed Rate (Screw Speed=50 rpm, Polymer Feed Rate =52 g/min, Nozzle Temperature = 140 ⁰ C)	109

Table 0.8: Shear Viscosity of Unprocessed Polyethylene Wax Pallets Measured via a Capillary Rheometer using a die with L/D ratio of 50/20 at 90 ⁰ C and 110 ⁰ C.....	110
Table 0.9: Shear Viscosity of Unprocessed Polyethylene Wax Pallets Measured via a Capillary Rheometer using a die with L/D ratio of 20/50 at 110 ⁰ C.....	110
Table 0.10: Shear Viscosity of Polyethylene Wax Particles (Produced at a Polymer Feed Rate 26 g/min, CO ₂ Feed Rate 45 ml/min, Nozzle Temperature 180 ⁰ C and Screw Speed 50 rpm) Measured via a Capillary Rheometer Using a Die with L/D Ratio of 50/20 at 90 ⁰ C and 100 ⁰ C.....	111
Table 0.11: Shear Viscosity of Polyethylene Wax Particles (Produced at a Polymer Feed Rate 26 g/min, CO ₂ Feed Rate 45 ml/min, Nozzle Temperature 180 ⁰ C and Screw Speed 50 rpm) Measured via a Capillary Rheometer Using a Die with L/D Ratio of 20/50 at 110 ⁰ C.....	111

LIST OF ABBREVIATIONS

"

" Inches

°

°C Degrees Celsius

ε

ε Error

Δ

ΔH_m Heat of melting

μ

μ Microns

μm Micrometers

μl Micro litres

η

η Viscosity

η_{atm} Viscosity at atmospheric pressure

A

A Constant

Å Angstrom

ANOVA Analysis of variance

ASTM American Society of Testing and Materials

B

B Constant

B' Pressure coefficient

C

cm	Centimetres
CAN-BD	Carbon dioxide Assisted Nebulization with a Bubble Dryer ®
CO ₂	Carbon Dioxide
CFC	Chlorofluorocarbons
CPCSP	Continuous Powder Coating Spraying Process

D

DCM	Digital camera module
DELOS	Depressurization of an expanded liquid organic solution
DSC	Differential Scanning Calorimeter

E

EEA	Ethylene Acrylic Acid
EGSEG	Expansion of gas-saturation with excess gas
EOS	Equation of State

F

f	Free volume fraction of the polymer
FTIR	Fourier transform Infra Red spectroscopy

G

g	Grams
g/cm ³	Grams per cubic centimetre
g/min	Grams per minute
GAS	Gas antisolvent process
GTP	Gas to polymer mass ratio

H

H ₂	Hydrogen gas
HDPE	High density polyethylene

K

K	Kelvin
KDU	Knock Detection Unit
kV	Kilovolts

L

LDPE	Low density polyethylene
L/D	Length to diameter ratio

M

min	Minute
min ⁻¹	Per minute
MLSR	Magnetically levitated sphere rheometer
ml	Millilitres
ml/min	Milliliters per minute
mm	Millimetres
MPa	Mega Pascal
mPa.s	Millipascal seconds
MSB	Magnetic suspension balance
mV	Millivolt

N

NH ₃	Ammonia
-----------------	---------

P

P	Pressure
P _c	Critical Pressure
Pa.s	Pascal second
PDMS	Poly(dimethylsiloxane)
PE	Polyethylene
PEG	Polyethylene glycol
PGSS	Particles from gas-saturated solution

PHBV	Poly(3-hydroxybutyrate-co-3-hydroxyvalerate)
PID	Proportional–integral–derivative
PP	Polypropylene
PPB	Propoxylated polyester
PS	Polystyrene
PSD	Particle size distribution
psi	Pound per square inch
psi ⁻¹	Per pound per square inch
PVC	Polyvinyl chloride

R

RCS	Refrigerated Cooling System
RESS	Rapid expansion of supercritical solutions
RESOLV	Rapid expansion of supercritical carbon dioxide solutions into a liquid solvent
rpm	Revolutions per minute

S

s	Seconds
s ⁻¹	Per second
SAA	Supercritical Assisted Atomization
SAS	Supercritical antisolvent process
SCF	Supercritical fluid
SEDS	Solution Enhanced Dispersion by Supercritical fluids
SEM	Scanning Electron Microscope
SL-EOS	Sanchez-Lacombe Equation of State
SS-EOS	Simha-Somcynsky Equation of State

T

T	Temperature
T _c	Critical Temperature
T _o	Thermodynamic second-order transition temperature
T _m	Melting point temperature

U

USA United States of America

V

V Volt

v_o Occupied volume

v_o^P Molecular volume of the polymer

VOC Volatile organic compounds

W

W Watt

w_{CO_2} Weight fraction of CO₂ dissolved in the polymer

WLD Wet laser diffraction

Wt-% Weight percentage

CHAPTER 1: INTRODUCTION AND OBJECTIVE

1.1 INTRODUCTION

The production of polymer microparticles is of interest in many industrial fields. Biomedical engineering, cosmetics, toners and paints, for example, are some areas that use micron sized polymer particles. Traditional techniques used for the production of micro particles, such as crushing/milling, spray- and freeze-drying, or re-crystallization from solvents, are operations that require large amount of energy, are characterized by low efficiencies and involve liquid solvents that can contaminate the product [1]. These processes may often incur undesired effects such as physico-chemical instabilities and poor product shelf-life. As far as the micronic particle structure is concerned, conventional manufacturing methods do not guarantee sufficient control on the powder characteristics. The main consequences are intra-batch particle size variability and broad size distribution. Moreover, the processes that use organic solvents require additional stages for the extraction of residual organic solvents, and generate waste streams which raise environmental concerns and industrial cost [2]. Due to the limitations associated with conventional techniques, the potential replacement of traditional techniques with supercritical fluid technology has received increasing attention from the scientific community in the past few years.

Supercritical fluid-based technologies represent a well-documented alternative for particle design and crystal engineering. Processes that use SCF technology for particle production, take advantage of some specific properties of gases at supercritical conditions, such as adjustable solvating power and selectivity that can be achieved by varying pressure and temperature. Use of supercritical fluid technology provides the possibility to achieve

crystallization conditions which may lead to very small particles with consistent particle size distribution, crystal structure and surface properties via the control of processing parameters and equipment, and they do not pollute the extracts, residues, and the environment [3-5]. Among all the possible supercritical fluids, supercritical carbon dioxide (SC-CO₂) is widely used for its nontoxic nature and easily attainable mild critical conditions that make it an ideal substitute to organic solvents. Use of supercritical carbon dioxide not only produces high purity products, but allows the micronization of thermolabile compounds. Moreover, carbon dioxide is gaseous at ambient conditions, which simplifies the problem of solvent residues [6].

Numerous supercritical fluids-based processes for micro-particle generation have been developed for taking advantage of supercritical fluid properties and review articles are available in the literature on these processes. Techniques like the rapid expansion of supercritical solutions (RESS), supercritical antisolvent precipitation (SAS), particle generation from gas-saturated solutions (PGSS), and new atomization processes (SAA) are some of the methods used in industry today for particle production [2,6,7]. However, it is to be noted that polymer is primarily produced in industry via an extrusion process, a well elaborated manufacturing technology which has been used in industry since the 1930s [8]. As such, polymer micro particle production via extrusion process would eliminate the need for secondary particle production steps (grinding, milling, PGSS, SAS etc.).

For particle production in an extruder, the supercritical fluid is first dissolved in the polymer matrix, where the dissolved CO₂ plasticizes and reduces the viscosity of the polymer to be micronized. The molten polymer-gas solution is then passed through a narrow die space and out through a micron-size nozzle hole where the vigorous expansion of the dissolved gas breaks up the polymer melt to produce micronized particles [9,10]. Here, the supercritical CO₂

has a dual functionality: it changes the rheological properties of the material, and behaves as an expansion agent.

Despite the widespread usage of extruders for polymer production, micron-size polymer particle production via extrusion process is relatively new. Only a limited number of studies have been conducted to produce particles via an extrusion process. Nalawade et al. produced submicron-size particles of polyester resins using supercritical fluid in an extrusion process. It was reported that various process parameters, such as pressure, temperature, flow rates, and nozzle diameter, can be utilized to control particle size and morphology of particles produced using supercritical CO₂ in an extruder [10,11].

1.2 RESEARCH OBJECTIVES

The work described in this thesis focuses on the extrusion of polymers in the presence of supercritical fluid. The first objective of this thesis is to investigate the feasibility of producing micron size particles using a supercritical fluid. Low molecular weight polyethylene wax and carbon dioxide were chosen for this purpose. The second objective of this thesis is the investigation of the effect of processing parameters on properties of the particles produced, such as particle size, size distribution and morphology.

This thesis is comprised of 5 chapters including this chapter containing the introduction and research objective. Chapter 2 focuses on the literature review related to this research, including a survey on properties and applications of supercritical fluids, and other similar processes that use supercritical fluids for particle production. For understanding the effects of shear viscosity and solubility of supercritical fluid, sections on CO₂ solubility in polymers and

the viscosity reduction effect of dissolved CO₂ on a polymer was integrated. References found in recent publications on materials micronized by supercritical fluid techniques, and a summary of the effects of different processing parameters on micronized particle properties is also included in this chapter. Chapter 3 provides a detailed description of the materials and equipment used for the micronization process. The design concepts used for the experimental setup and design of the screw configuration is outlined. In an effort to establish a steady micronization process and understand the effects of processing parameters on particle production, preliminary experiments were conducted. A summary of the observations made during preliminary experiments performed is provided in this chapter. Chapter 4 comprises the results and discussion concerning the polyethylene wax particles produced. Particle analysis was performed using scanning electron microscopy (SEM) and optical microscopy to evaluate particle size, size distribution and to analyze the morphology of the particles. The results are presented in terms of the effects of processing parameters on the above mentioned particle properties. Finally, conclusions and recommendations are presented in chapter 5.

CHAPTER 2: LITERATURE REVIEW

2.1 INTRODUCTION

The polymer industry produces over 20 million tons of volatile organic compounds (VOCs) each year [12]. Conventional well known processes for micronization (particle generation), such as milling, grinding, spray drying etc., are known to generate aqueous waste streams, and emit hazardous VOCs and chlorofluorocarbons (CFCs). Other concerns associated with these processes are control of the particle size and particle size distribution [2,13]. Use of supercritical fluids is a viable “green” alternative to noxious VOCs and CFCs. A supercritical fluid is defined as a substance for which both pressure and temperature are above the critical values. Advantages of SCFs include low surface tension, low viscosity, high diffusivity, and density-dependent solvent power. The density and as such the solvating power, of a SCF can be tuned from gas-like to liquid-like values through changes in pressure and temperature [14].

Among all SCFs, supercritical carbon dioxide has received a lot of attention due to its non-toxic, chemically inert and inexpensive nature. Dissolved CO₂ causes a considerable reduction in the viscosity of molten polymers resulting in less energy consumption during processing. The versatile operating conditions that are possible with supercritical fluids also provide flexibility in controlling the particle size and particle size distribution [11,14,15].

Particle formation technologies that use supercritical fluids have evolved in many different forms during the last 20 years. Several review articles have already appeared in the literature, presenting a variety of particle formation processes. These include the rapid

expansion of supercritical solutions (RESS), the gas antisolvent process (GAS), supercritical antisolvent process (SAS), and the particles from gas-saturated solution (PGSS) processes [2,16-18] and many more [2,7,17]. However, in the polymer industry, extrusion is the primary method for polymer processing. Micronization of polymers in an extrusion process will allow elimination of secondary particle generation steps such as grinding, milling as well as the recently developed processes such as GAS, SAS and RESS. Unfortunately, supercritical fluids have hardly been applied for micronization of polymers during extrusion. As a result, the effects of SCFs on polymer in an extrusion process and on extrusion performance have not been clarified thoroughly [19]. This chapter will review literature studies on properties and uses of supercritical fluid, polymer/SCF solution behaviour such as solubility, and effects of CO₂ on polymer rheology and morphology.

2.2 POLYMER

2.2.1 Polyethylene Wax

Low molecular weight polyethylene is known as polyethylene wax (PE wax). It is a synthetic wax produced during the polymerization of low molecular weight polyethylene. The ethylene used is generally obtained by cracking petroleum naphtha or from natural gas [20]. Figure 2.1 shows a molecule of polyethylene which is made by subsequent addition of many ethylene monomer units forming a long and linear chain of carbon atoms.

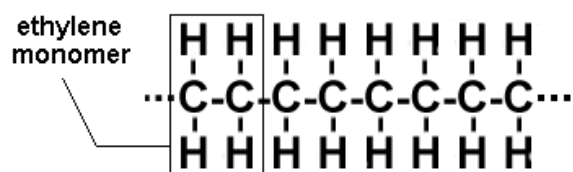


Figure 2.1: Structure of Polyethylene Molecule

Polyethylene wax has good dispersion and fluidity, good electrical and remoulding properties, good light resistant and chemical-resistant properties. It is well known for increasing abrasion resistance and providing excellent barrier protection. It also improves surface appearance by providing a non-sticky wax surface [21]. It is soluble in various polymers such as polyethylene, polypropylene, polyvinyl acetate, ethylenepropylene rubber, butyl rubber, and various aromatic hydrocarbons. It is also used for temperature and viscosity modification of other polymers. Polyethylene wax is non-toxic in nature and is available in the market in various forms and grades differing in viscosity, softening point, hardness, density and molecular weight [22,23]. Some of the characteristic properties of PE wax are listed in Table 2.1.

Table 2.1: Characteristic Properties of PE Wax [23,24]

CHARACTERISTICS	POLYETHYLENE WAX
Melting point, °C	95-100
Molecular Weight (g/mol)	2,000-4,000
Density (g/cm ³)	0.93-0.94
Viscosity at 140°C, mm ² /s	50-1000
Tensile strength, N/cm ²	1000-1300
Elongation at break, %	240
Melt index (g/10 min)	~3.5
Colour	White

A little more than 10-wt% of PE produced in the USA finds use in typical wax applications [24]. The application itself depends on the form of wax and its characteristic properties. PE wax as homopolymer is used in elastomers, hot melt adhesives, inks, lubricants, coatings, plastics, solvent polishes, personal care products and wax blends. Copolymers provide greater compatibility and solubility than comparable homopolymers. These

copolymers produce emulsions with very light colors that resist yellowing. Major use of copolymers includes adhesives, polishes, textiles, candles, paper coatings and color concentrates. Oxidised PE wax is known to emulsify with anionic, non-ionic and cationic surfactants. These emulsions permit the use of oxidised PE wax as coating for citrus and in the leather, paper, polish and textile fields. It is also used in PVC formulation as a lubricant, in wax blends and in industrial coatings. Micronized polyethylene wax is used for applications such as stir-in wax for inks and coatings and suspending and texturing agents in personal care products [21-23].

2.3 SUPERCRITICAL FLUID

2.3.1 Supercritical Fluid

A homogeneous fluid generally exists in either a liquid or gas phase, which is clearly defined by phase boundaries, as shown in Figure 2.2. As pressure and temperature increase above the critical point, the phases become indistinguishable. This critical point is thermodynamically defined by the conditions

$$\left(\frac{\partial P}{\partial V}\right)_T = 0 \quad \text{and} \quad \left(\frac{\partial^2 P}{\partial^2 V}\right)_T = 0 \quad (2.1)$$

where P is the pressure, V is the molar volume and T represents the absolute temperature. Beyond the critical point, the substance exists as a supercritical fluid. The critical point of any substance is defined by its critical temperature and critical pressure. A list of critical pressures and critical temperatures of some common substances is provided in Table 2.2.

Table 2.2: Critical Temperature and Critical Pressure of Some Common Substances [14]

Substance	Critical Temperature (K)	Critical Pressure (MPa)
Acetone	508.1	4.70
Carbon Dioxide	304.1	7.38
Dimethyl Ether	400.0	5.24
Propane	369.8	4.25
Toluene	591.8	41.1
Water	647.3	22.1

In the supercritical fluid region, physico-chemical properties of the material are intermediate between those of a liquid and a gas, as shown in Table 2.3 [12]. Like a gas, SCFs show lower viscosity and higher diffusivity relative to the liquid. These properties facilitate mass transfer phenomena, such as matrix extraction or impregnation. Like a liquid, SCFs show high density which improves its solvating power. As a result, it has been successfully used as a solvent, antisolvent or plasticizer in polymer processing: e.g. polymer modification, polymer composites, polymer blending, microcellular foaming, particle production, and in polymer synthesis [9,26].

Table 2.3: Physical Properties of Gas, Liquid and SCF [12]

Property	Liquid	SCF	Gas
Density (g/cm^3)	1	0.5 – 1	10^{-3} - 10^{-2}
Diffusivity (cm^2/s)	10^{-6}	10^{-3}	10^{-1}
Viscosity (Pa-s)	10^{-3} – 10^{-2}	10^{-5}	10^{-6}

Compared to other organic solvents, supercritical fluids provide improvement in product quality. The advantages of SCFs include low surface tension, low viscosity, high

diffusivity, and density-dependent solvating power. As suggested by equation 2.1, SCFs have high compressibility, which allows for density alteration with pressure change resulting in solvent power variation [27-32]. It is also possible to induce phase change from liquid to gas without passing through a distinct phase transition by following the B-A path, as shown in Figure 2.2. These characteristics allow for a wide range of application of SCFs [12].

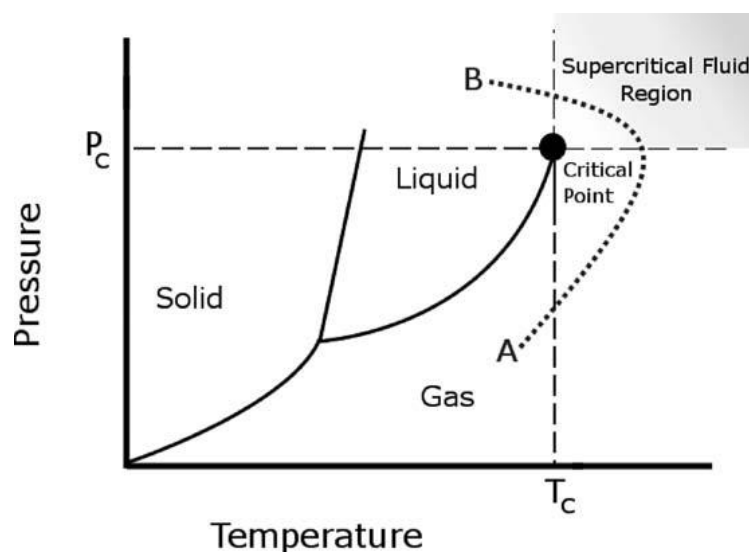


Figure 2.2: Phase Diagram of a Pure Compound

2.3.2 Carbon Dioxide as a Supercritical Fluid

Supercritical carbon dioxide has attracted a lot of attention in polymer production and processing applications as a “green” alternative to noxious VOCs and CFCs. It is non-toxic, non-flammable, and chemically inert in nature. It is also inexpensive and is abundant in the atmosphere. Large amounts are available as a by-product from NH_3 , H_2 and ethanol production. Its supercritical conditions are easily attained ($T_c = 304 \text{ K}$, $P_c = 7.38 \text{ MPa}$) in comparison to other supercritical fluids. Moreover, many polymers are plasticized in the presence of CO_2 , allowing processing at lower temperatures [33,34]. As a result, in terms of the supercritical

fluid being used as a solvent in material processing, CO₂ occupies the majority (86%) of published work with water being next, contributing at 10% [14,16,35].

Dissolved supercritical CO₂ is known to alter the physical properties of polymers, such as to decrease viscosity, decrease density, and increase swollen volume [14]. In addition, due to high diffusivity of the compressed gas, residual CO₂ removal is easily achieved by simple depressurization, unlike organic solvents [36]. These characteristic properties have stirred the attention of many researchers towards the use of supercritical CO₂ for polymer processing.

2.4 APPLICATION OF SUPERCRITICAL FLUIDS FOR PARTICLE PRODUCTION

Supercritical fluid technology has evolved in the last 20 years. Various review articles have been published [2,13,16-18,37,38], where the use of supercritical fluids has been proposed for particle production using different methods. These methods can be classified into four categories based on the role of the supercritical fluid: processes where SCF acts as a solvent (RESS, RESOLV); processes where SCF acts as an antisolvent (SAS, GAS, SEDS); particles from gas-saturated solutions (PGSS, DELOS); and CO₂-assisted spray-drying (SAA, CAN-BD).

2.4.1 Supercritical Fluid as a Solvent Processes (RESS, RESOLV)

In Rapid Expansion of Supercritical Solution (RESS) process, the polymer is first dissolved in a solvent, such as supercritical CO₂, and then this high-pressure solution is rapidly depressurized into a collection chamber through a heated nozzle that leads to polymer

precipitation. A schematic of the overall process is provided in Figure 2.3. Some of the advantages of this process include very fine particle production; controllable particle size and morphology by control of process parameters and geometry of process equipments (spraying nozzle); and solvent-free product. However, it is to be noted that RESS process is used when the polymer has some degree of solubility in the supercritical fluid. As discussed in section 2.6.1., CO₂ is not particularly a very powerful solvent for polymers, for which high pressure and sometimes high temperature is required to dissolve even a small quantity of material. As a result, operation and capital cost for this process has been reported to be high, which is one of the disadvantages associated with the RESS process [1,19,39-41].

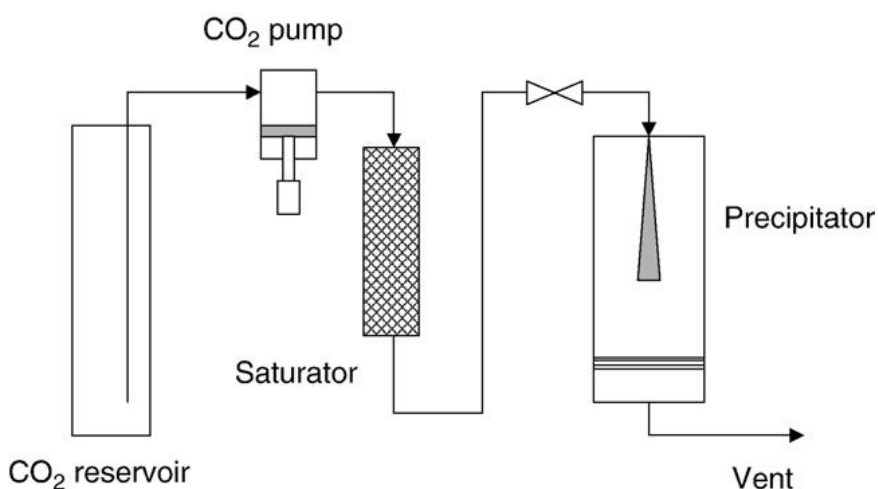


Figure 2.3: Schematic Representation of RESS Process [26]

The Rapid Expansion of a Supercritical Solution into a Liquid Solvent (RESOLV) process is a variation of RESS process presented in Figure 2.3. In the RESOLV process, the supercritical solution is depressurized through an orifice into a collection chamber containing an aqueous solution containing surfactants or reducing agents at room temperature. The aqueous medium is used to minimize particle aggregation experienced during the jet expansion

in a RESS process. In addition, the surfactants and reducing agents help form and stabilize the nano-sized particles [16,36].

2.4.2 Supercritical Fluid as an Antisolvent Processes (GAS, SAS, SEDS)

Supercritical antisolvent processes involve recrystallization techniques for processing solids that are insoluble in SCF. The technique is especially suitable for polymers because the majority of polymers are not soluble in supercritical fluids or gases. In this method, the solute is first dissolved in an organic solvent. The solution is then exposed to an antisolvent, such as supercritical CO₂. As the gas starts dissolving in the organic solvent, the solid compound initially in solution starts to precipitate. A schematic of two of the supercritical antisolvent processes is provided in Figure 2.4. The basic operating principle is the same for all antisolvent processes; the only difference being the way solution and antisolvent contact or mixing is achieved. In the Gaseous Antisolvent (GAS) process, the precipitation vessel is initially loaded with the solution and then the antisolvent is added to the vessel until the final pressure is reached. Alternatively, in the Supercritical Antisolvent (SAS) process, the antisolvent at supercritical conditions is first pumped inside the high-pressure vessel until the system reaches the fixed pressure and temperature, and then the organic solution is sprayed through a nozzle into the vessel. The Solution Enhanced Dispersion by Supercritical Fluids (SEDS) process is similar to the SAS technique except that, in this case, the solution and the antisolvent are simultaneously sprayed into the precipitation vessel [6,13,16,26,42].

Advantages of antisolvent processes include fine particle production, easily controllable particle size and morphology with the use of appropriate process equipment, such as spraying

nozzle, and applicability for a wide variety of substances insoluble in supercritical fluid. Disadvantages include use of organic solvent, dilute product stream, particle stripping from residual organic solvent, and further processing of waste stream for separation of gas and solvent [2,16].

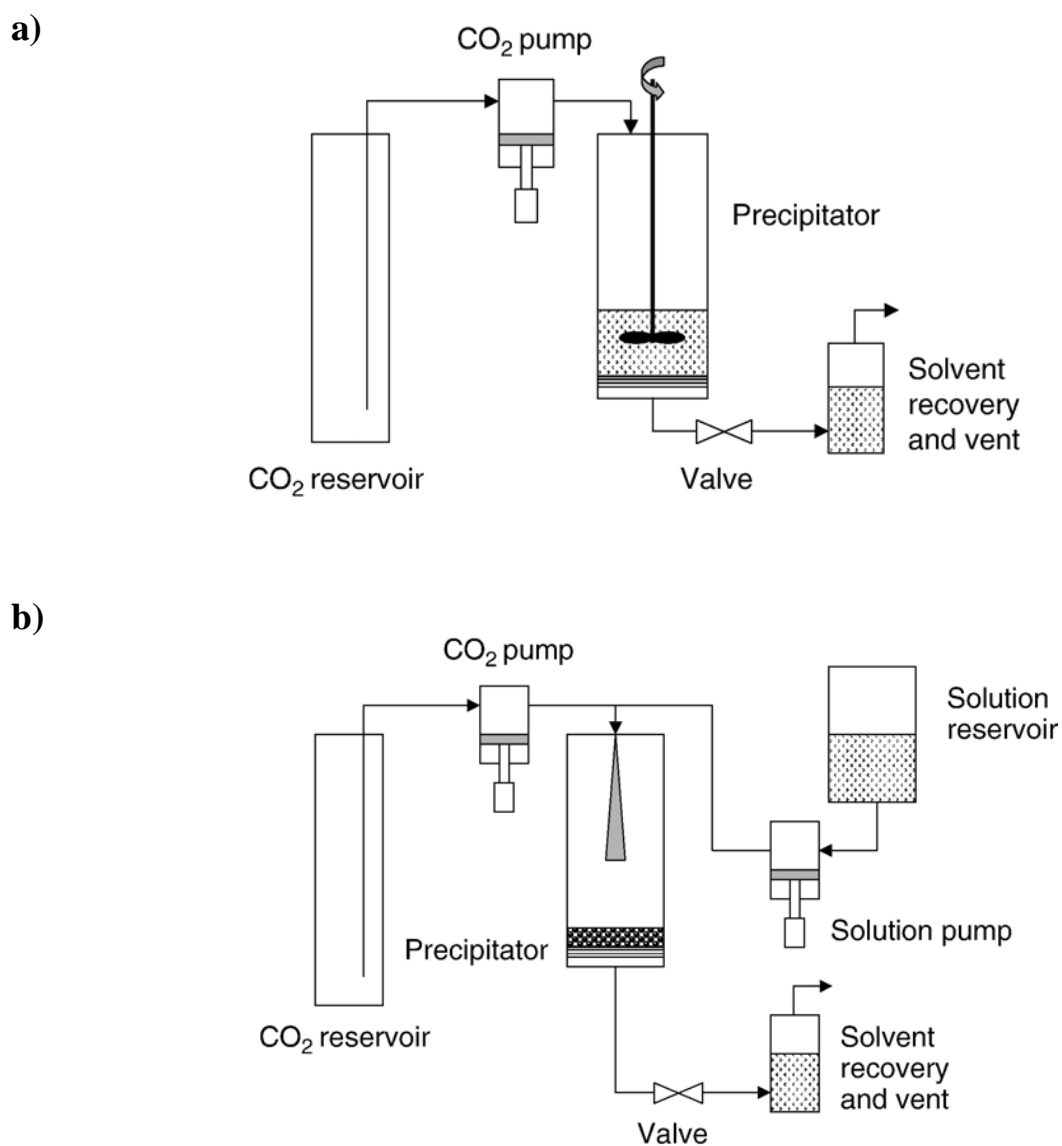


Figure 2.4: Schematic Representation of: a) GAS Process, and b) SAS Process [26]

2.4.3 Particles from Gas-Saturated Solution (PGSS, DELOS)

In a PGSS process, a substance insoluble in SCF is put into a molten or liquid state by heating and then allowed to absorb a large amount of gas under sub- or supercritical conditions that causes swelling and decreases the melting point of the substance. The absorbed gas reduces the viscosity of the solution (gas absorbed solution) increasing the free volume and further allowing more gas to be dissolved into the solution. The solution is then allowed to depressurize in a chamber where the solution is rapidly expanded over a nozzle leading to particle formation by precipitation. Currently, the running industrial application of this technology is mostly on non-polymeric materials. However, this technique has great promise and is highly suitable for polymer powder production. Schematic representation of a PGSS process is illustrated in Figure 2.5.

PGSS process has numerous advantages. It can produce fine particles with narrow particle size distributions, and improved product quality compared to other conventional processes used for particle production. It uses moderate pressure, consumes less gas, and generates solvent free product. PGSS process is also an easy to scale up process [2,7].

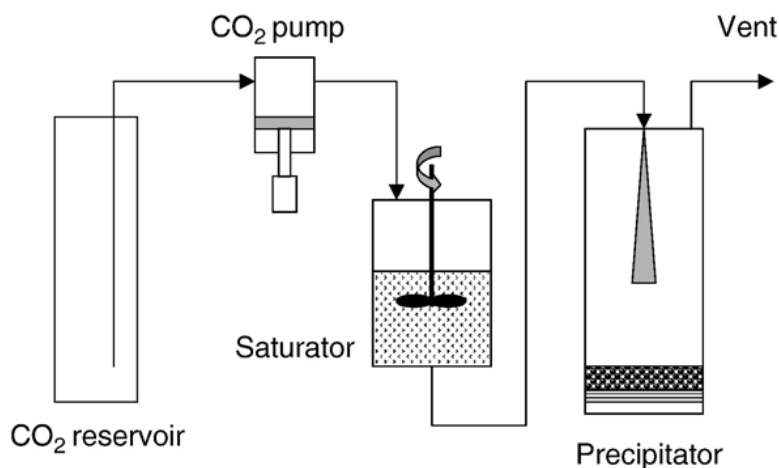


Figure 2.5: Schematic Representation of PGSS process [26]

The Depressurization of an Expanded Liquid Organic Solution (DELOS) has been developed based on the principle of PGSS process. The only difference between the PGSS and the DELOS method is that in the DELOS method CO₂ does not act as an antisolvent, but rather a co-solvent in addition to an organic solvent. The use of organic solvent allows processing at lower temperature and the production of fine particle of thermolabile compounds using the DELOS method [16,36].

2.4.4 Carbon Dioxide assisted Spray Drying (SAA, CAN-BD)

In carbon dioxide assisted spray drying processes, the supercritical carbon dioxide plays the role of both a co-solvent, as it is mixed with the solution to be treated, as well as a pneumatic agent to atomize the solution into fine droplets. In this process, the substance to be micronized is first dissolved in water or ethanol or both and then mixed with supercritical CO₂, producing an emulsion, in a packed bed saturator. The emulsion is then sent to a thin wall injector and allowed to rapidly depressurize through a suitable device into the precipitator at atmospheric pressure to generate aerosols of micro-bubbles and micro-droplets that are dried by a flux of warm nitrogen [43,44].

The main difference between CAN-BD (Carbon dioxide Assisted Nebulization with a Bubble Dryer®) and SAA (Supercritical Fluid-Assisted Atomization) processes is the initial mixing equipment utilized to generate the emulsion. In the case of SAA, the supercritical CO₂ and the solution are mixed in a vessel loaded with stainless steel perforated saddles which assures a large contact surface between liquid solution and the SCF [44,45]. On the other hand, in the CAN-BD process, the supercritical CO₂ and the solution are pumped through near zero

volume channels to produce the emulsion, which is then allowed to depressurize in the precipitator [46-48].

The advantages of the SAA process include its capability for processing both water-soluble and non-water-soluble compounds. Moreover, both SAA and CAN-BD processes provide good control over particle size and particle size distribution [43,44].

2.4.5 Selection of Methods for Particle Production

Several techniques are currently available for particle production based on SCF technology. The selection of the process to be used is dependent on the characteristics of the material to be treated and/or the final product. For instance, if the polymeric material is soluble in the SCF the RESS technique can be used, whereas if SCF is soluble in the polymer the PGSS process can be used. In case of low solubility, an anti-solvent method can be used. However, it is to be kept in mind that anti-solvent methods use organic solvents that are associated with issues such as solvent removal and waste stream generation. When organic solvents have to be avoided, *i.e.* in the case of biological products, processes such as CAN-BD or SEDS could be selected. Finally, the characteristics of the desired product (particle size, particle size distribution, shape etc.) would drive the selection of the technology as well. Other issues such as cost and availability can also derive the choice of process to be used.

2.5 EXTRUSION IN PARTICLE PRODUCTION

Since the 1930s, the extrusion process has been widely used for manufacturing and processing of polymeric material. The overall extrusion system can be divided into two units:

(a) the extruder (Figure 2.6); known as the conveying unit that is used to melt, mix and convert the raw material into a product of uniform shape and density, and (b) the die unit which is used to shape the material by forcing it through a narrow outlet under controlled conditions. Based on design, extruders can be divided into types: single-screw and twin-screw extruders. Irrespective of the type of extruder, most commercial extruders have a modular design, providing a choice of screws (single screw vs. twin screw) with interchangeable sections as well as various die designs available to meet production requirements. Advantages of an extrusion process include short residence time, self wiping adjustable screw profile, and versatility for processing different kinds of material [8]. Among the two types of extruders available, twin-screw extruders are more commonly used than single screw extruders in mixing operations due to their superior mass and heat transfer characteristics [8,49].

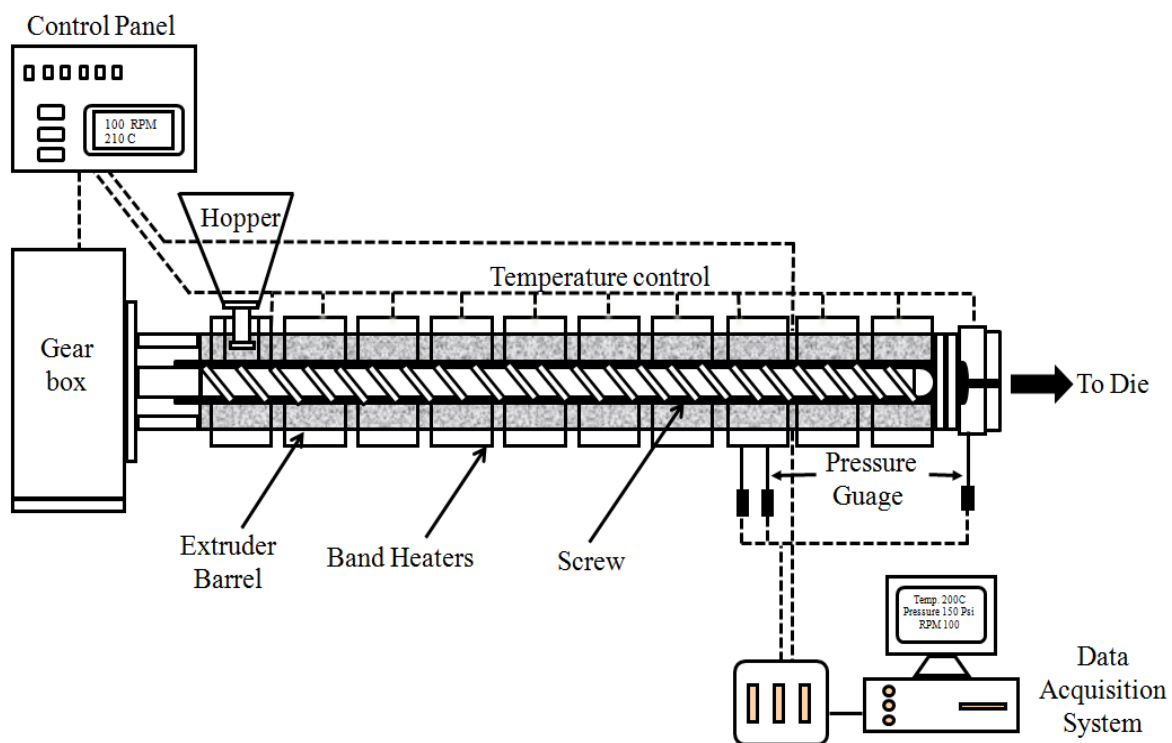


Figure 2.6: Typical Extrusion Process

For particle production using an extruder, the supercritical fluid is first dissolved in the polymer matrix, where the dissolved CO₂ plasticizes and reduces the viscosity of the polymer to be micronized. The molten polymer-gas solution is then passed through a narrow die gap and out through a micron-size nozzle hole. The high pressure difference between the upstream and downstream of the nozzle causes thermodynamic instability due to reduction of gas solubility in the solution resulting in supersaturation. This supersaturation causes nucleation of bubbles, an illustration of which is provided in Figure 2.7. A vigorous expansion of these bubbles break up the solution to produce micronized particles [9,10]. Due to an excess of CO₂ used for particle production, this method has been termed as expansion of gas-saturation with excess gas (EGSEG) [15].

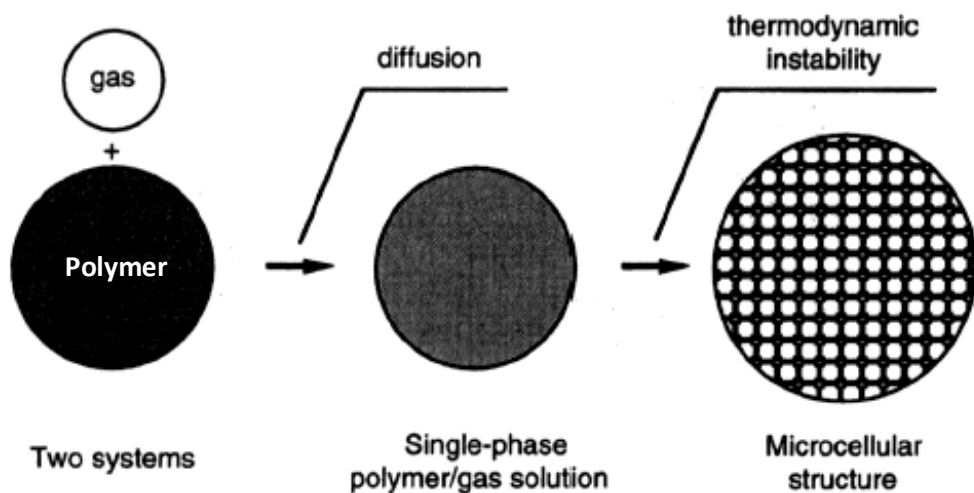


Figure 2.7: Morphology Change of a Polymer-Gas System in an Extrusion Particle Production Process Using Supercritical Fluid Solution [50]

One of the advantages of using extrusion for particle production is that the particle shape, size, and size distribution can be controlled via control of processing parameters, nozzle size and geometry. Use of extrusion for particle production can help eliminate issues associated with conventional powder production methods, such as broad particle size distribution in milling process and heat generation during grinding process [9]. The plasticizing effect of dissolved CO₂ permits operation at lower temperatures, allowing micronization of thermolabile compounds using extrusion [8,9,51]. In addition, since polymers are primarily produced in industry via extrusion processes, micronization of polymers using an extruder will allow elimination of secondary particle generation steps such as for GAS, SAS and RESS.

Only a limited number of studies have been conducted to produce particles via an extrusion process. Nalawade et al. [10,11] produced submicron-size particles (fibres) of polyester resins using an extrusion process. They reported that the effect of various process parameters such as pressure, temperature, flow rates, and nozzle diameter plays a crucial role for particle production in an extruder and further details are discussed in section 2.7.

2.6 POLYMER/ SUPERCRITICAL FLUID SOLUTION

When a polymer melt is exposed to a high-pressure gas, two competing mechanisms affect the specific volume of the polymer-gas mixture: (1) the hydrostatic pressure, and (2) swelling. Hydrostatic pressure decreases the specific volume. Swelling, on the other hand, caused by dissolved gas under high pressure increases the specific volume. The latter is typically higher than the hydrostatic pressure effect. The increase in specific volume due to swelling enhances the overall activity of the polymer-gas solution, thus creating more free volume. This increase in free volume causes an increase in gas solubility and diffusivity. The

increase in free volume also increases chain mobility, decreases viscosity and surface tension of the polymer [52,53].

All of the above mentioned parameters, such as solubility, diffusivity, viscosity and surface tension, are affected by swelling (or increase in free volume) and are crucial for understanding the foaming behaviour in an extrusion process. To attain a stable particle production process using supercritical CO₂, detailed knowledge of these process variables is required. A discussion regarding some of these characteristic properties of polymer-supercritical fluid solution is provided in this section.

2.6.1 Solubility

Solubility is defined as the maximum amount of solute that can be dissolved in a solvent at a specific temperature and pressure without phase separation. The solubility of CO₂ in polymer or polymer in CO₂, are both determined by the intermolecular forces acting between the polymer and the CO₂ molecules. It was found that the quadruple moment and Lewis acidity of CO₂ contributes to its solubility in polymers. Several studies have been carried out to explore the interactions between polymer and CO₂ [14,54]. The evidence of Lewis acid-base interaction was first provided by Kazarian et al. [54] in 1996 where he used a Fourier transform IR spectroscopy to analyze the interaction between CO₂ and polymers.

Carbon-dioxide solubility also depends on processing temperature and pressure. At elevated temperature and pressure, the quadruple moment of supercritical CO₂ is disrupted by the thermal energy leading to a non-polar behaviour of CO₂, allowing dissolution of a non-polar solute, such as polymer, into supercritical CO₂. However, it is to be noted that the critical dissolution pressure and temperature rises with increasing molecular weight, i.e. larger

molecules show limited solubility in CO₂. Polymers with flexible backbones and high free volume (hence low glass transition temperature) show higher solubility in CO₂ [14].

The quantity of CO₂ dissolved in a polymer can also be affected by the weak intermolecular interactions between CO₂ and functional groups, such as carbonyl groups, ether groups, aromatic groups etc., available in a polymer. Evidence of such interactions has been of much interest to research studies for years and is highlighted in several publications [54-57]. For example, an FTIR study indicated that interactions between CO₂ and carbonyl groups of poly(methyl methacrylate) and cellulose acetate was the reason for CO₂ solubility in these polymers [55]. In another study, Shah et al. [56] investigated the solubility of carbon dioxide in silicone polymers: silicon(dimethyl silmethylene) and poly(tetramethyl silhexylene siloxane). It was found that the solubility of carbon dioxide decreases with increasing polymer backbone substitution or side chain substitution. They argued that this decrease in solubility was a result of decrease in specific free volume (i.e. fractional free volume) in these polymers.

Various theoretical models such as lattice fluid theory, off-lattice theory, cubic equation of state, are readily used to estimate CO₂ solubility in polymers. Apart from theoretical models, several experimental methods, for example phase separation method, gravimetric method, pressure decay method, are employed for solubility measurements. Many articles are available that provide detailed description of the experimental principles and apparatus used for these methods [9,58-60]. Among the various methods available for solubility measurement, the gravimetric method (uses a Magnetic Suspension Balance (MSB) apparatus) is one of the most popular as it has some advantages over the other methods available. High sensitivity and short measurement time are two such advantages reported in the literature [9,58].

When using an experimental method for solubility measurements, it should be kept in mind that gas dissolution in polymer melt causes swelling which must be taken into account for accurate measurement of solubility. Thus, theoretical models are often paired with experimental measurement to correct the solubility results obtained and to include the volume swelling of polymer melts [61].

The solubility of different grades of polypropylene (PP) and polyethylene (PE) has been widely investigated and published in literature. Li et al. measured the solubility of carbon dioxide in solid state isotactic polypropylene by pressure-decay method for a temperature range from 373.15 to 423.15 K and pressure up to 15 MPa [59]. Sato et al. measured the solubility and diffusivity of CO₂ in melts of polymers, such as polypropylene (PP), high-density polyethylene (HDPE) etc., at temperatures: 433.2, 453.2, and 473.2 K and pressures up to 17 MPa using pressure decay method combined with Sanchez-Lacombe equation of state (SL-EOS). The EOS was used to estimate the swollen volume due to dissolved gas. Both these studies indicated a decrease in CO₂ solubility with increase in temperature [62,63].

Areerat et al. also analyzed the solubility of supercritical CO₂ in low-density polyethylene (LDPE), high-density polyethylene (HDPE), polypropylene (PP), and polystyrene (PS) for a temperature range of 423.15K to 473.15 K and pressures up to 12 MPa using MSB. They analyzed the effect of pressure and temperature on solubility and concluded that CO₂ solubility increases with increase in pressure and decreases with increase in temperature for all polymer/CO₂ systems. The absolute value of solubility varies from polymer to polymer. The magnitude of the solubility in different polymer types is PP, HDPE, LDPE, EEA and PS in descending order as shown in Figure 2.8 [64].

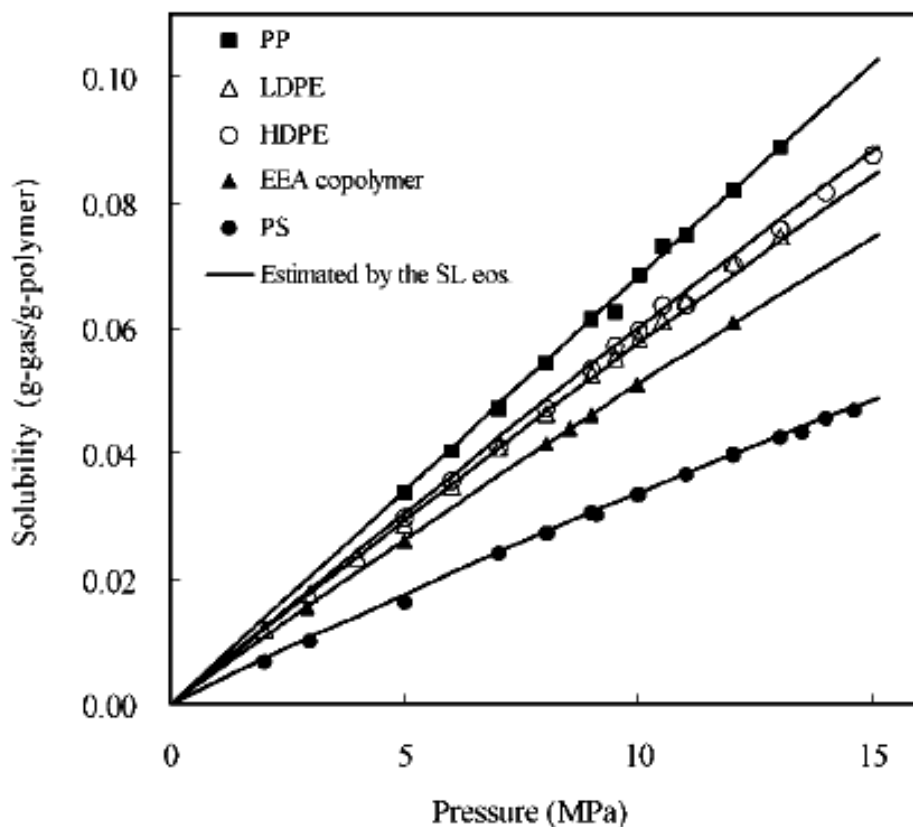


Figure 2.8: Solubility of CO₂ in Different Polymer Melts at 473.15 K Under Different Saturation Pressure (The symbols represent experimental results whereas the straight line is the estimation from SL-EOS) [64]

Li et al. [65] carefully studied the solubility of CO₂ in polypropylene at temperatures from 313.2 to 483.7 K and pressure up to 25 MPa by using MSB method and SL-EOS for swelling correction. It was found that at a given temperature, when pressure increases, the solubility increases almost linearly at low pressure, but increases to large values with a non-linear trend at high pressure (Figure 2.9). Comparison of the CO₂ solubility with and without swelling degree correction was also performed. It was found that solubility values that included the swelling degree correction was higher than those that did not include the correction, and the differences between the values became higher at high pressure (Figure 2.9). The solubility

values that included the solubility correction were close to the ones available in the literature, which implied that the contribution of swelling cannot be ignored.

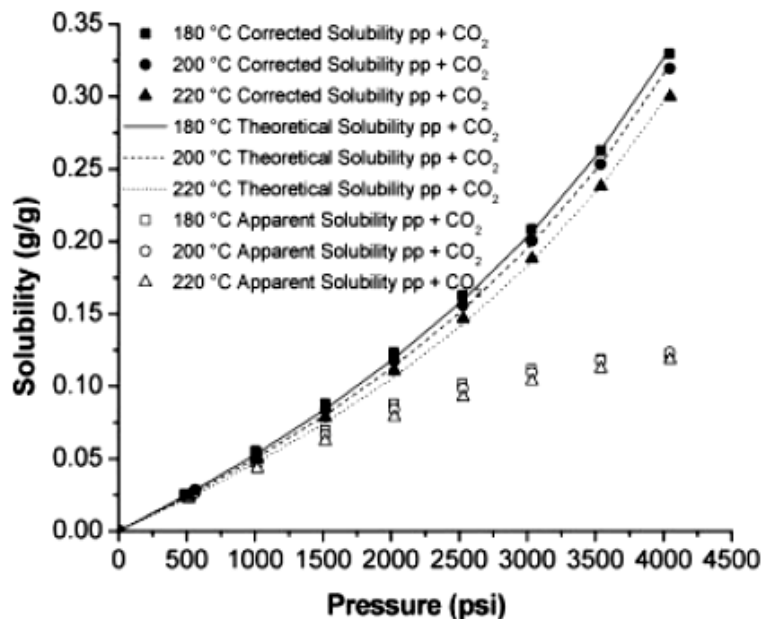


Figure 2.9: Solubility of CO₂ in PP Polymer Melts at Different Temperatures with and without Swelling Degree Correction [65].

The difference in CO₂ solubility in linear and branched polypropylene (PP) was investigated by Li et al. [52,61,65,66] using a magnetic suspension balance for temperature range of 453 to 493 K and at pressure of up to 31MPa. It was noted that linear polypropylene absorbs more gas than branched polypropylene due to the entanglement effect of the branched polypropylene. Carbon dioxide solubility in PP melt was compared with semiempirical data (calculated by empirically measuring gas uptake and EOS corrected swelling effect) and theoretical values calculated with the Sanchez-Lacombe equation of state (SL-EOS) and the Simha-Somcynsky equation of state (SS-EOS). The authors concluded that SS-EOS predicted the swelling effect more accurately compared to SL- EOS, for both semiempirical and theoretical cases.

2.6.2 Viscosity

Viscosity is a fluid property which describes its resistance to deformation under shear or tensile stress. Shear viscosity is a key factor in the breakup of molten polymers in micronization. The higher the viscosity the more difficult it is to break up the polymer melt. Hence, it is crucial to understand the effect of polymer and polymer-gas solution viscosity in order to design a successful micronization process.

The viscosity of a polymer is a strong function of molecular weight and it increases with increasing molecular weight. High molecular weight (i.e. high viscosity) polymer processing is associated with various challenges. A possible solution to this dilemma is the use of organic solvents. However, waste stream generation and VOC emission are concerns associated with organic solvent usage. An alternative solution is to control process temperature to adjust solution viscosity. Viscosity is a strong function of temperature and an increase in temperature decreases viscosity. This temperature-viscosity correlation was first proposed by Tamman and Hesse in 1926 in the form of an Arrhenius equation:

$$\eta = A \exp\left(\frac{B}{T - T_0}\right) \quad 2.2$$

where A and B are constants, η is the viscosity, T is the temperature and T_0 represents the thermodynamic second-order transition temperature [67]. Equation 2.2 shows that viscosity is inversely proportional to temperature. However, at elevated temperature the risk of polymer degradation is a concern.

A proposed alternative for polymer viscosity reduction is the use of supercritical CO₂. After years of research to understand the effect of dissolved CO₂ in molten polymers, it is now

well established that supercritical CO₂ has a significant effect on polymer viscosity. The dissolution of CO₂ in a polymer matrix causes plasticization, which is evident by a decreased glass transition or melting point temperature of the polymer [34,68-71]. This in turn increases the chain mobility [69,71-73] and reduces polymer viscosity [73]. Thus, the use of CO₂ allows processing of polymers at low temperatures and polymer degradation is avoided.

Another approach to understanding the above mentioned viscosity reduction phenomenon is by the free volume theory. In a polymer-gas system, the dissolved gas under high pressure causes the polymer to swell and increase the specific volume, which enhances the overall activity of the polymer/gas system, and thus creates more free volume for the CO₂ molecule to penetrate into. This increase in specific volume decreases polymer viscosity [33,52,74-77]. The relationship between the viscosity and free volume was first proposed by Doolittle [78],

$$\eta = A \exp \left(\frac{B}{f} \right) \quad 2.3$$

where A and B are constants, and f is the free volume fraction of the polymer. The free volume fraction is defined as the ratio of volume accessible for chain motions to the specific volume of the melt. The accessible volume is the difference between the specific volume of the melt and the occupied volume. For a polymer-gas mixture, the occupied volume is defined as

$$v_o = w_{CO_2} v_o^{CO_2} + (1 - w_{CO_2}) v_o^P \quad 2.4$$

Where, v_o is the occupied volume, v_o^P is the molecular volume of the polymer and w_{CO_2} is the weight fraction of CO₂ dissolved in the polymer [9].

Viscosity is not only a function of temperature, but also a function of pressure. The pressure dependence of polymer viscosity has been studied by many researchers. Duvdevani et al. [79] measured the pressure effect on viscosity for low density polyethylene using a capillary rheometer and proposed the following relation

$$\eta = \eta_{\text{atm}} \exp (B'P) \quad 2.5$$

where η_{atm} is the viscosity at atmospheric pressure, P is pressure, and B' is a pressure coefficient which is a function of temperature. The pressure coefficient was calculated to be around $3 \cdot 10^{-5} \text{ psi}^{-1}$ for the polyethylene-gas mixture. However, it should be noted that the pressure coefficient is a function of shear rate and temperature and it increases with increasing shear rate and temperature.

Numerous viscosity measurements have been performed by individual research groups to understand the effects of process variables on viscosity and to develop viscosity models incorporating the effects of these variables. Experimentally, viscosity measurement can be performed using extrusion rheometers such as a slit die [80], capillary die [81,82], and wedge die [77]. Various theoretical models based on Doolittle's free volume theory have also been proposed for predicting viscosity with respect to changes in pressure, temperature, CO_2 content etc.[77,80]. Some of the related publications are summarized in the following paragraphs.

Lee et al. [83] proposed a free volume model using the generalized Cross-Carreau equation and Doolittle's free volume theory to describe the viscosity model of PS- CO_2 theoretically. In this work, the fractional free volume term of Doolittle's theory was expressed as a power law series in order to include the effects of temperature, pressure and CO_2 concentration.

Royer et al. [80] developed a free volume method using the Williams-Landel-Ferry equation, a modified version of Doolittle's equation, to determine the glass transition temperature and melting point depression due to dissolved CO₂. The results indicate CO₂ is an effective plasticizer for polystyrene, lowering the viscosity of the polymer melt by as much as 80%. Experimental measurements of viscosity as a function of shear rate, pressure, temperature, and CO₂ concentration were also conducted to analyze the effect of process variables on viscosity.

Royer et al. [84] also designed a magnetically levitated sphere rheometer (MLSR) to measure viscosity of fluids exposed to high-pressure carbon dioxide. Viscosity measurements of poly(dimethylsiloxane) melt plasticized by high-pressure CO₂ were performed to illustrate the utility of the new rheometer under high-pressure conditions. It was found that the MLSR can be used for measuring rheological properties, specifically zero shear viscosities, of transparent high-pressure materials to a precision of about 5%.

Areerat et al. [81] studied the melt viscosities of low-density polyethylene (LDPE)/supercritical CO₂ solutions using a capillary rheometer attached to a foaming extruder. The viscosity measurements were performed by varying the CO₂ content in the range of 0 to 5.0-wt% and temperature in the range of 150°C to 175°C. The experimental results indicated that the viscosity of LDPE/CO₂ solution was reduced to 30% of that of the neat polymer by dissolving CO₂, up to 5.0 wt% at a temperature of 150°C. Doolittle's free volume concept combined with the Cross-Carreau model were employed to develop a mathematical model for predicting the viscosity reduction of the polymer/gas solution. In this model the free-volume fraction of LDPE/CO₂ solution was calculated using the Sanchez-Lacombe equation of state and the solubility data obtained during experimental measurements.

An important consideration to solution viscosity is the effect of shear. At high pressures, the effect of shear was reported for LDPE-CO₂ solution by Nobelen et al. [82]. In this study, a capillary tube die attached to a twin screw extruder was used to show the PE/CO₂ solution viscosity dependence on shear rate, temperature, pressure, and CO₂ concentration. A theoretical model based on a power law was proposed to describe the pseudoplastic behavior of PE/CO₂ solutions with different shear rates. Correction factors were included to take into account the effects of temperature, pressure, and CO₂ concentration.

Viscosity has been measured as a function of shear rate for a number of polymer- SCF systems, for example PDMS-CO₂ [85], PS-CO₂ [34] etc. These measurements show that the shape of the viscosity curves (shear viscosity vs. shear rate) for polymer-SCF solutions appear identical in shape to the viscosity curve for the pure polymer melt. This observation led to the successful application of classical viscoelastic scaling theory to reduce the viscosity data for polymer-SCF systems to a master curve of scaled viscosity vs. scaled shear rate. The master curve allows the rescaling (shifting) of viscosity data from a reference situation to different processing conditions [10].

2.7 EFFECT OF PROCESS VARIABLES ON MICRONIZATION

In a polymer particle production process, polymer particle size, particle size distribution and morphology of particles are a function of process variables, such as molecular weight, temperature, pressure, nozzle diameter etc. Effects of some of these variables are discussed below.

2.7.1 Effect of Pressure and Temperature

The effect of pressure and temperature in controlling particle size and morphology is tremendous. However, contradictory results have been reported by different authors about the influence of these parameters on particle size during batch and continuous operations. For example, for an increase in pressure some authors found a particle size increase [86], some found the process insensitive to this variable [11,87] and others observed a particle size decrease [11,88,89]. Same problem occurred for increasing temperature, where particle size increased for some authors [11,87], some observed no effect [90], while others reported a decrease in particle size [86,88]. Some of these findings are discussed below.

Costa et al. [88] investigated the effect of temperature and pressure on poly(3-hydroxybutyrate-co-3-hydroxyvalerate) (PHBV) particle size and particle size distribution for particles produced using supercritical antisolvent technique. The results indicate a decrease in the mean particle size from 7.0 to 5.9 μm for an isobaric increase in temperature from 35 to 40°C. In addition, a pressure increase from 80 to 90 bar caused a significant decrease in the particle size. However, a further increase in pressure did not significantly influence the diameter of the particles. The authors referred to the findings of Reverchon et al. [91] and concluded that for pressures larger than the asymptotic volume expansion, there is no significant effect of pressure in the particle size and particle size distribution of the particles precipitated.

In the gas antisolvent precipitation study, Chen et al. [89] noted that for a pressure increase from 9–18 MPa the crystal size decreases and shorter and thinner particles were formed. It was suggested that the decrease in particle size was favoured by the increase in

nucleation at higher pressure. Under isobaric conditions, experiments were carried out at 3 different temperature settings ($T=298, 308$ and 318 K) to investigate the effect on particle size. They reported an increase in particle size with increase in temperature.

Nalawade et al. [11] performed an experimental study to understand the effects of process variables on particle size, size distribution and shape of particles produced using supercritical CO_2 in a batch process. A wet laser diffraction (WLD) apparatus, Malvern Mastersizer®, was used to measure the particle size and particle size distribution, whereas a scanning electron microscope (SEM) was used to observe the morphology and shape of the particles. It was reported that the particle size increased with increasing temperature above its melting point for polyethylene glycol (PEG) under isobaric conditions. They argued that the increase in particle size was due to the decrease in CO_2 solubility with increasing temperature. They also reported an absence of pressure effects on PEG particle size, particle size distribution and shape.

2.7.2 Effect of Molecular Weight

As mentioned earlier, shear viscosity of a polymer plays an important role in polymer micronization. The higher the viscosity of a polymer, the harder it is to break it up to produce particles. The viscosity of polymer is directly proportional to its molecular weight, i.e. the viscosity increases with increasing molecular weight.

Nalawade et al. investigated the effect of molecular weight on micronization of several different polymers, such as polyethylene glycol (PEG), propoxylated polyester resin (PPB) etc. They found that long fibre shape particles were produced for a PEG sample with higher molecular weight, instead of round particles [11]. They argued that for high molecular weight

polymer, high shear and extensional viscosity inhibit the breakup of the polymer melt. As a result, excess of CO₂ is necessary in order to break up the polymer melt. In the presence of excess CO₂, i.e. at a high gas to polymer mass ratio, the polymer melt is subjected to intense instabilities at the surface of the melt present in the form of a thin film and hence, the breakup of the melt is enhanced [10].

2.7.3 Effect of Spraying Nozzle Diameter

Investigation of the effect of nozzle diameter on PEG particles size was performed by Nalawade et al. [11,9]. It was found that the average particle diameter decreases with decrease in nozzle diameter. They explained this behaviour using the pressure drop rate effect in a nozzle, suggested by Park et al. In a microcellular foaming study, Park et al. [92] examined the effect of pressure drop on particles and found that the pressure drop rate across the nozzle determines the solubility drop rate, which in turn determines the nucleation rate of CO₂ bubbles. By analyzing the pressure drop rate across two different nozzles, Nalawade et al. [11,9] found that the pressure drop rate is very high in the smaller diameter. An order of magnitude of pressure drop rate for the smaller nozzle diameter is around 25 times higher than for the bigger nozzle diameter. On the other hand, the pressure drop rate was only 3 times higher in case of different pressures for the same nozzle.

In another study, Nalawade et al. observed that nozzle diameter also has a significant effect on product quality. It was found that for a high molecular weight polyester resin, as the nozzle diameter increased, the product changed from agglomerated fibres to irregular shaped particles [15]. They argued that this observation was a result of the viscoelastic nature of polymers. Before the breakup of a viscoelastic material, long threads are always formed along

with droplets that inhibit the breakup. Polymer molecules with long chains intermingle into each other. As a result, when the melt enters the nozzle from large cross section to small cross section it is subjected to elongation. The smaller the diameter of the nozzle, the higher is the extensional effect experienced by the polymer molecules. In addition, high shear experienced by the larger molecules in the nozzle also keeps them aligned. This elongation prevents the breakup of the polymer molecules into particles even at elevated pressure. Hence, agglomerated fibres are formed for high molecular weight polymers when processed through a smaller nozzle [93].

The nozzle geometry is a key factor in micro-particle production processes. The geometry of a nozzle allows working at higher Reynolds (good mixing) and Weber (small droplet size) numbers by increasing the velocity of the fluid [36]. This leads to an improved mass transfer and nucleation rate resulting in the production of particles with small size and little agglomeration [94]. Therefore, special attention should be given to nozzle geometry when designing a particle production process.

2.7.4 Effect of CO₂ Content

In their publication for PEG particle production, Nalawade et al. [95] investigated the effect of increasing gas to polymer mass ratio (GTP) on the flow behaviour. They observed that when GTP ratio increases a transition from one flow regime to another takes place. This increase in GTP forces the foaming polymer strands to break up and produce particles. They argued that at higher ratios, the expansion of excess CO₂ causes intense instabilities at the surface of the polymer melt which enhances the breakup. However, it should be noted that foam is produced even at higher ratios if the temperature and pressure are low.

Nalawade et al. [9,95] also investigated the dependency of particle size, size distribution, and morphology on GTP. The results indicate that particle size decreased with increasing GTP. At high ratios, the influence of pressure on particle size is less pronounced, than at low GTP. Photographs and diagrams presented in this work indicate that even the particles that have similar sizes, differ in morphology for varying GTP.

2.7.5 Effect of Solidification Time

The time available for particles to solidify defines the shape of particles produced. Both pressure and temperature play a vital role in determining solidification time. From the PEG micronization study by Nalawade et al. [11], it was observed that more spherically shaped particles are formed at higher temperature in a PGSS process. This is because as the temperature of the polymer melt increases, more heat needs to be dissipated for particles to solidify for which the solidification process gets delayed. This delayed solidification facilitates retraction of molten polymer into a spherical shape by both visco-elastic relaxation and surface tension. Moreover, the amount of dissolved CO₂, a function of temperature and pressure, also contributes to solidification in the form of heat of evaporation. At higher temperature and lower pressure, the amount of dissolved CO₂ is reduced. As a result, less energy is utilized for evaporation of CO₂, which increases the solidification time. On the other hand, for lower temperature, a large amount of CO₂ was found to be retained inside PEG particles due to rapid cooling, for which porous particles were formed.

CHAPTER 3: EXPERIMENTAL

3.1 INTRODUCTION

Polymer micronization in the presence of supercritical CO₂ using an extruder is a new process which has not yet been fully understood and tested. A steady micronization process requires special techniques for flow control of CO₂ and dissolution of the injected CO₂. It also requires special equipment for CO₂ injection, spraying and collection of particles. As a result, various methods were tested and used to achieve a steady particle production process via screw configuration change and process pressure control. Several extrusion methodologies and devices were specially designed to fit a typical twin screw extrusion process to perform the experiments. Experiments performed were used to analyze the effects of supercritical CO₂, pressure, temperature and RPM on the micronization process. Analysis of particle size and morphology was performed to understand the effects of these process variables. A description of the equipment and techniques used for the experiments performed and for the analysis of the particles collected is described in this chapter.

3.2 MATERIALS

3.2.1 Polyethylene Wax

Polyethylene wax, known as Licowax® PE 520, was used for micronization using supercritical CO₂ in the extrusion process. It is a medium molecular weight non-oxidized non-polar PE wax produced by Clariant USA. It was reported by the manufacturer that the viscosity of this polymer is approximately 650 mPa.s, density is in the range of 0.92-0.94 g/cm³ (at 23°C) and the drop point is 117-123°C (ASTM D3954). The crystallization temperature and

melting point (T_m) were measured using Differential Scanning Calorimetry (DSC) and were found to be 58.15°C and 106.84°C respectively. The effect of shear on polymer viscosity was also measured using a capillary rheometer in the lab (data presented in appendix D), and the results obtained are illustrated in Figure 3.1.

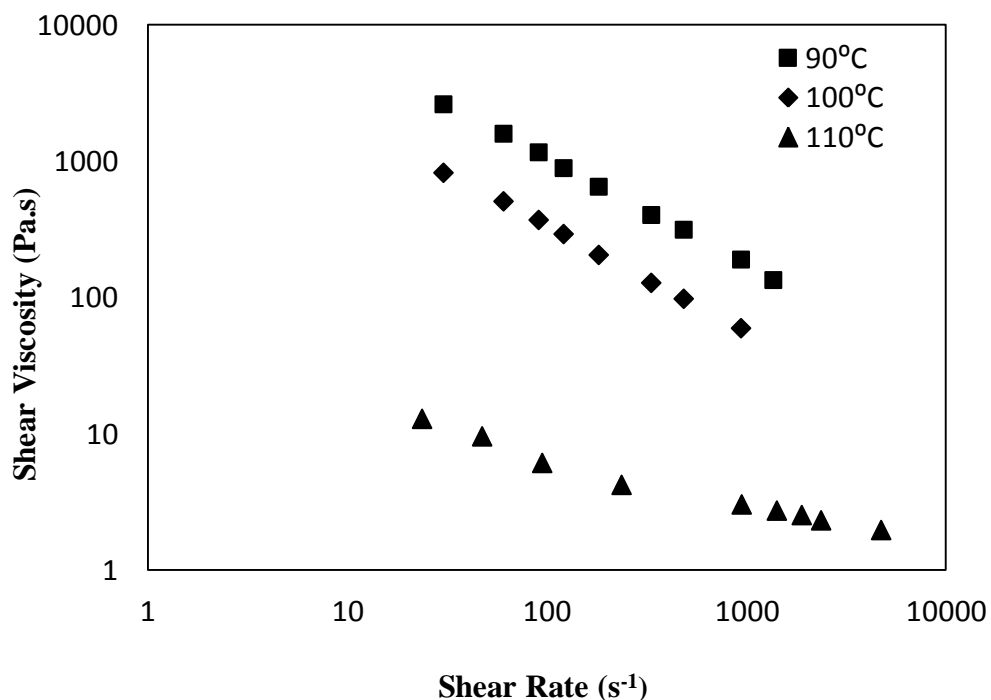


Figure 3.1: Shear viscosity of Polyethylene Wax at Various Temperatures

3.2.2 Supercritical Carbon Dioxide

The carbon dioxide used as the supercritical fluid in this experiment was supplied by Praxair Canada. The cylinder was supplied with a high-pressure helium headspace, to help maintain the high pressure required to maintain supercritical conditions for the experiments. The product was supplied at 99.997% product purity with an initial cylinder pressure of about 1900 psi.

3.3 EQUIPMENT

3.3.1 Leistritz LSM 30.34 Twin-Screw Extruder

The extrusion system used in these experiments was a twin-screw extruder with fully intermeshing and co-rotating screws of 34 mm diameter and 30 L/D ratio. The extruder comprised of 10 barrel segments, where each segment came with its own temperature control. At barrel segment number 1, ground polymer powder or pelletized polymer was fed into the extruder using a Brabender flex-wall feeder regulated by a KDU controller. Barrel segment number 7 was equipped with a SCF injection port for the delivery of CO₂. The extruder was also equipped with a converging die and a high resistance spraying nozzle. The temperature of the die and spraying nozzle were controlled by band heaters and PID controllers. The schematics of the twin-screw extrusion system are shown in Figure 3.2.

An ISCO positive displacement pump was connected to the injection needle to meter the CO₂ into the extruder and an OPTO22 data acquisition system was used to control the extruder screw speed and monitor the pressure and temperature in the extruder barrel. A special screw configuration was used to ensure dissolution of CO₂ into the polymer matrix, stable injection of CO₂, pressure generation and constant spray of micronized polymer particles. Details of the screw design concepts are discussed in section 3.5.

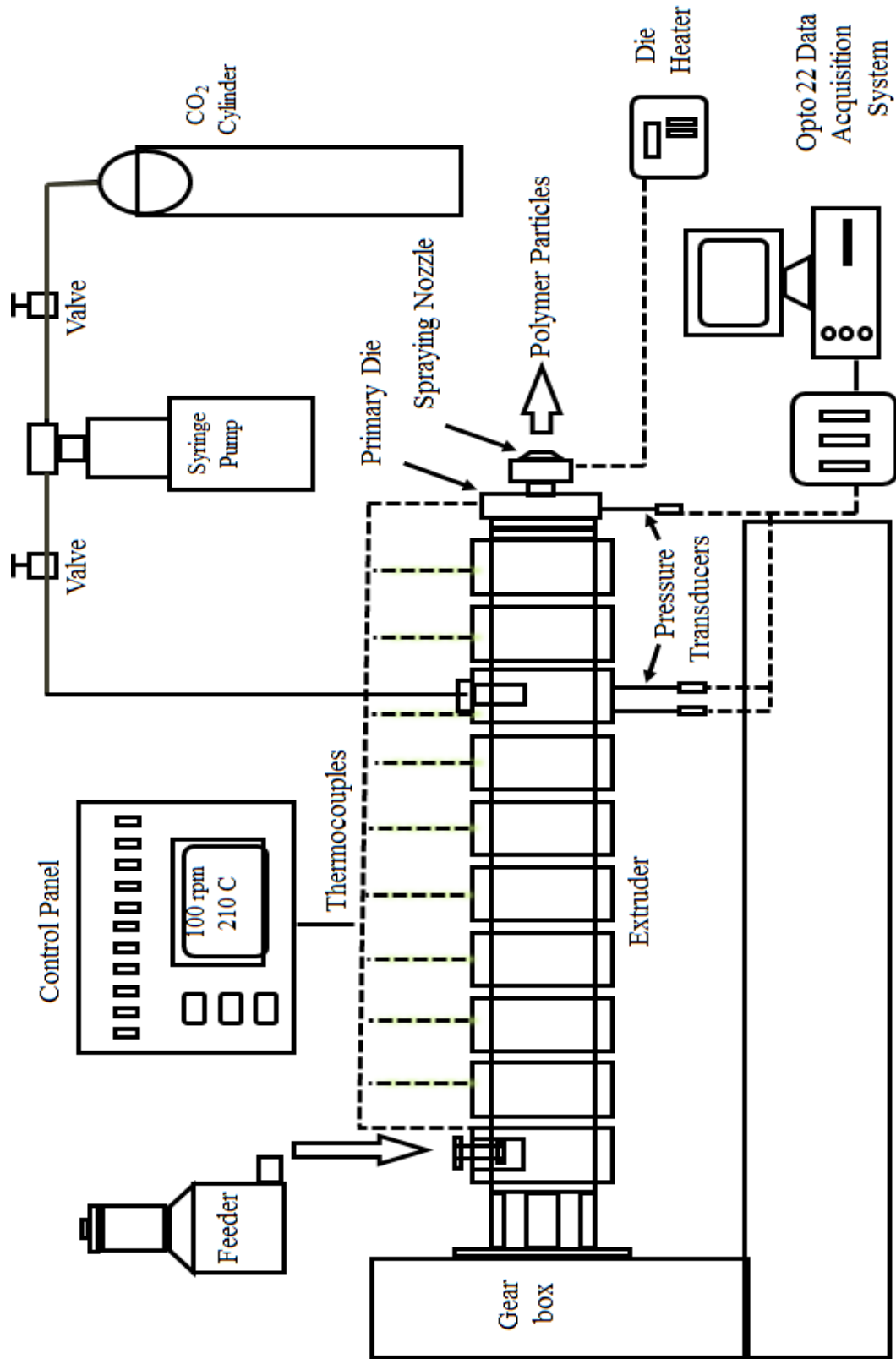


Figure 3.2: Schematic of the extrusion system

3.3.2 ISCO Positive Displacement Pump

SCF was injected using an ISCO positive displacement pump. For injection purposes, an ISCO D series syringe pump model 260D was used. Some of the specifications of the pump are provided in Table 3.1.

Table 3.1: Positive Displacement Pump Specifications

	ISCO-260D
Cylinder Capacity (ml)	266.05
Pressure Range (psi)	10-7500
Pressure Accuracy (%)	± 2.0
Flow Rate Range (min^{-1})	0.01 μl - 107 ml
Flow Rate Accuracy (%)	± 0.5

The ISCO positive displacement pump is capable of delivering SCF in constant pressure mode or constant flow mode. During the experiment, constant flow mode was used to meter a known volumetric flow rate of CO₂ into the polymer melt. If required, the volumetric flow rate may be converted into mass flow rate using the CO₂ density obtained from the literature. During the experiment, the ISCO pump cylinders were first filled up with CO₂ from CO₂ cylinders delivered by Praxair Canada with initial pressure of 1900 PSI. Carbon dioxide was then delivered from the pump to the extruder through the injection device using 1/8" tubing of 0.02" wall thickness. The pump and the Praxair CO₂ cylinder were also connected via a 1/8" tubing of 0.02" wall thickness and several Swagelok connectors.

3.3.3 SCF Injection Device

An injection device was designed to supply CO₂ into the twin-screw extruder. The liquid/gas injection stem used for this purpose was supplied by Leistritz which had a hollow 0.4 mm (1/64") space and two pinholes at the stem tip. The gas flowed through the hollow space and was injected in-between the meshing of the two screws as suggested in Figure 3.4. A series of Swagelok compression fittings and 1/8" metal tubing were used to connect the injection stem to the CO₂ supply pump. The injection stem was inserted into the barrel through the locking bolt and it sat in a narrow oval-shaped aperture.

During the experiments, the extruder barrel was fully filled under the injection device with polymer melt to generate high pressure and to ensure that the injected CO₂ was directly swept by the polymer melt and was dissolved quickly. However, due to high pressure build-up in the extruder, polymer sometimes filled up the hollow space in the CO₂ injection stem, and constant injection of gas could not be achieved. Therefore, a start-up procedure was implemented to minimize clogging. The design of the CO₂ injection device designed for a twin-screw extruder is shown in Figure 3.3. The location of the injection needle stem inside the extruder barrel is shown in Figure 3.4.

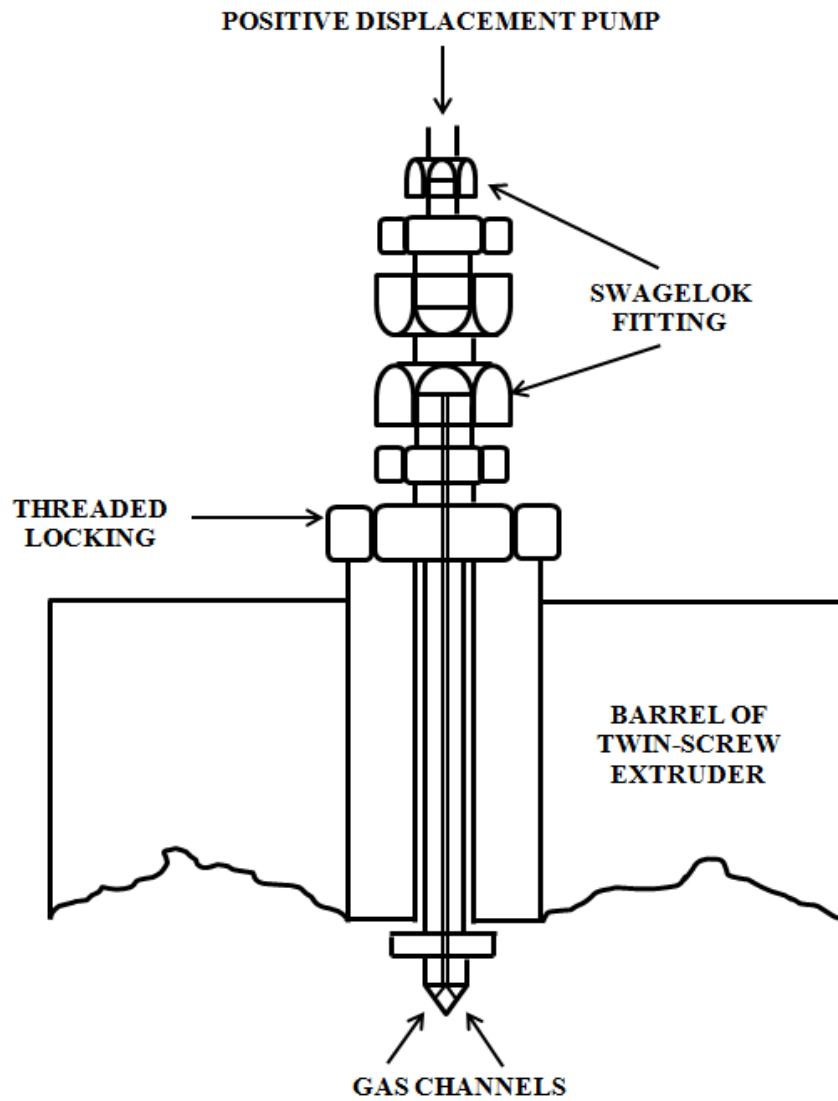


Figure 3.3: The CO₂ Injection Device for Twin-Screw Extruder

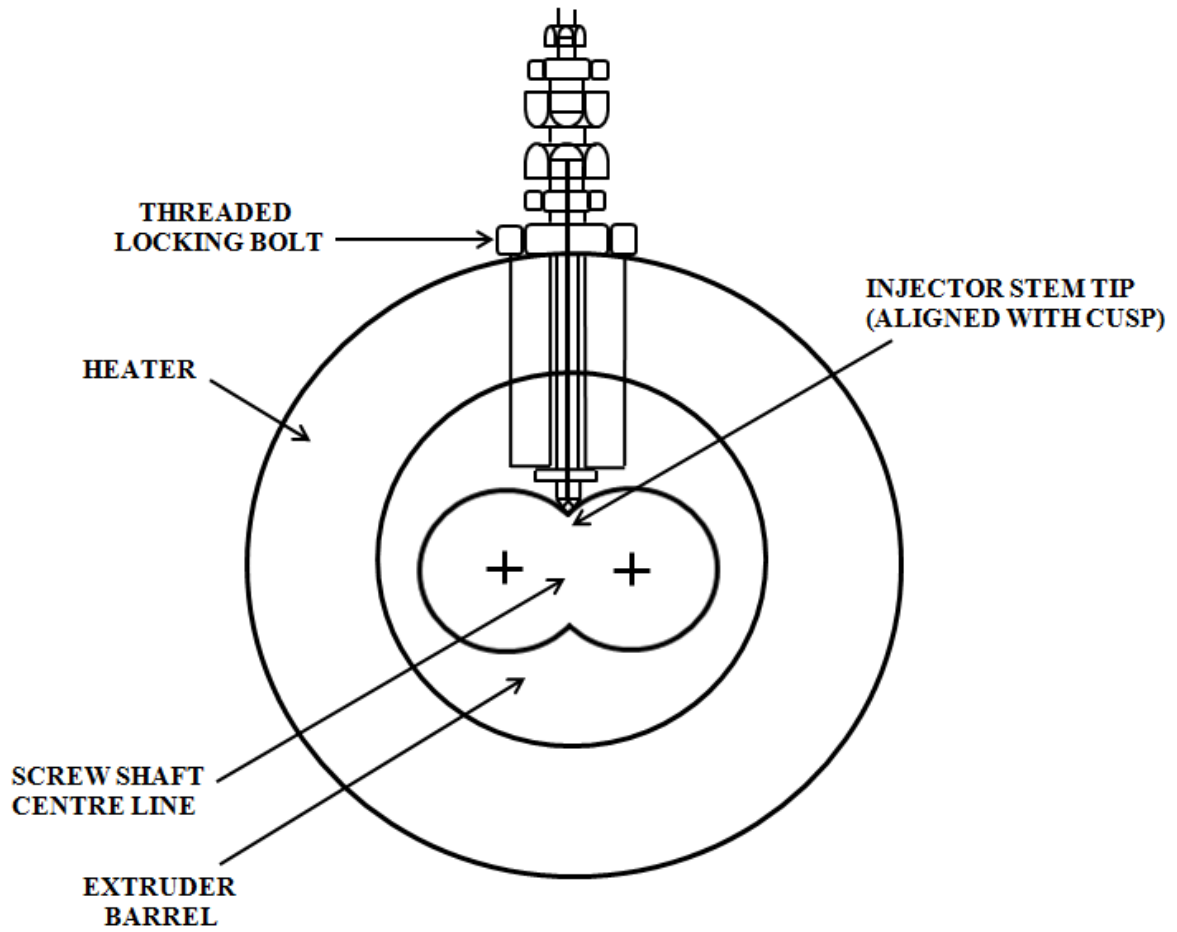


Figure 3.4: The Barrel Cross Section of a Twin-Screw Extruder Showing the Injection Location

3.3.4 Spraying Nozzle

An air atomizing spraying nozzle from Spraying Systems Co. was customized for the production of polymer particles. The nozzle comprised of two inlet caps, a fluid cap and an air cap that was capable of delivering the fluid (molten polymer-gas mixture) and air, respectively. Due to the incorporated air cap, this nozzle can be used for air assisted particle production or air assisted cooling of micronized particles. The spraying nozzle used has a fluid cap capillary diameter of 0.4 mm and length of 1.66 mm, with a nozzle orifice L/D ratio of 4.15. The temperature of the spraying nozzle was maintained by a 400 W band heater controlled via a Zesta temperature controller. A schematic diagram of the spraying nozzle is shown in Figure 3.5.

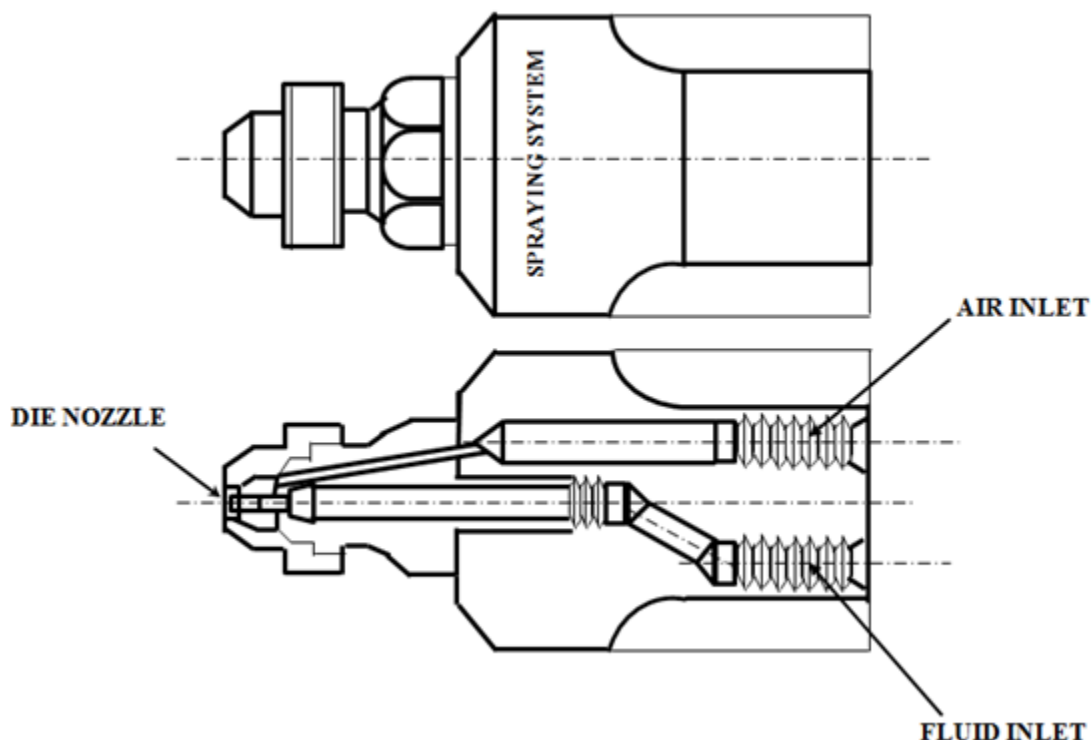


Figure 3.5: Schematic of Spraying Nozzle Used

3.3.5 OPTO22 Data Acquisition System

The temperature readings from temperature probes, pressure readings from both pressure transducers and positive displacement pump, and the extrusion screw speed were converted to digital signals using an OPTO22 Controller. OPTO22 Data Acquisition System is primarily comprised of a mother board, an input and an output module. The type of module used depended on the type of signal sent and received and the voltage used. For the pressure transducers OPTO AD9T was used, which converted output signals between 0 and 50 mV. For temperature probes and for the positive displacement pump an OPTO AD7 and OPTO AD12 were used, respectively. The converted digital signals were sent to the data-logging computer via an RS-232C cable. LabVIEW graphics program (Version 4.0) was used to write the user interface and display for the data acquisition system. The digital signals were recorded every 6 seconds and displayed on the screen.

3.3.6 Polymer Collection Chamber Design

A 72" * 25" * 36" polymer collection chamber was designed for the collection of particles. Half inch thick clear Lexan sheets were used for making this chamber. The chamber was mounted on a metal frame sitting on four wheels for easier mobility. The chamber was divided into two sections as shown in Figure 3.6. The particles blown out of the spraying nozzle entered the chamber through an 8 inch opening and settled in the bigger chamber from where they were collected for sample analysis. The smaller chamber was designed to allow the suction of excess air through an air filter.

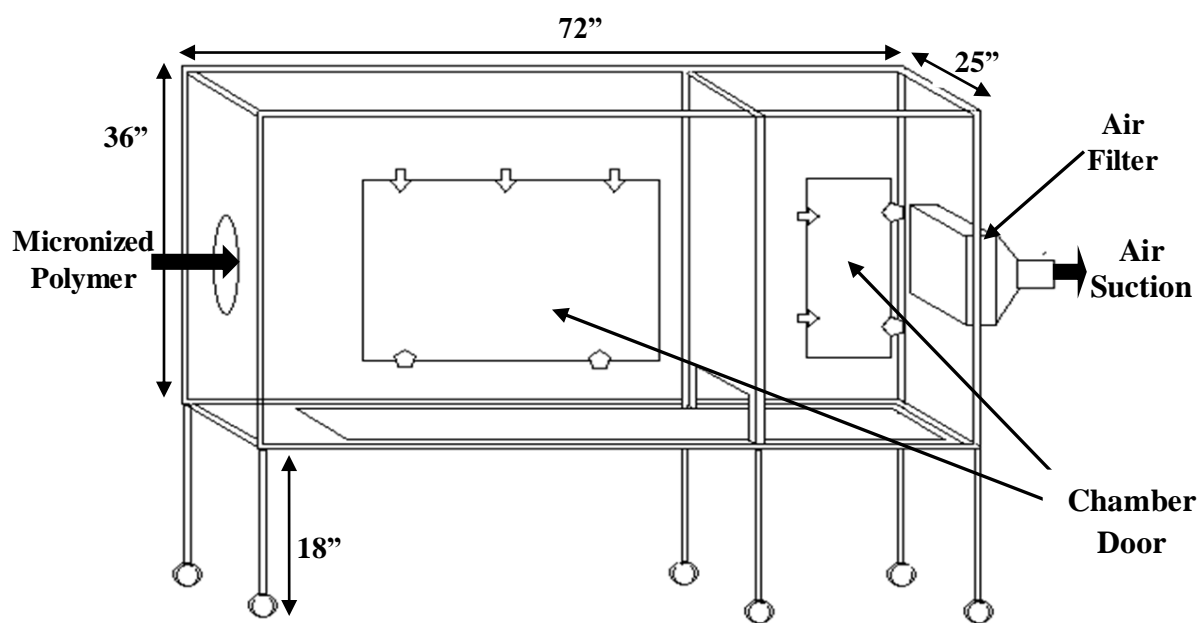


Figure 3.6: Micronized Polymer Collection Chamber

3.3.7 Design of Twin-screw Configuration

The screw configuration is an important feature for establishing a stable micronization process in an extruder. Here, the screw configuration is not only used to ensure dissolution of CO₂ into the polymer matrix, but also for pressure generation, stable injection of CO₂ and constant spray of micronized polymer particles. In this section, the design criterion of the twin-screw configuration is discussed.

The extruder consists of 10 barrel segments, where the polymer feed was introduced in the 1st barrel segment and CO₂ was injected into the 8th barrel segment. The screw elements inside the first six barrel segments were used for polymer melting, polymer conveying and pressure generation inside the extruder barrels. The screw design for these segments was similar to any conventional screw configuration with a series of conveying screw elements, starting with screw elements with higher pitch value and then introducing elements with smaller pitch values as the polymer entered the extruder and moved forward towards barrel segment 8. In these barrel segments, the decrease in pitch was from 45 mm to 20 mm. A short section of kneading blocks was introduced in barrel segment 5 in order to help in polymer melting.

Carbon dioxide was injected at barrel segment 8, before which a set of reverse screw elements was introduced to prevent CO₂ backflow and to generate a melt seal. After the reverse elements, sets of kneading blocks, including neutral and forward staggered ones, were introduced to assist in vigorous mixing and complete dissolution of supercritical CO₂ in the polymer melt under limited residence time. The kneading blocks also assured high pressure generation. As CO₂ solubility is a function of pressure, high pressure is essential for the preparation of the polymer/CO₂ solution. Additionally, maintaining the pressure above the

solubility pressure prevents CO₂ precipitation. Nevertheless, kneading blocks exhibit more pressure fluctuation than conveying elements. Consequently, conveying elements were used to stabilize the pressure before the polymer melt entered the die and spraying nozzle. The complete screw configuration is illustrated in Figure 3.7.

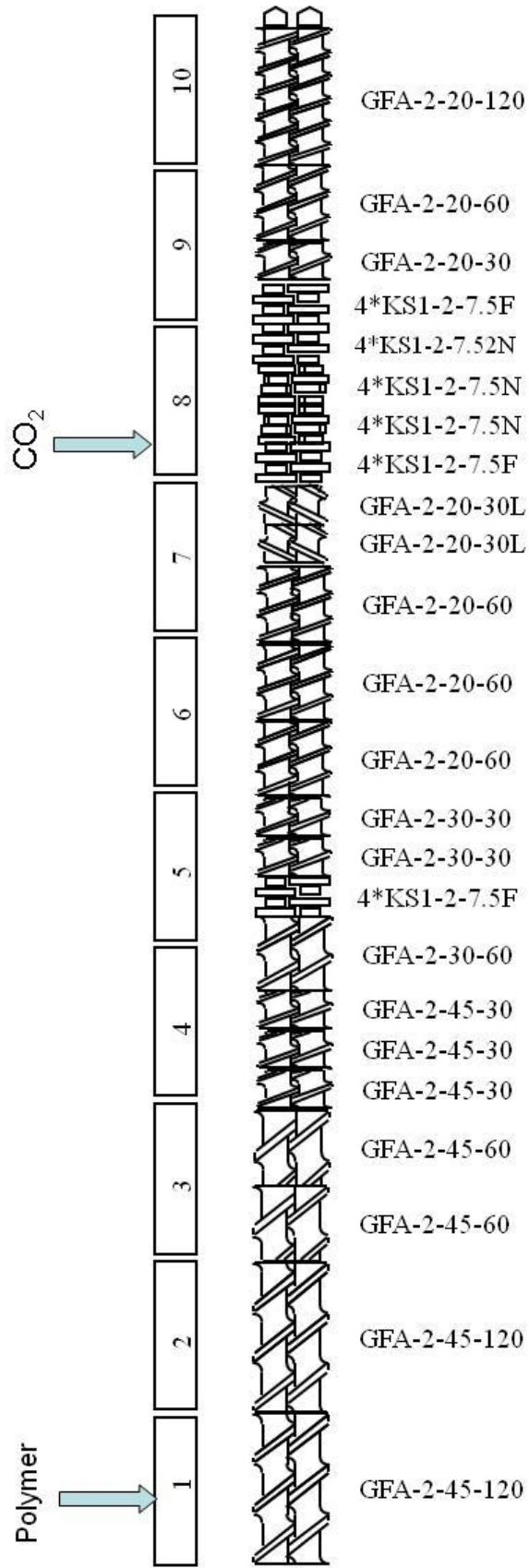


Figure 3.7: Schematic of the Twin-Screw Configuration

3.4 EXTRUDER OPERATION AND SAMPLE COLLECTION PROCEDURE

The extruder barrel sections were preheated to 20/20/20/70/90/90/90/90/90/100°C with the die temperature set at 140°C. The extruder temperatures and melt temperature were monitored via thermocouples, whereas the die temperature was monitored and controlled using a ceramic band heater. The pressures in barrel segments 8, 9 and 10 and the die pressure were monitored using four pressure transducers. Prior to their use, these pressure transducers were calibrated using a Dynisco Portable Pressure Source PPS1100. An ISCO injection pump and injection needle setup was used to supply supercritical CO₂ into the extruder. The screw configuration used for the micronization process was shown in Figure 3.7.

A start-up procedure was introduced to avoid polymer clogging of the injection needle. After the barrel temperature reached the set temperature, the extruder screws were initiated followed by injection of CO₂. When CO₂ started to escape through the nozzle and the feeder opening, the polymer feed was commenced. This startup procedure allowed the CO₂ pressure in the injection needle to resist clogging when the barrel filling up with polymer and pressure increased inside the extruder barrel.

The polymer feed rate calibration was performed before the start of the experiment. After the start-up, the extruder was allowed to be completely filled with polymer and the extruder pressure was allowed to stabilize. The CO₂ feed rate was gradually increased to the desired pressure setting to stabilize the micronization process. This was also done to minimize the initial CO₂ waste during start-up. Once a stable process was established, the polymer melt

temperature and pressure readings were recorded via the Opto22 data acquisition system. The CO₂ pump pressure was recorded directly from the pump display.

For each process variable change, such as polymer feed rate, screw speed, CO₂ feed rate etc., particles samples were collected to analyze the effect of the process parameter on particle size, size distribution and morphology. After the initial change, the system was first allowed to stabilize for 15 minutes. The stabilization was indicated by the pressure readings obtained via the Opto22 data acquisition system. Once a stable process had been established, the particles were collected from the particle collection chamber at two different locations, front of the chamber (6 inches away from the spraying nozzle) and the back of the collection chamber (33 inches away from the front of the spraying nozzle) . Particles were allowed to accumulate on a foil paper for 10 minutes before collection. The collected samples were then examined using SEM and optical microscopy.

3.5 CHARACTERIZATION

3.5.1 Capillary Rheometer

The shear viscosity of the virgin polyethylene wax and the micronized polyethylene wax was measured using a Kayness Galaxy V capillary rheometer. Readings were taken at three different temperatures using two different capillary dies. The capillary diameters were 0.05 and 0.02 inch with an L/D ratio of 2.5 and 0.4, respectively. The capillary with the bigger L/D ratio was used to measure the viscosity at lower temperatures (90°C and 100°C), whereas the capillary with the smaller L/D ratio was used to measure the viscosity at 110°C. This is because at higher temperature, the polymer viscosity is too small to be measured using a die

with a large L/D ratio. Bagley Correction was not used to calculate the viscosity since the L/D values were high (Figure 3.1).

3.5.2 DSC

Differential scanning calorimetry is a thermal analysis technique used for collecting data that quantitatively describes the heat flow and temperatures associated with thermal transitions of a specific material in a controlled atmosphere. For determining the glass transition temperature, melting point (T_m) and heat of melting (ΔH_m) of both virgin and micronized polyethylene wax, DSC measurements were performed on a TA ® Instrument DSC Q2000 V24.4 equipped with a Mass Flow Control and Refrigerated Cooling System (RCS). The measurements were performed at steady heating rate of 5°C/min for a temperature range of 0°C to 150°C. The analysis was performed on each sample to study the effect of micronization and to understand the influence of process variables on thermal transition properties (melting point temperature, glass transition temperature, etc.) of the polymer.

3.5.3 Microscopy

Optical microscopic analysis was carried out to estimate the particle size and generate particle size distributions for both virgin and micronized polymer. The microscope used was manufactured by Southern Instrument Co. and was equipped with a DCM300 digital camera and ScopePhoto imaging software. The particle size measurements were done at three different magnifications, 2X, 5X and 10X for all samples. Three slides were prepared and analyzed for each sample, from which the average particle sizes (arithmetic mean diameter, sauter mean diameter and volume mean diameter) were calculated.

3.5.4 SEM

Particle morphology and particle size was also analyzed using a Zeiss LEO 1530 Gemini Scanning Electron Microscope (SEM). For SEM imaging, the specimen to be studied must be electrically conductive, at least at the surface. As polymers are non-conductive in nature, PE wax samples were first coated with an ultra thin layer of gold, an electrically-conducting material. For coating, thin layers of polymer powders were dispersed on adhesive tapes previously stuck on aluminum stubs. The aluminum stubs were then placed inside a low vacuum sputter coater, where a thin layer of gold (thickness 250 Å) was deposited on to the polymer samples in 12 minutes. Gold coated samples were then analyzed under the microscope at 5kV and at three different magnifications: 100X, 500X and 2000X. Three samples were examined for each experimental run and each sample was measured at 3 different locations under the microscope to verify the powder uniformity.

3.6 PRELIMINARY EXPERIMENTS

In order to determine the optimal operating conditions for the micronization process, the effect of process variables such as nozzle diameter, screw speed, polymer feed rate, CO₂ feed rate, etc. were investigated. The extruder barrel temperature was set to 20/20/20/70/90/90/90/ 90/90/100°C with the die temperature at 140°C, which was heated with a 400W ceramic band heater controlled via a Zesta temperature controller. The barrel segments 8, 9 and 10, and the die pressure were monitored using Dynisco pressure transducers. The extruder pressure and the pressure generation at the ISCO pump were monitored to understand the effects of the above mentioned process variables on pressure and to establish a steady particle spray/micronization process.

3.6.1 Effect of Polymer Feed Rate

The effect of polymer feed rate was investigated at a CO₂ feed rate of 25 ml/min and screw speed of 70 rpm. Polymer feed rate was varied from 10 g/min to 25 g/min keeping all other variables constant. It was observed that the barrel pressure, die pressure and the pump pressure increases with increasing polymer feed rate. This increase in pressure is expected as high polymer feed rate increases the degree of fill. Maintaining high pressure (pressure above the CO₂ solubility pressure) inside the extruder is essential for complete dissolution of CO₂ in the polymer matrix and to prevent CO₂ precipitation [11]. Thus, it is recommended to use a high polymer feed rate for maintaining a high pressure during micronization process.

3.6.2 Effect of Screw Speed

The effect of screw speed on pressure was investigated at a constant polymer feed rate of 25 g/min and CO₂ feed rate of 25 ml/min. The screw speed was varied within the range of 30 to 150 rpm. It was observed that the increase in screw speed decreased the barrel, die and pump pressure. This is because the degree of fill within the barrel decreases at a higher screw speed due to increase in conveying capacity. As a result, it is recommended that a lower screw speed is used for polymer micronization in order to maintain a high pressure. However, decrease in screw speed means decrease in mixing. Hence, a decision was made to use a minimum screw speed of 50 rpm for conducting further experiments.

3.6.3 Effect of CO₂ Feed Rate

The effect of CO₂ feed rate and CO₂ pump pressure on the extrusion process was also studied. The screw speed and polymer feed rate were set at 50 rpm and 25 g/min, respectively. Carbon dioxide feed rate from 5 ml/min to 70 ml/min was tested. It was observed that a steady micronization process cannot be established below a CO₂ feed rate of 25 ml/min for the given polymer feed rate. In addition, an increase in CO₂ feed rate above 25 ml/min increases the extruder barrel pressure and die pressure. Hence, a better polymer spray rate at higher CO₂ feed rate is observed. This behaviour can be explained using the solubility limit of CO₂. As the solubility limit of CO₂ in a given polymer is reached, the additional amount of CO₂ will not dissolve. As a result, a two-phase mixture would be generated and the excess of CO₂ will pressurize the mixture resulting in an increase in system pressure. The excess CO₂ also creates a lubricating effect in the barrel. This phenomenon in turn assists in polymer spraying and particle generation in the extrusion process [9].

3.6.4 Effect of Nozzle Diameter

An investigation on the effect of nozzle diameter on the micronization process was performed at polymer feed rate of 15 g/min, CO₂ feed rate 25 ml/min, and screw speed of 50 rpm. Two different nozzle fluid caps, SU1 and SU4, with diameters 0.508 mm and 1.524 mm, respectively, were chosen for this purpose. It was found that the bigger nozzle was unable to produce PE particles at the given condition, and only foamed PE strands were being produced. To overcome this issue, polymer feed rate and/or CO₂ feed rate was increased gradually to generate higher pressure. However, a stable micronization process could not be established. This phenomenon could be explained using the effect of pressure drop rate inside the nozzle. The pressure drop rate across a nozzle determines the solubility drop rate, which in turn determines the nucleation rate of CO₂ bubbles [11]. A higher pressure drop rate is required for nucleation and particle generation, which could not be achieved in the larger nozzle (SU4). In contrast, the smaller nozzle (SU1) was able to generate particles at the given process conditions. For this reason, only the SU1 fluid cap was used for the micronization of PE in later experiments.

CHAPTER 4: MICRONIZATION OF POLYETHYLENE WAX

4.1 INTRODUCTION

The formation of small polymeric particles with a narrow size distribution is an important process for paint, paper, polish and various other polymer industries [21-23]. Supercritical fluids provide a number of ways of achieving this by rapidly exceeding the saturation point of a solute by dilution, depressurization or a combination of these. In an extrusion process, the polymer-gas solution is expanded through a nozzle from a high to low pressure which causes a sudden reduction of solubility of the gas dissolved in the polymer [9,10]. This results in nucleation of bubbles and a vigorous expansion of these bubbles generates micron size particles. In this work, feasibility of particles production in an extrusion process using supercritical CO₂ has been studied.

One of the advantages of using extrusion for particle production is that the particle morphology, size, and size distribution can be controlled via control of processing variables, nozzle type and size. Use of extrusion for particle production can help eliminate issues associated with conventional powder production methods, such as broad particle size distribution in milling process and heat generation during grinding process. In addition, the plasticizing effect of dissolved CO₂ permits operation at lower temperature which will allow micronization of thermolabile compounds in an extruder [8,9,51]. As many polymer grades are produced in industry via an extrusion process, extrusion micronization will allow elimination of secondary particle generation steps with only some setup and equipment changes to the traditional extrusion process.

For particle production in an extruder, among various supercritical fluids available, supercritical CO₂ has been used in this study for its inexpensive, non-toxic, and chemically inert nature. Dissolved supercritical CO₂ is known to alter physical properties of polymer, causing a decrease in viscosity, decrease in density, and an increase in swollen volume, thus allowing easier polymer processing [14]. In addition, residual CO₂ removal is easily achieved by simple depressurization, as CO₂ exists in a gaseous state at ambient conditions [33,34].

In this study, micron size particles of low molecular weight polyethylene, known as polyethylene wax, were produced using supercritical CO₂. Micronized polyethylene wax is commonly used in paint, toner and personal care products, such as stir-in wax for inks and coatings, and suspending and texturing agents in personal care products. As the melting point (T_m) of polyethylene wax is low (around 95°C), milling and grinding is not an easy task. As a result, industries are always looking for methods and technologies for producing particles without using organic solvents. Use of supercritical CO₂ in the micronization of polyethylene wax can eliminate the need of organic solvents currently used for particle production.

4.2 EXPERIMENTAL DESIGN

4.2.1 Design of Experiments

The experimental study was divided into two parts. In the first part, a factorial design was used to analyze the effect of polymer feed rate and nozzle temperature on particle size, shape and particle size distribution. In the second part, a completely randomized design was used to analyze the effect of CO₂ feed rate and pump pressure on polymer particles and particle size distribution.

Part 1: Factorial design

Based on observations made during preliminary experiments, it was found that for a polymer feed rate of 10 g/min (or higher) and a screw speed of 50 rpm, a minimum of 25ml/min of CO₂ feed rate is required to establish a steady and continuous particle production process. As a result, a constant flow of 25 ml/min CO₂ was used to analyze the effects of nozzle temperature and polymer feed rate on particle production. For this purpose, three different polymer feed rates (13, 25 and 52 g/min) and four different nozzle temperatures (140, 160, 180 and 200 °C) were chosen.

Part 2: Completely Randomized Design

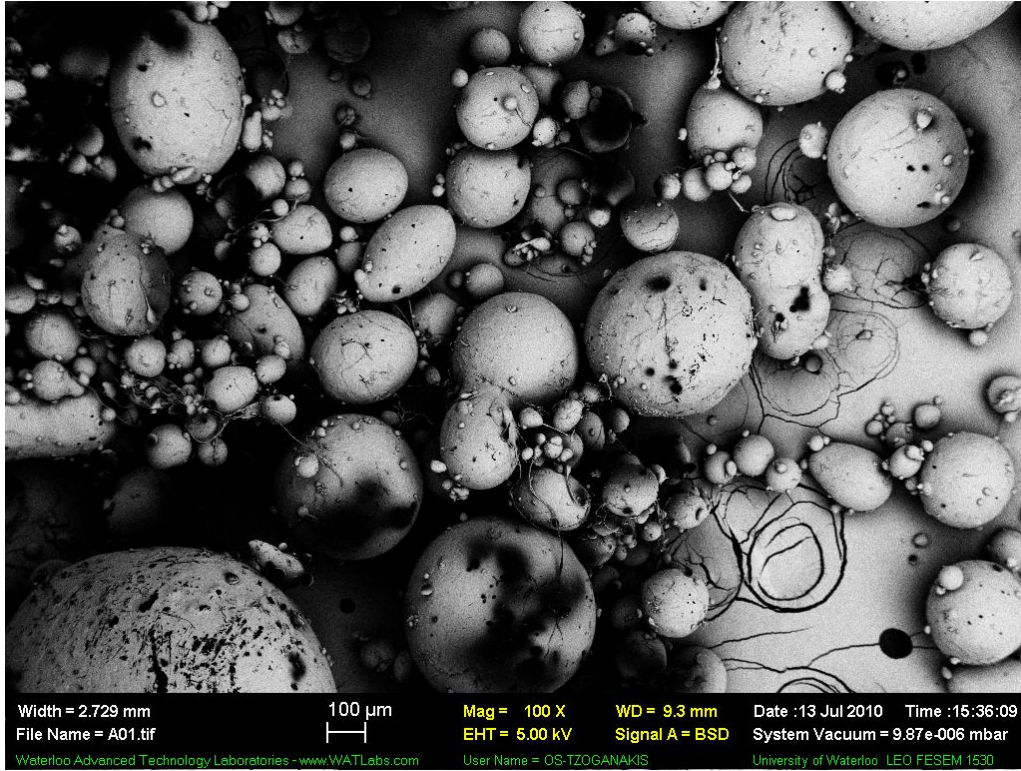
For the polymer feed rate of 52 g/min, CO₂ feed rate of 25 ml/min was not sufficient to establish a steady pressure and hence a steady particle generation process. To overcome this issue, CO₂ feed rate was varied (15 to 55 ml/min) and the effect of increasing CO₂ feed rate on particles' size, morphology and size distribution was studied. During these experiments, the nozzle temperature was kept constant at 140°C and the polymer feed rate was set at 52 g/min.

4.3 RESULTS AD DISCUSSION

Particle analysis using SEM and optical microscopy (images provided in appendix E and F) indicate a successful production of micron size particles using CO₂ in an extrusion process. All the powder samples of polyethylene wax collected were examined and the results are presented in terms of the processing variables used, such as nozzle temperature, polymer feed rate, and CO₂ feed rate.

SEM images indicate that the most spherically shaped particles were produced at CO₂ feed rate of 25 ml/min, screw speed of 50 rpm, and nozzle temperature of 200°C for both polymer feed rates of 13 g/min and 26 g/min, respectively, as illustrated in Figure 4.1. This phenomenon indicates that an optimal operating condition exists which can ensure generation of more spherically shaped polymer particles with reduced agglomeration, and least amount of fibres. In addition, a narrow particle size distribution can also be obtained via control of process variables, details of which are discussed in section 4.3.2.

(a)



(b)

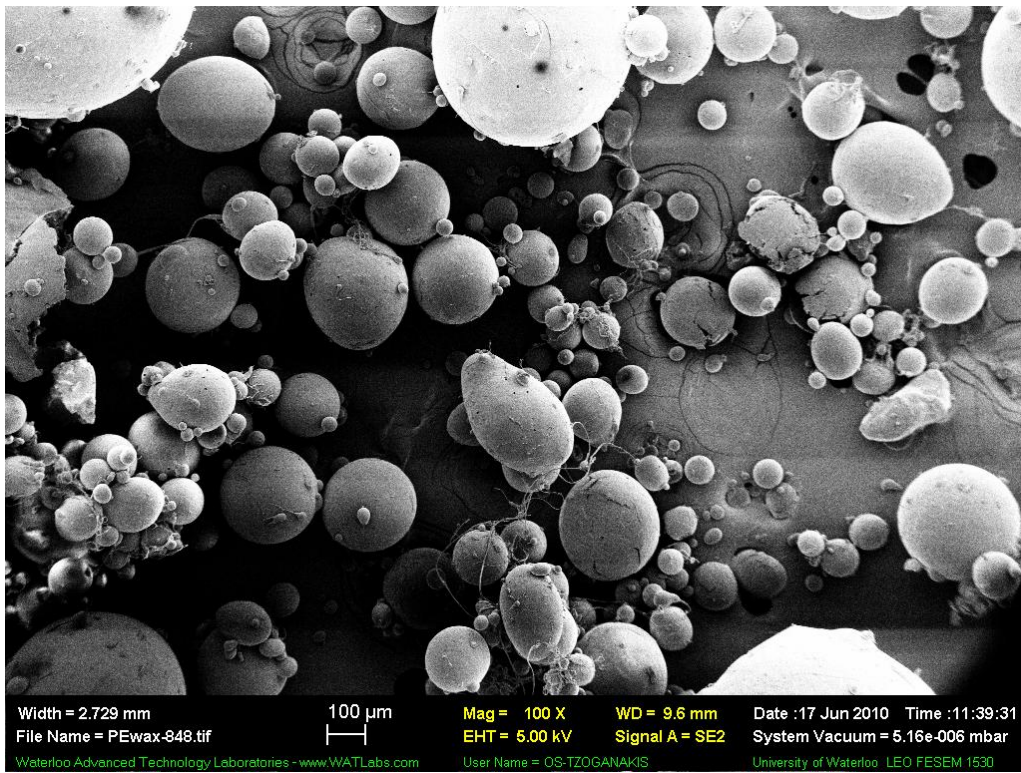


Figure 4.1: SEM Images of Particles Produced at CO₂ Feed Rate of 25 ml/min, Screw Speed of 50 rpm, and Nozzle Temperature at 200°C:

(a) Polymer feed rate = 13 g/min, and (b) Polymer feed rate= 26 g/min

4.3.1 Particle Size

Particle size measurements were performed using an optical microscope equipped with a DCM300 digital camera and scope photo imaging software (measured particle sizes presented in appendix B). The results obtained indicate that the polyethylene wax particles produced had sizes in the range of 0.01 to 190 μm . Contrary to the optical microscopy results obtained, the SEM images indicate that particle sizes larger than 190 μm were also present for several samples analyzed (for example see figure 4.1). This error in analysis could either be the result of powder sampling or due to the limitations associated with optical microscopic measurements. It is indicated in the literature that an optical microscopic method should be used to measure particles from about 0.8 μm to 150 μm in size [96]. Above the 150 μm limit, sieve and microscope analysis should be merged. One of the major limitations of an optical microscope is its small depth of focus; for a wide range of particle sizes only a limited number of particles are in focus in any field of view. Further, the edges of particles are blurred due to diffraction effects [96]. Additionally, during measurements it was sometimes observed that the measurements were not always inclusive of misshapen particles or particles that were agglomerated (refer to Figures presented in appendix E). Consequently, the results and discussion on particle size in this section is drawn from both SEM and microscopic image analysis.

The particle size measurements performed via an optical microscope indicate the arithmetic mean particle size of polyethylene wax produced was in the range of 5.5 to 9.73 μm . The Sauter mean and volume moment mean diameter was in the range of 10.97 to 26.56 μm and 13.21 to 35 μm , respectively (formulas used for mean particle size calculation are shown

in appendix A). These mean particle sizes were found to be a function of process variables, the effects of which are discussed in the following sections.

4.3.1.1 Effect of Nozzle Temperature

Polymer viscosity is a function of temperature and an increase in temperature reduces the shear and extensional viscosity of polymers. Thus, it is easier to break up the polymer melt into particles at higher processing temperatures. As a result, variation in temperature is supposed to have a significant effect on micronization process. The effect of temperature on particle size has been studied and reported by many authors. However, the reported results indicate a contradictory influence of temperature on particle size. For an increase in temperature some authors found a particle size increase [11,87], some observed no effect [90] while others reported a decrease in particle size [86,88].

In this report, the effect of increased nozzle temperature on particle size was examined. At a constant screw speed of 50 rpm and CO₂ feed rate of 25 ml/min, the mean particle sizes at different temperatures and polymer feed rates are displayed in Table 4.1. Note that the data for the particles produced at polymer feed rate of 52 g/min are not presented in the Table. This is due to the fact that at 52 g/min polymer feed rate, the production process was not stable. In addition, the small amount of particles produced was found to be agglomerated and the particle size estimation using optical microscope was not reliable.

The particle size analysis indicates a considerable effect of nozzle temperature on particle size of polyethylene wax. The experimental results demonstrate that an increase in nozzle temperature from 140 to 200°C causes an increase in mean particle diameter. This phenomenon can be explained by the effect of temperature on CO₂ solubility in the polymer.

From the solubility studies of Areerat et al. it was found that CO₂ solubility increases with increase in pressure and decreases with increase in temperature for all polymer/CO₂ systems [64]. This decrease in solubility decreases the rate of nucleation at higher temperature and increases particle size during expansion. A similar trend was observed for Sauter Mean and Volume Mean Diameter, with the exception of particles produced at 140°C nozzle temperature.

Table 4.1: Mean Particle Diameter at Different Polymer Feed Rates and Nozzle Temperatures (CO₂ feed rate =25 ml/min, screw speed= 50 rpm)

Polymer Feed Rate (g/min)	Nozzle Temperature (°C)	Mean Diameter (µm)	Sauter Mean Diameter (µm)	Volume Mean Diameter (µm)
13	140	5.4	17.5	29.0
	160	5.9	11.0	13.7
	180	6.3	11.6	13.2
	200	6.7	26.6	35.5
26	140	5.5	18.9	26.2
	160	5.6	12.3	16.6
	180	9.6	16.7	19.1
	200	9.7	19.3	24.5

At 140°C nozzle temperature, the Sauter Mean and Volume Mean Diameters seem to be high in the case of both polymer feed rates (Table 4.1). However, it should be noted that the particle size obtained for 140°C is unreliable. From careful analysis of the microscopic images it was found that particles were significantly agglomerated at 140°C. As discussed above, due to the limitations associated with optical microscopic analysis, the particle size calculated for a

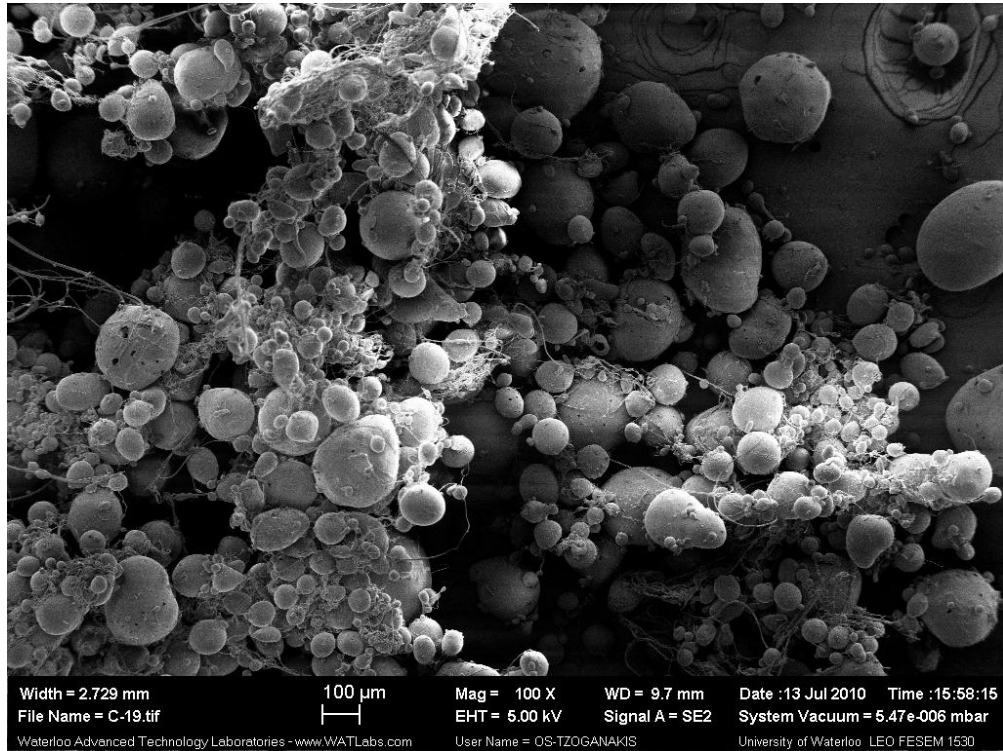
140°C nozzle temperature setting is associated with error and should not be used to draw any conclusions.

From the data presented in Table 4.1, it is observed that unlike Mean Diameter, there is a significant increase in Sauter Mean and Volume Mean Diameter for a nozzle temperature increase from 180 to 200°C, in the case of both polymer feed rates. It is to be noted that in electron microscopic measurement, the diameter of particles are measured with a graticule, then summed and divided by the number of particles measured to obtain the Mean Particle Diameter. When this diameter is converted to the Sauter Mean Diameter or Volume Mean Diameter, the error associated with the measurements gets amplified due to the nature of conversion (see formulas in appendix A). As a result, the effect of increasing nozzle temperature (from 180 to 200°C) on particle size seems more prominent for Sauter Mean and Volume Mean Diameter than Mean Diameter. In addition, the National Bureau of Standards (NBS) recommends that a minimum of 10,000 images must be examined for statistical validity [98]. Yet, due to manual laborious technique used for optical microscopic measurement, it is difficult to examine large number of images, which poses a real danger of unrepresentative sampling. As a result, the data obtained and used in this thesis for particle size analysis should not be used beyond the level of simple judgement.

4.3.1.2 Effect of Polymer Feed Rate

The influence of polymer feed rate was the second variable studied. From the results obtained (Table 4.1), it can be concluded that there is a significant effect of polymer feed rate on particle size. Similar conclusions can be drawn from examining the SEM images (Figure 4.2) of particles produced at different polymer feed rates. This observation can be credited to the effect of pressure and GTP on particle size. As polymer feed rate increases, the barrel and die pressure increases and the GTP decreases. The decrease in GTP causes an increase in particle size. This particle size dependency on GTP was suggested by Nalawade et al. [93,95] in several of his publications. In addition, it was found that at lower GTP ratio, the influence of nozzle temperature on particle size is more pronounced than at higher GTP (Table 4.1). Polymer feed rate also has a significant effect on particle size distribution and particle morphology, which is discussed in sections 4.3.2 and 4.3.3, respectively.

(a)



(b)

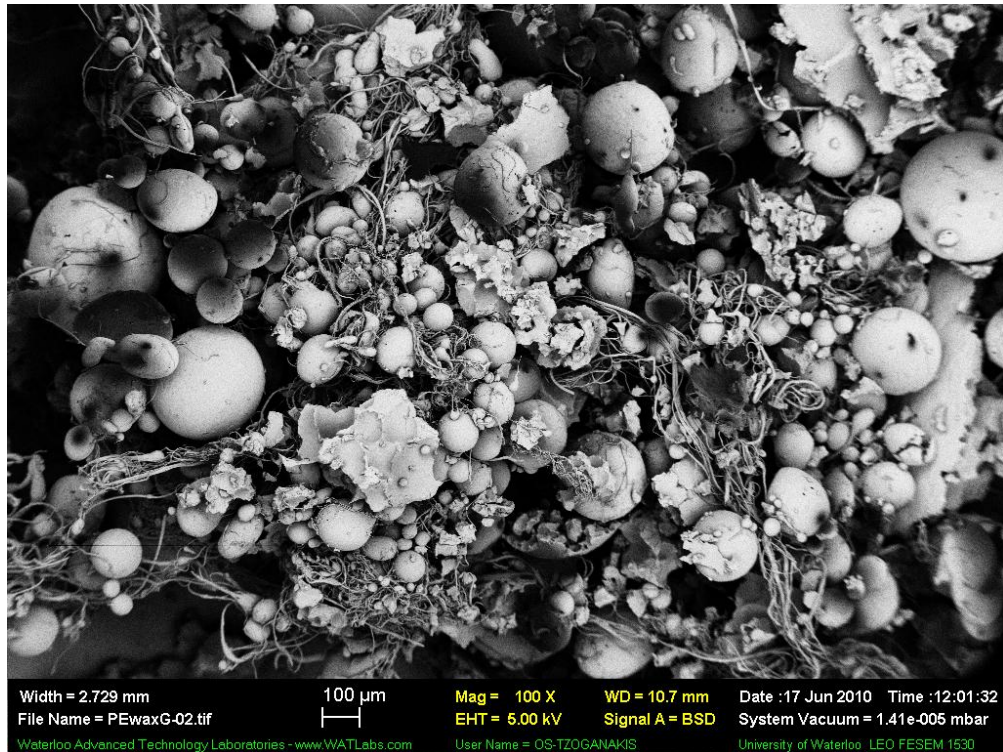


Figure 4.2: SEM Images of Particles Produced at Different Polymer Feed Rate (CO₂ feed rate = 25 ml/min, screw speed = 50 rpm, nozzle temperature = 160°C): (a) 13 g/min and (b) 26 g/min

4.3.1.3 Effect of CO₂ Feed Rate

The increase in CO₂ feed rate represents an increase in GTP ratio. The increase in GTP ratio causes a transition from one flow regime to another when the polymer melt is allowed to pass through the small diameter nozzle. At lower GTP ratio, polymer foaming is observed while particles are produced as the ratio increases. This is because at high GTP ratio, the expansion of excess CO₂ causes an intense instability at the surface of the polymer melt which enhances breakup of polymer melt and particle production [10].

Experiments with different CO₂ feed rates were performed to investigate the effect of CO₂ on particle size. For similar operating conditions, it was found that the mean particle size increases with an increase in CO₂ feed rate (Table 4.2), with the exception of CO₂ feed rate of 55 ml/min. SEM images indicate that particles were agglomerated at CO₂ feed rate of 55 ml/min, and as such the particle size calculated for this point is unreliable (due to limitations associated with optical microscope).

Table 4.2: Mean Particle Diameter at Different CO₂ Feed Rates for a Constant Polymer Feed Rate of 52 g/min (Screw Speed = 55 rpm and Nozzle Temperature = 140°C).

CO ₂ Feed Rate (ml/min)	Mean Diameter (µm)	Sauter Mean Diameter (µm)	Volume Mean diameter (µm)
15	8.1	17.9	21.0
25	8.5	19.5	34.8
35	10.3	31.8	45.1
45	20.5	77.5	97.7
55	9.7	20.2	24.9

Note: particle spray was not constant at CO₂ feed rate of 15 ml/min.

4.3.1.4 Statistical Analysis of Particle Size

In order to analyze the effect of each process variable on mean particle sizes, estimated (Table 4.1) from the optical microscopic measurements, the size data was modeled using factorial design. Factors studied for this analysis were polymer feed rate and nozzle temperature. In order to reduce the number of experiments, it was decided to omit the effect of CO₂ (feed rate =25 ml/min) on particle size from this part of the study. From inspection of the results presented in Table 4.1, it can be concluded that the mean particle size of the micronized polyethylene wax increased with increasing polymer feed rate and nozzle temperature. For statistical analysis, an Analysis of Variance (ANOVA) of the data was conducted (Table 4.3).

Table 4.3: ANOVA Table

Source	SS	df	MS	F_{observed}
Polymer Feed Rate	4.59	1	4.59	2.48
Nozzle Temperature	12.46	3	4.15	2.24
Error	5.55	3	1.85	
Total	22.61	7		

Note: SS=sum of squares, df= degrees of freedom, MS= mean squared value

From the data presented in the ANOVA Table, it can be concluded that there is a significant effect of nozzle temperature on particle size at a 75% confidence level (F-value = 2.02). However, there is no significant effect of nozzle temperature for a confidence level of 90% or higher (F-value = 5.54). Similarly, no significant effect of polymer feed rate was observed at 90% confidence level. However, there is a notable effect of polymer feed rate at 75% confidence level.

4.3.2 Particle Size Distribution

Based on the particle size data obtained by means of the optical microscope, particle size distributions were plotted for particles produced at different processing conditions (data used for this purpose is presented in appendix C). Approximately 150 particles divided in 26 size classes linearly spaced between 0.05 to 25 μm were used to produce these particle size distributions. To generate the plots, the particle sizes were plotted against the percentage frequency of occurrence of particles in a given size class. These distribution plots are provided in Figures 4.3 to 4.6. As seen in these figures, most particles were found to be sized in the ranged of 0.1 to 25 μm . However, occasionally particles in the size range of 25 to 150 μm were observed; particles which were not included in these plots as they did not contribute to and lay far from the distribution curve.

By visual inspection of the plots, it can be concluded that processing variables have a considerable effect on particle size distributions. In order to study the effect of these variables and compare the different distributions, the frequency distribution curves were normalized, so that the area under the curve is 100%. It is to be noted that only about 150 particles were used to generate the particle size distribution plots. For more accurate and reliable particle size distribution plots, a larger sample of particles (1000 particles) should be considered. As SEM results indicate the presence of larger particles than the ones measured using the optical microscopic, sieve measurements should be combined with microscopic data to obtain a better estimation of particle size, and hence size distribution. In addition, examining samples from different locations in the sample bag (particles from top of the bag vs. particles at the bottom of the bag) would also reduce any errors associated with PSDs. For the purposes of this thesis, it

was not possible to perform other measurements due to the lack of suitable measurement techniques and equipment available in the facility.

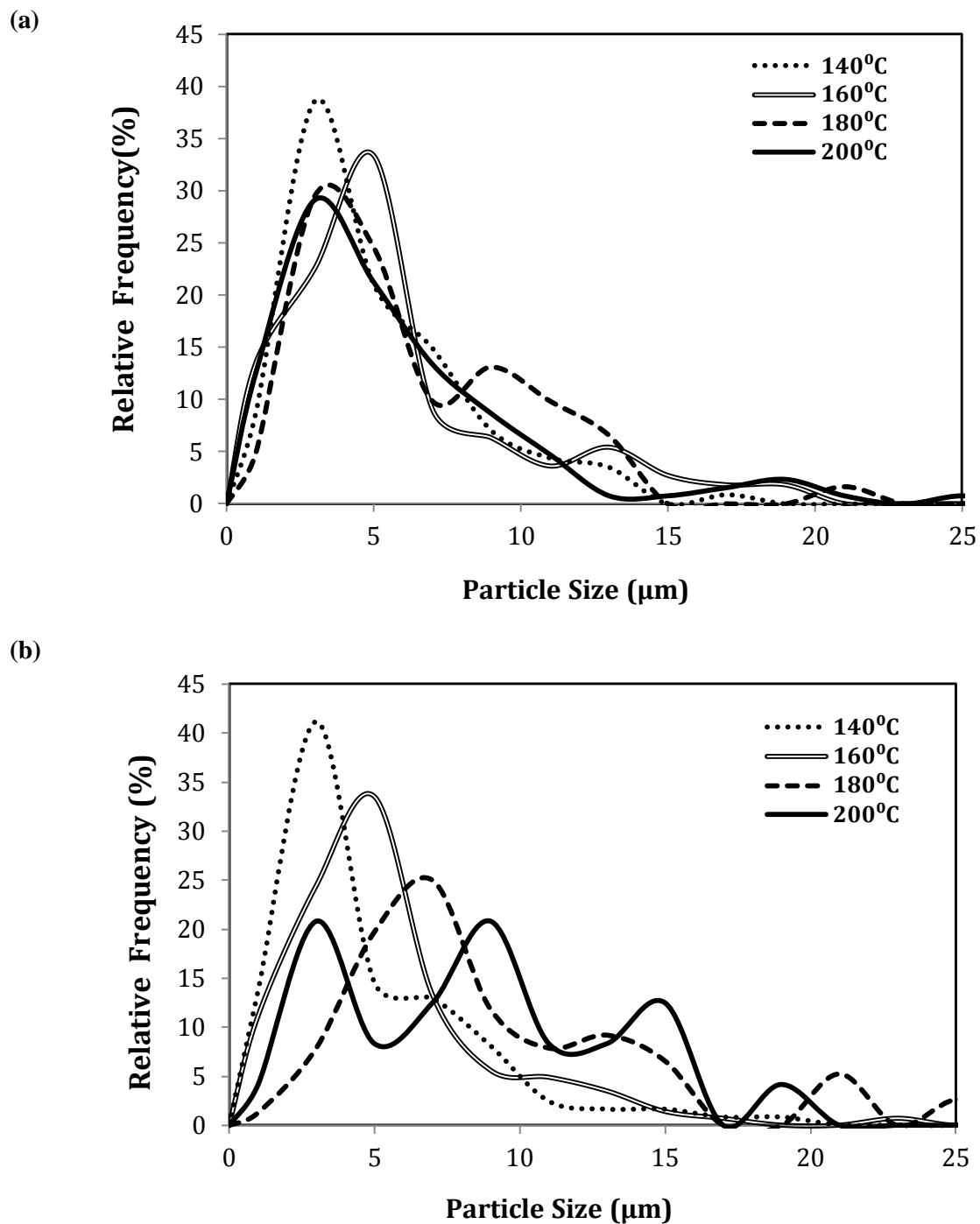


Figure 4.3: Normalized Particle Size Distributions at Different Polymer Feed Rates (CO₂ Feed Rate = 25 ml/min, Screw Speed = 50 rpm): (a) 13 g/min and (b) 26 g/min

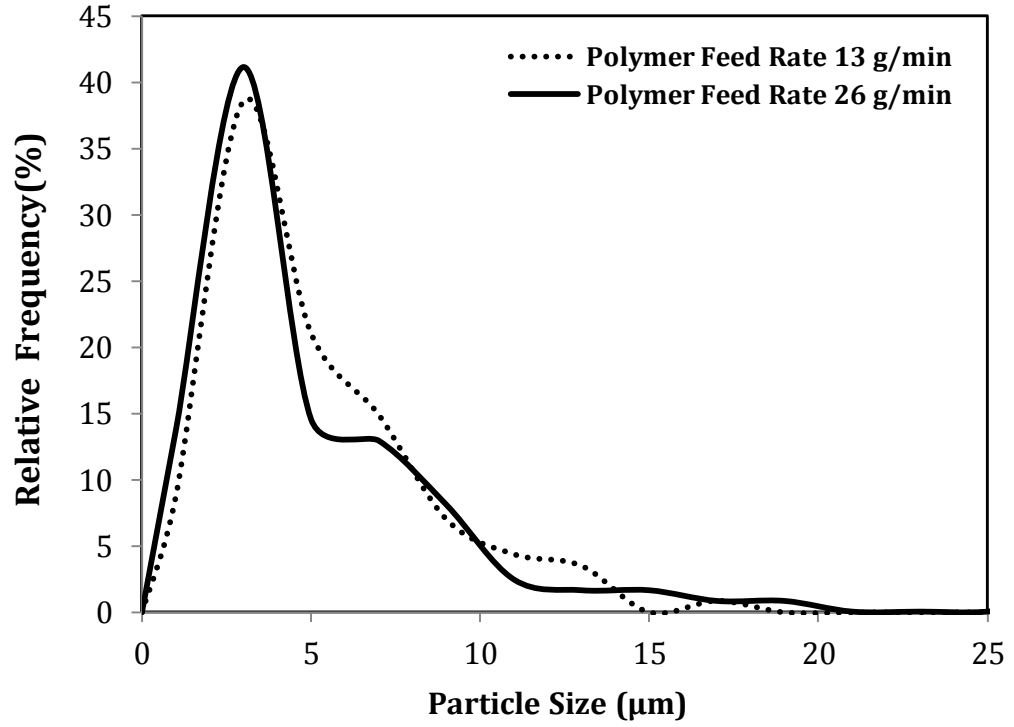
4.3.2.1 Effect of Nozzle Temperature

A considerable effect of nozzle temperature on particle size distribution was observed for polyethylene wax. It was found that particle size distribution broadens as the nozzle temperature increases. However, this phenomenon was only observed at higher polymer feed rate (26g/min). In other words, no significant effect of nozzle temperature on particle size distribution was observed for a polymer feed rate of 13 g/min (Figure 4.3 (a)). This behaviour could be attributed to the fact that at lower polymer feed rate (high GTP ratio) the residence time of polymer melt in the nozzle is relatively short to cause any significant effect on particle size. An illustration of the effect of nozzle temperature on particle size is provided in Figure 4.3 (b). In addition to the shape of PSDs, the position and the number of modal peaks on the particle size distributions were also affected by the nozzle temperature at higher polymer feed rate. For example, the distribution curve at 140°C was unimodal, at 160°C was bi-modal, at 180°C was tri-modal and at 200°C was quad-modal.

4.3.2.2 Effect of Polymer Feed Rate

The effect of polymer feed rate on particle size distribution is shown in Figures 4.4 and 4.5. From the PSD curves in Figure 4.4, it can be seen that the effect of polymer feed rate at lower temperatures (140 and 160°C) is insignificant. In other words, at lower temperatures the distributions for both high and low polymer feed rate look identical. However, at higher temperatures (180 and 200°C), the distributions differ in both breadth and shape/modality (Figure 4.5). A broader distribution was observed for a higher polymer feed rate.

(a)



(b)

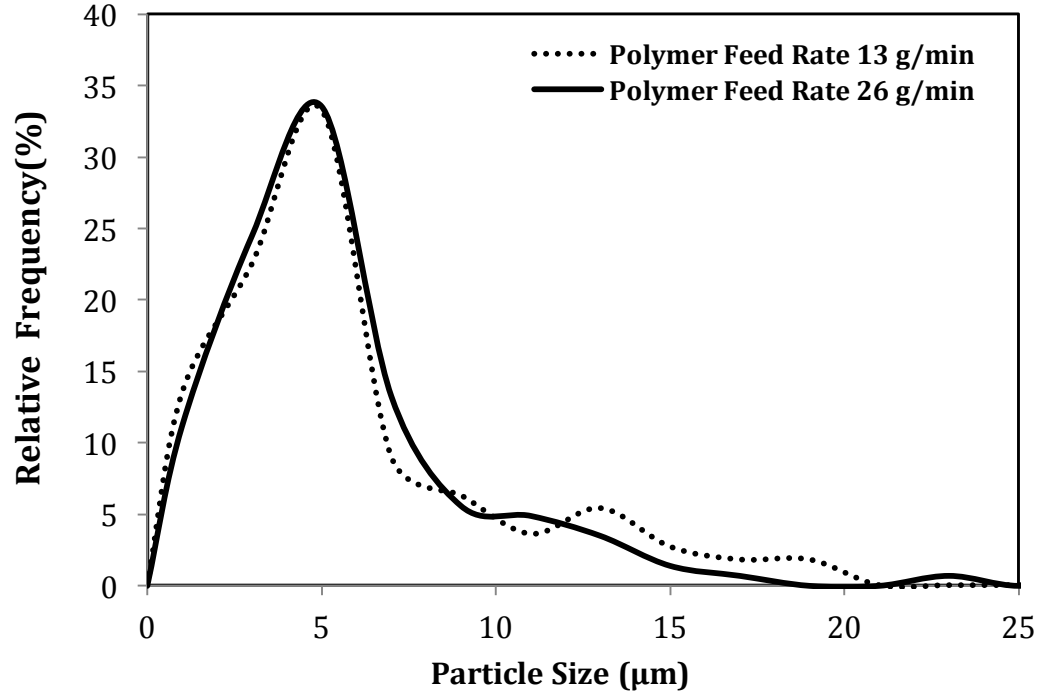


Figure 4.4: Normalized Particle Size Distribution at Lower Nozzle Temperatures (CO₂ Feed Rate = 25 ml/min, Screw Speed = 50 rpm):
(a) 140 °C and (b) 160 °C

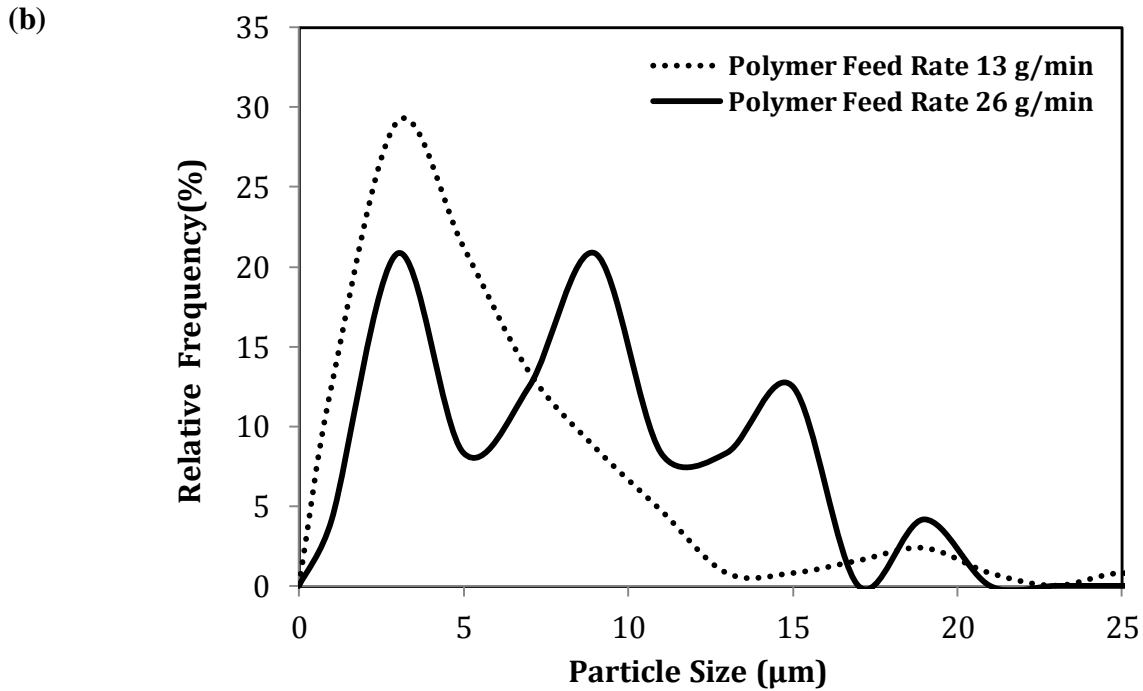
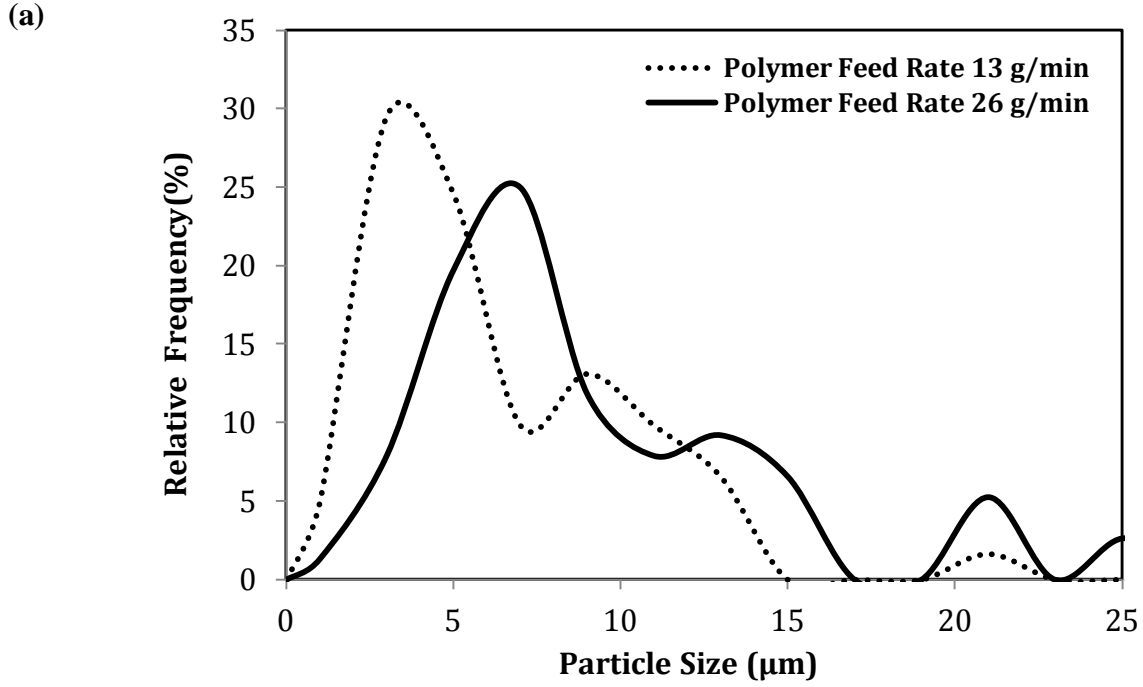


Figure 4.5: Normalized Particle Size Distribution at Higher Nozzle Temperatures (CO₂ Feed Rate = 25 ml/min, Screw Speed = 50 rpm): (a) 180°C and (b) 200°C

4.3.2.3 Effect of CO₂ Feed Rate

For a polymer feed rate of 52 g/min, an initial CO₂ feed rate of 15 and 25 ml/min was not sufficient for establishing a steady spray of particles. To overcome this issue, the CO₂ feed rate was increased and the effect of increase in CO₂ feed rate on particle size distribution was studied. The particle size distribution plots presented in Figure 4.6 demonstrate that an increase in CO₂ feed rate produces narrower particle size distributions; the most narrow distribution was obtained for the CO₂ feed rate of 55 ml/min. This phenomenon further proves that processing variables, such as CO₂ feed rate, have a significant effect on particle size and size distribution, which can be manipulated to obtain particles with tailored size and size distribution in extrusion micronization using supercritical CO₂.

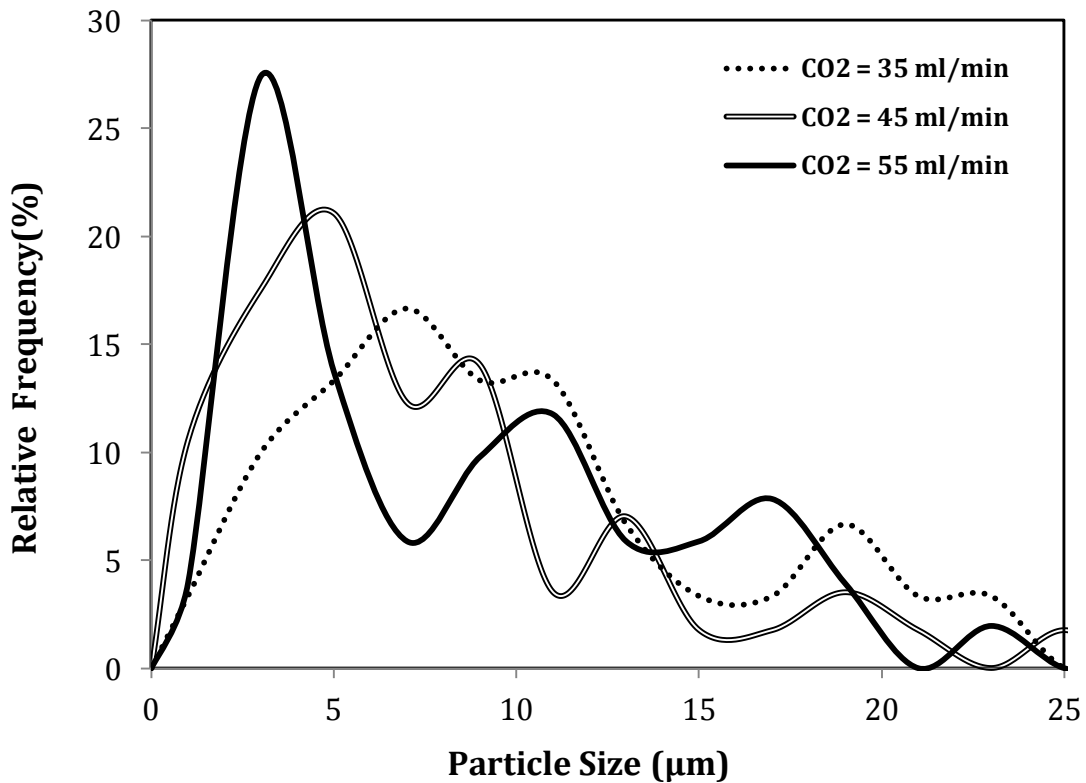


Figure 4.6: Normalized Particle Size Distribution at Different CO₂ Feed Rate (Polymer Feed Rate = 52 g/min, Screw Speed = 50 rpm, Nozzle Temperature = 140°C)

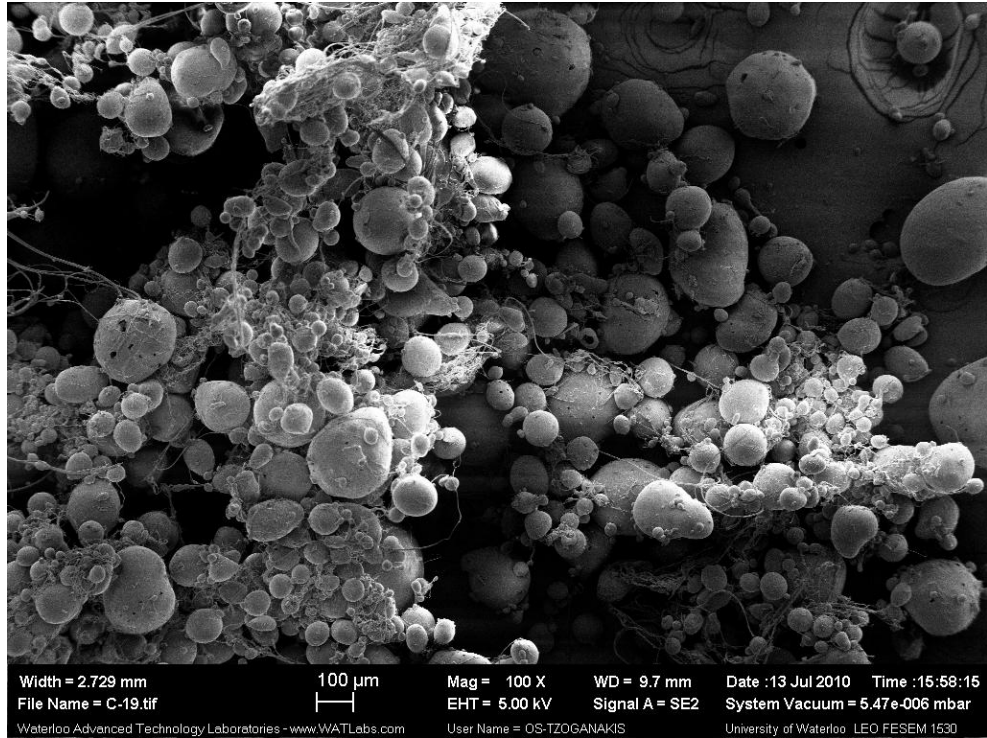
4.3.3 Morphology

In addition to particle size and particle size distribution, particle morphology was also found to be a function of polymer feed rate, nozzle temperature and CO₂ feed rate. The effects of these variables are discussed in detail below.

4.3.3.1 Effect of Nozzle Temperature

In an extrusion micronization process, the time available for particles to solidify defines the shape of particles produced. Both pressure and temperature play a vital role in determining this solidification time. As the nozzle temperature increases, the temperature of the polymer melt increases, which in turn causes a delay in solidification as more heat needs to be dissipated for particles to solidify. This delayed solidification facilitates retraction of molten polymer into a spherical shape by both visco-elastic relaxation and surface tension. Moreover, the amount of dissolved CO₂, a function of temperature and pressure, also contributes to solidification in the form of heat of evaporation. At higher temperature and lower pressure, the amount of dissolved CO₂ is reduced. Consequently, less energy is utilized for evaporation of CO₂, which increases the solidification time [11]. As a result, more spherically shaped particles of polymers were produced at higher nozzle temperature, an illustration of which is provided in Figure 4.7 and 4.8. Furthermore, at higher flow rates, careful analysis of the SEM images indicates a decrease in the amount of fibres produced at a higher temperature. Agglomeration also tends to decrease with an increase in nozzle temperature. This could be attributed to the fact that at higher temperature, shear and external viscosity of polymer melt decreases. As a result, it is easier to break up polymer melt into particles at higher nozzle temperature.

(a)



(b)

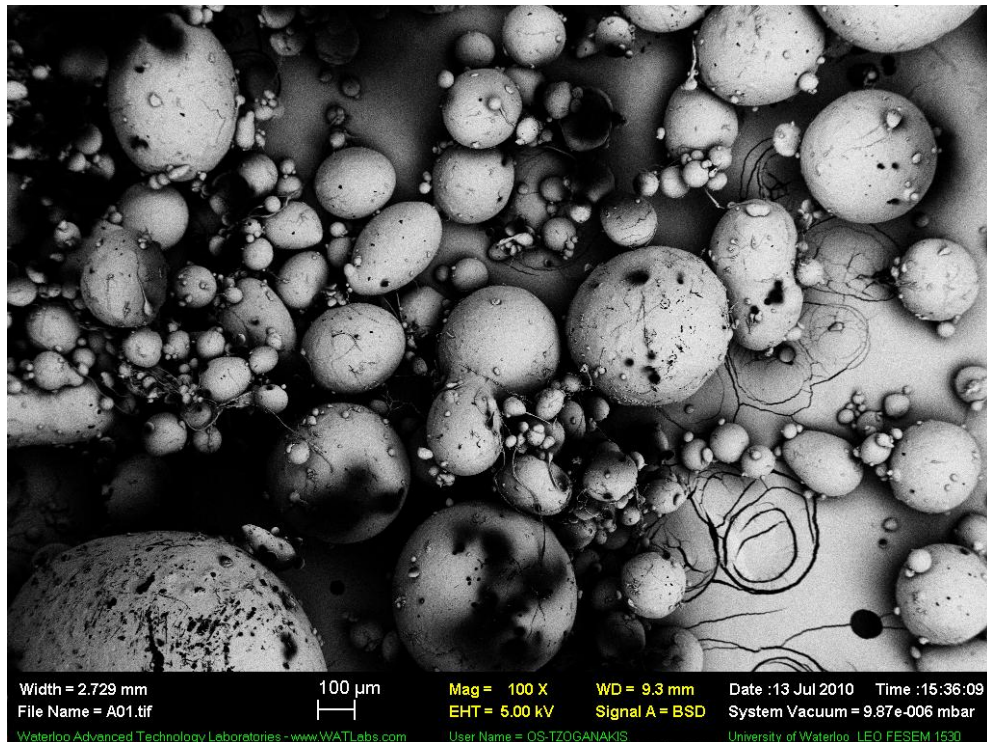
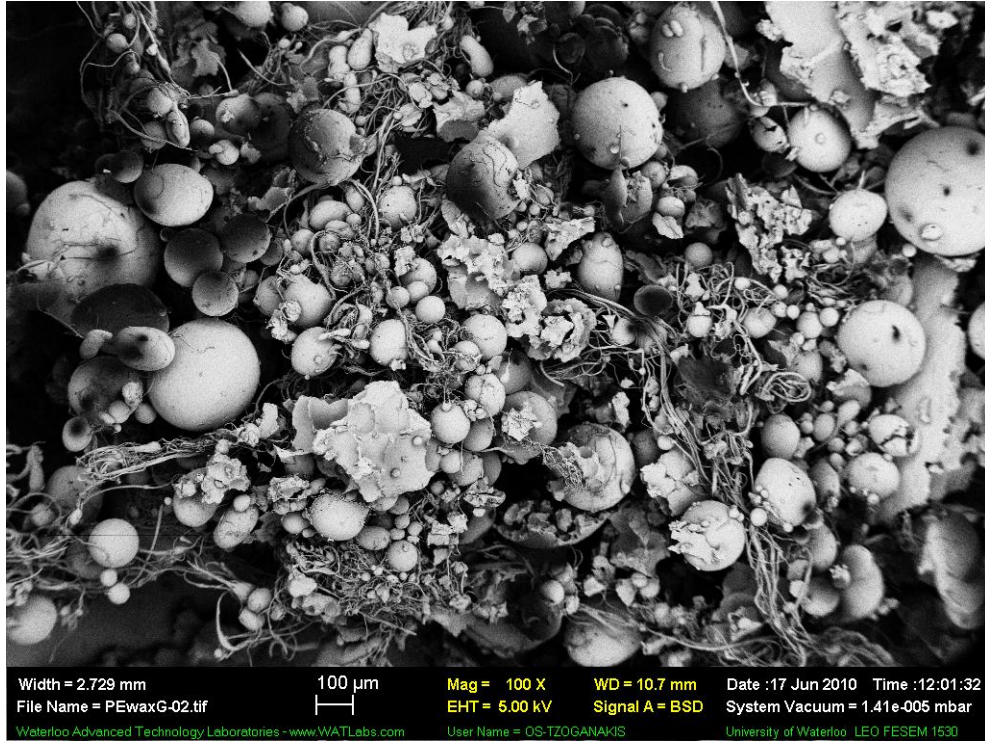


Figure 4.7: SEM Images of Particles Produced at Different Nozzle Temperatures at a Polymer Feed Rate of 13 g/min (CO₂ Feed Rate = 25 ml/min, Screw Speed = 50 rpm): (a) 160°C and (b) 200°C

(a)



(b)

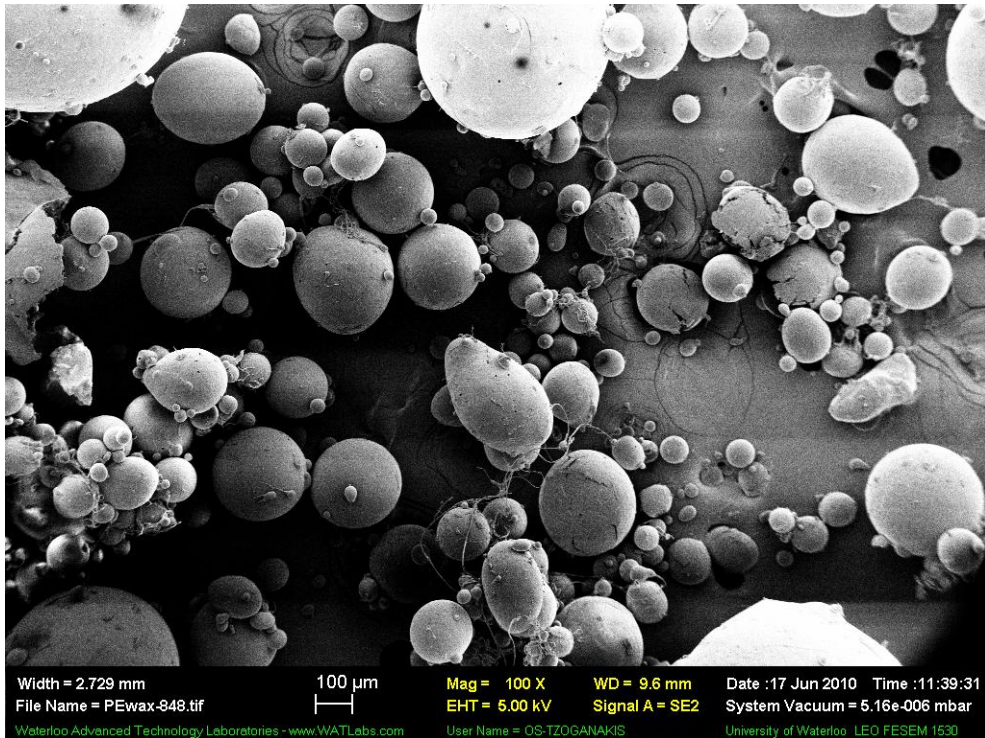
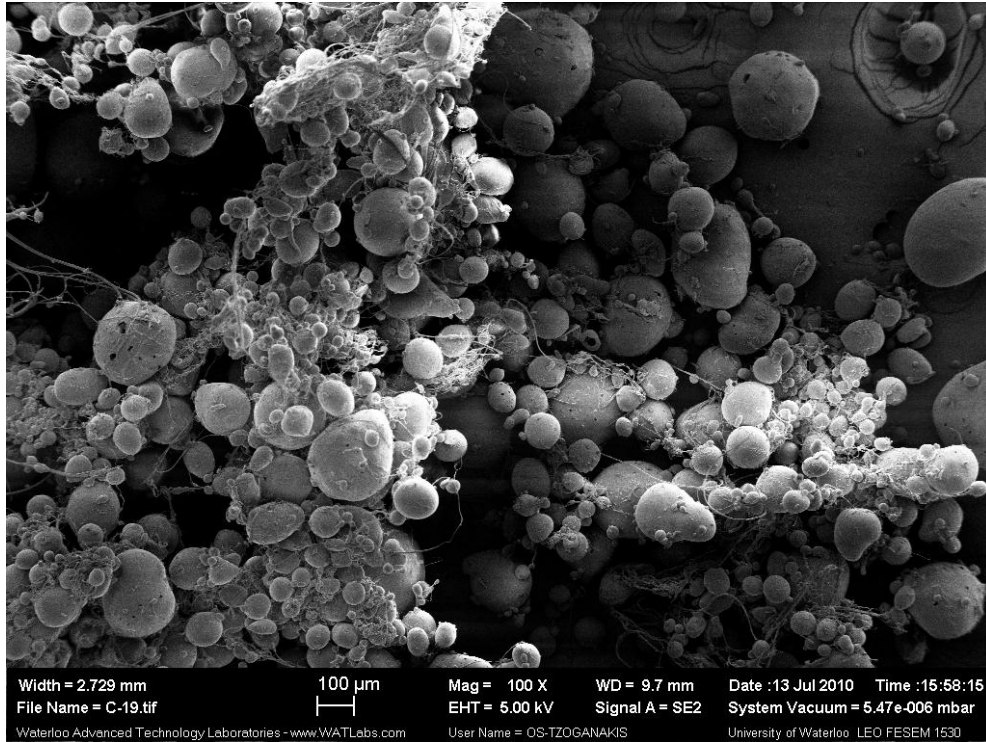


Figure 4.8: SEM Images of Particles Produced at Different Nozzle Temperatures at a Polymer Feed Rate of 26 g/min (CO₂ Feed Rate = 25 ml/min, Screw Speed = 50 rpm): (a) 160°C and (b) 200°C

4.3.3.2 Effect of Polymer Feed Rate

From inspection of SEM images of particles produced at similar operating conditions and different polymer feed rates, it can be concluded that particle agglomeration increased with increase in polymer feed rate, as illustrated in Figures 4.9 and 4.10. In addition, more fibrous product was formed at higher feed rate. This behaviour is probably due to reduced nucleation because of the reduction in GTP ratio. A change in particle shape with the increase in polymer feed rate was also observed in the SEM images. For an increase in polymer feed rate from 13 to 26 g/min , particles were found to contain holes and were more deformed (Figure 4.9). This observation can be attributed to the fact that an increase in polymer feed rate causes an increase in pressure. This increase in overall pressure causes a larger thermodynamic instability due to the rapid depressurization of the polymer melt, and the quick escape of the CO₂ gas results in the formation of particles with holes. The holes in the particles further assist in the breakup of the wax polymer particles producing irregular shaped particles.

(a)



(b)

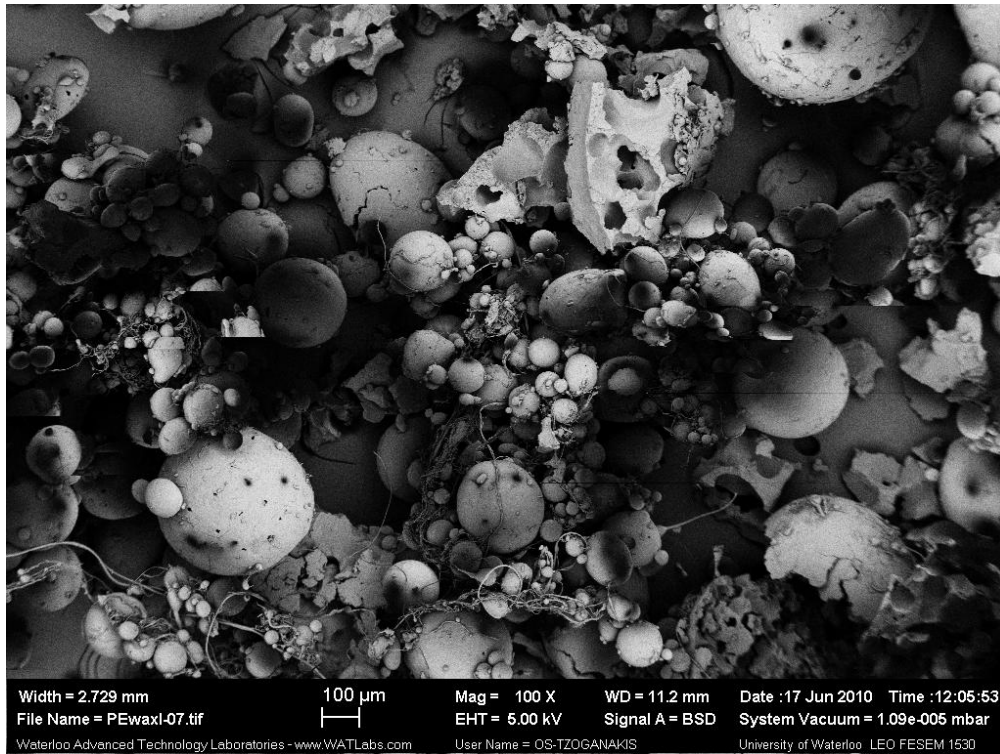
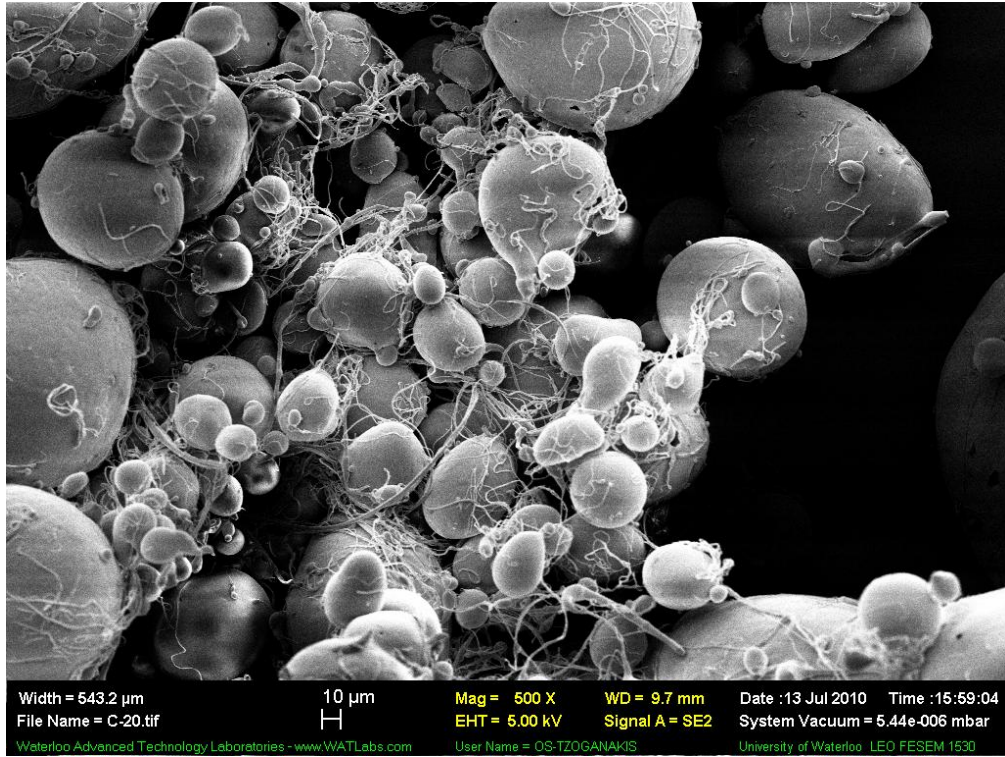


**Figure 4.9: SEM Images of Particles Produced at Different Polymer Feed Rates at Nozzle Temperatures 160°C (CO₂ Feed Rate = 25 ml/min, Screw Speed = 50 rpm):
(a) 13 g/min and (b) 26 g/min**

(a)



(b)



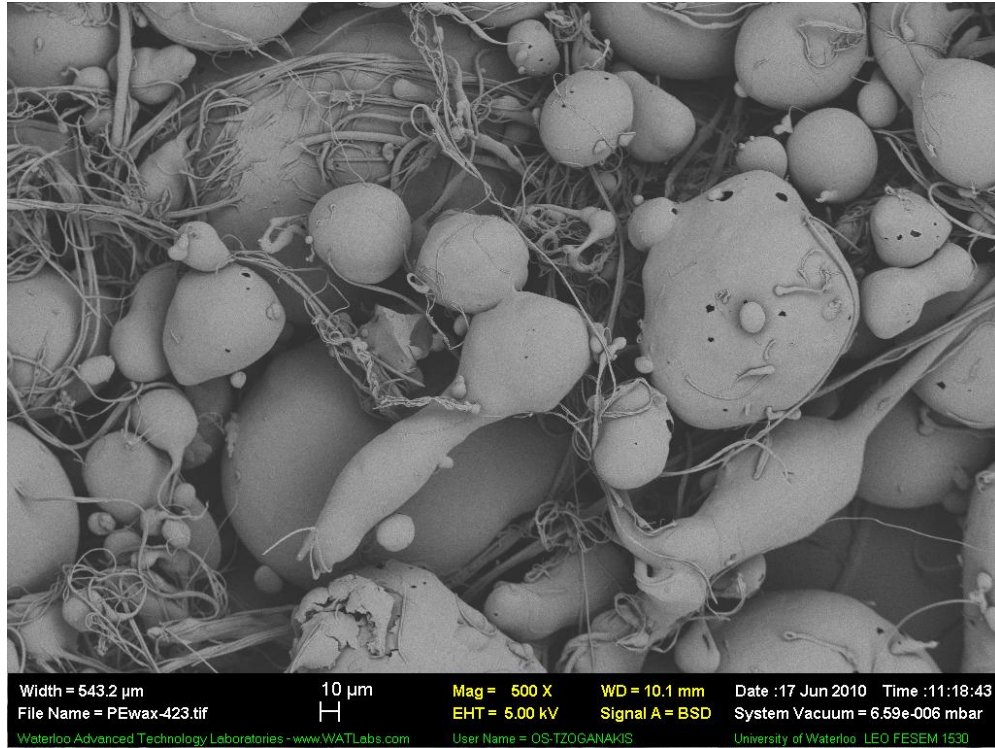
Figure 4.10: SEM Images of Particles Produced at Different Polymer Feed Rates at Nozzle Temperatures 180°C (CO₂ Feed Rate = 25 ml/min, Screw Speed = 50 rpm): (a) 13 g/min and (b) 26 g/min

4.3.3.3. Effect of CO₂ Feed Rate

Experiments at different CO₂ feed rates were performed to investigate the effect of CO₂ on particle morphology. From the SEM images obtained it can be concluded that particle agglomeration increased with increase in CO₂ feed rate (Figure 4.12). In addition, more fibres are produced at higher CO₂ feed rate, an illustration of which is provided in Figures 4.11 and 4.12. At high CO₂ feed rate, the GTP ratio increases causing rapid depressurization of the polymer melt through the nozzle. The high pressure release of the polymer melt causes the hot particles to collide and form clusters resulting in an increase in agglomeration.

As shown in Figures 4.11 and 4.12, particles produced with higher CO₂ feed rate were also found to be more deformed compared to the particles produced with lower CO₂ feed rate. Additionally, increase in CO₂ feed rate results in an increase in holes in the particles. This phenomenon could be the result of an increase in pressure at high CO₂ feed rate. When the polymer-CO₂ solution is allowed to pass through a narrow die space and out through a micron-size nozzle hole, the high pressure difference between the upstream and the downstream of the spraying nozzle causes thermodynamic instability due to reduction of gas solubility in the solution resulting in supersaturation. This supersaturation causes nucleation of bubbles. At higher CO₂ feed rate, the nucleation of bubbles increases (since the pressure increases) resulting in the production of particles with holes once the gas escapes from the polymer melt. These holes further assist in breaking of the easily breakable waxy polymer particles resulting in the formation of deformed particles, as shown in Figures 4.11 (b) and 4.12 (b).

(a)

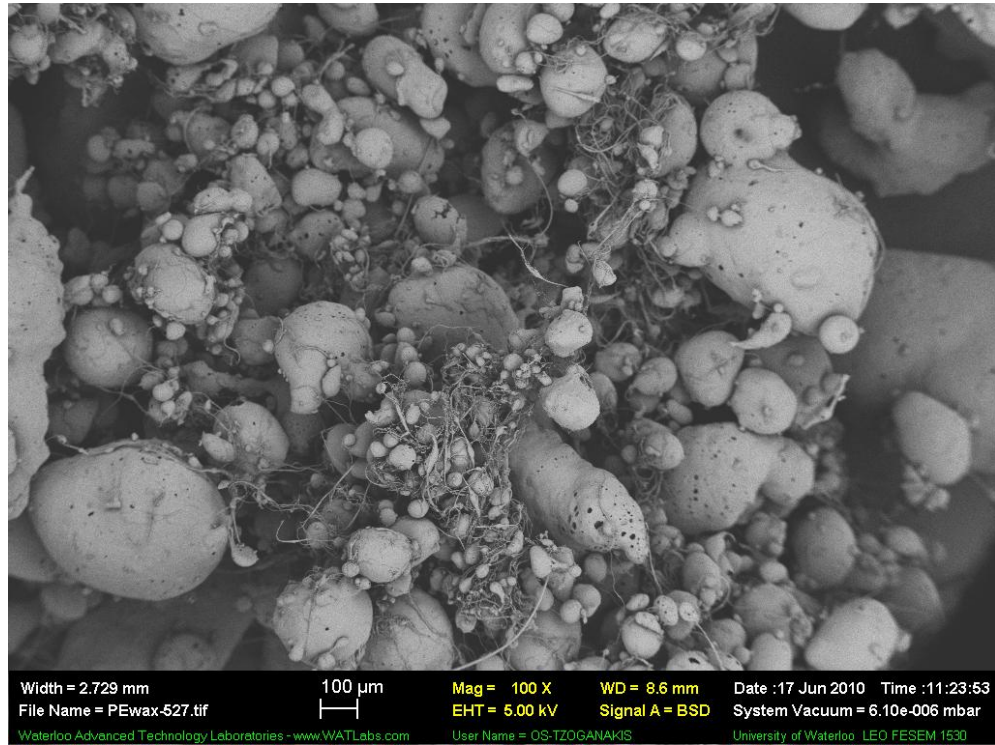


(b)



Figure 4.11: SEM Images of Particles Produced at Different CO₂ Feed Rate at 500X Magnification (Polymer Feed Rate= 55 g/min, Screw Speed = 50 rpm, Nozzle Temperature = 140°C): (a) 45 ml/min and (b) 55 ml/min

(a)



(b)

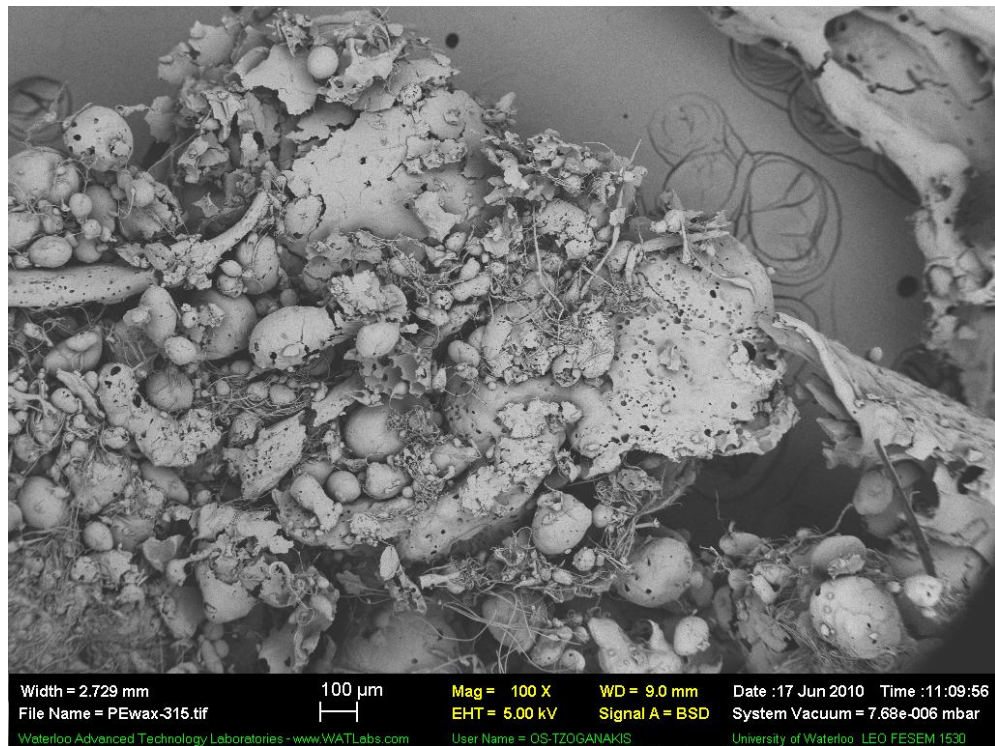


Figure 4.12: SEM Images of Particles Produced at Different CO₂ Feed Rate at 100X Magnification (Polymer Feed Rate= 55 g/min, Screw Speed = 50 rpm, Nozzle Temperature = 140°C): (a) 35 ml/min and (b) 55 ml/min

4.3.4 Melting Point and Glass Transition Temperature

In a micronization process, polymer particles are produced by stretching and breaking long chain polymer molecules. As the polymer molecules are elongated and broken during micronization, this procedure is expected to reduce the molecular weight and viscosity of the polymer. Due to the decrease in molecular weight, physicochemical strength of the polymer is also affected by the micronization process.

Differential Scanning Calorimetric measurements, on both unprocessed and processed (micronized) polyethylene wax, were performed to examine the effect of micronization on thermal transition temperatures, such as melting point temperature. From the graphical representation of thermal transition data presented in Figure 4.13 and 4.14, the melting point temperatures of micronized polymers at various processing conditions were found (listed in Table 4.4). The data obtained indicate no significant evidence of decrease in melting point temperature due to micronization. Melting point temperatures of both processed and unprocessed polyethylene wax are found to be approximately similar. However, ΔH (change in enthalpy) was affected by the micronization process (Figure 4.13 and 4.14). In addition, particles produced at different conditions display differences in ΔH values (Table 4.4). This phenomenon indicates a change of crystallinity of the polymeric material due to micronization.

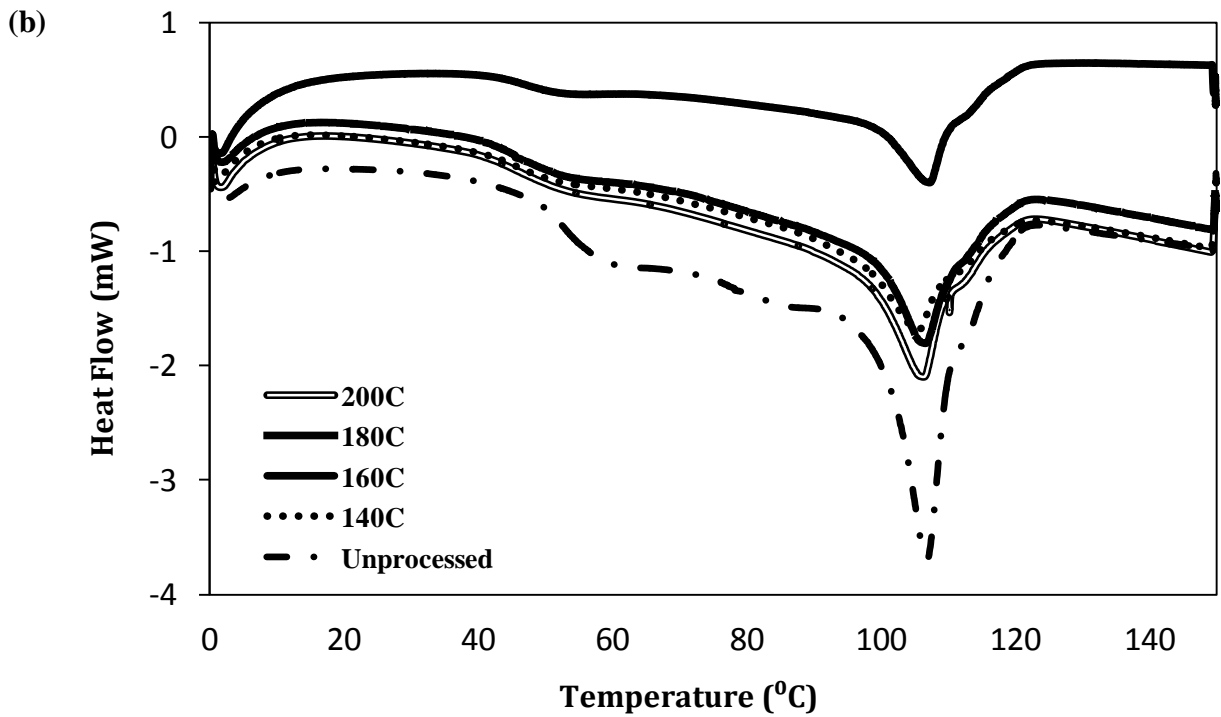
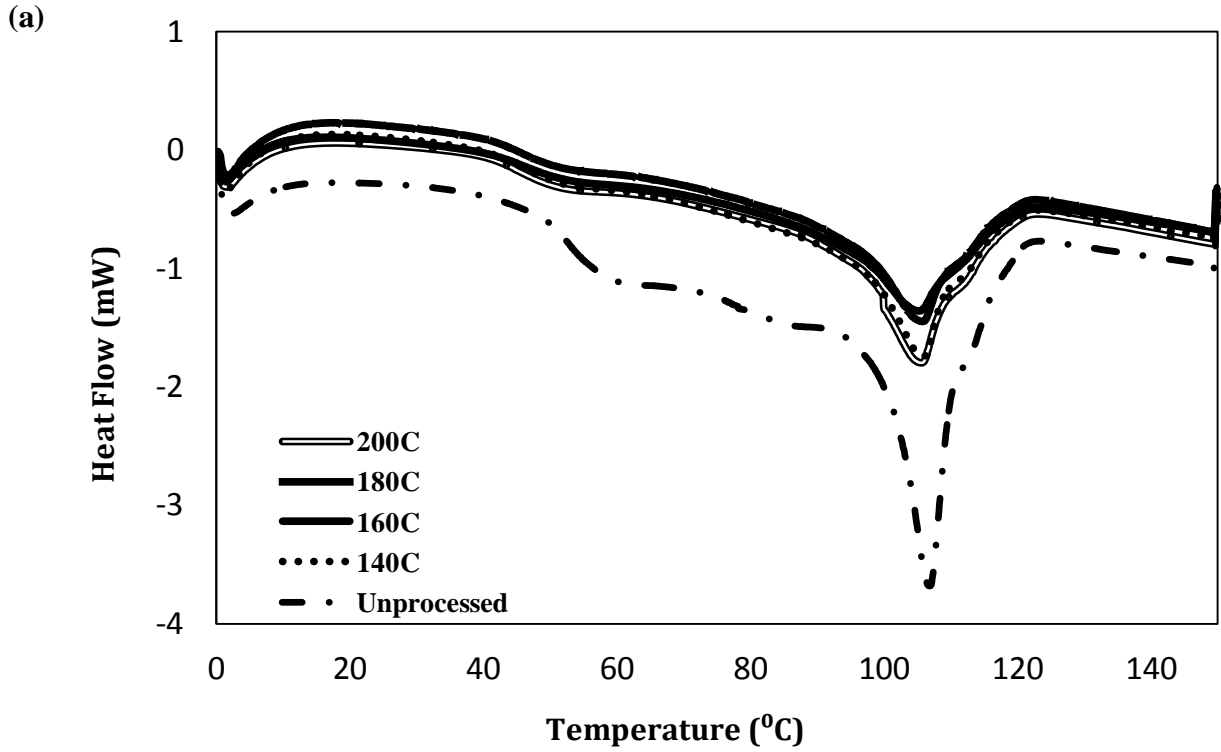


Figure 4.13: DSC of Micronized and Unprocessed Polyethylene Wax at Various Nozzle Temperatures and Two Different Polymeric Feed Rates (CO_2 Feed Rate = 25 ml/min, Screw Speed = 50 rpm): (a) 13 g/min, and (b) 26 g/min

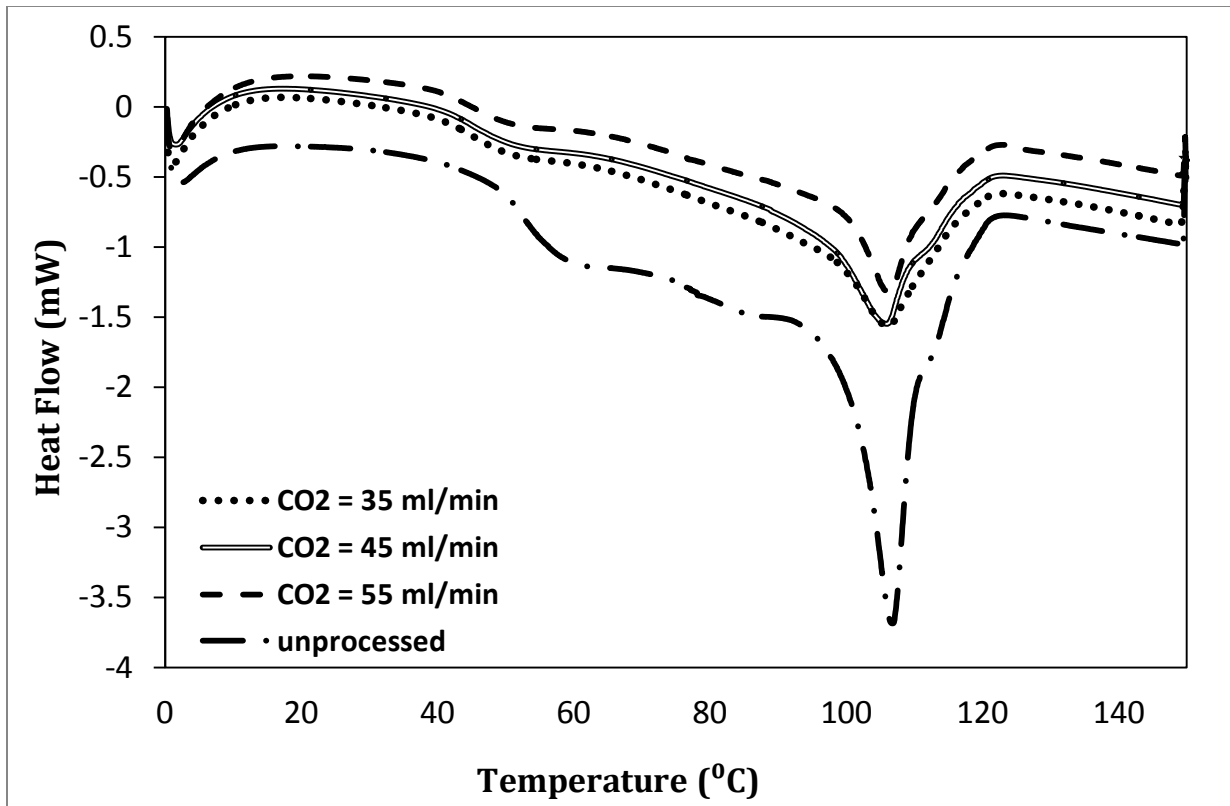


Figure 4.14: DSC of Micronized and Unprocessed Polyethylene Wax at Various CO₂ Feed Rates (Nozzle Temperature= 140°C, Polymer Feed Rate = 55 g/min, Screw Speed = 50 rpm)

**Table 4.4: Effect of Micronization on Melting Point Temperature of Polyethylene Wax
(Screw Speed= 50 rpm)**

	Polymer Feed Rate (g/min)	Nozzle Temperature (°C)	CO₂ Feed Rate (ml/min)	Melting Point (°C)	ΔH (J/g)
Unprocessed	-	-	-	106.8	123.8
Processed	13	140	25	106.0	89.0
		160	25	105.3	85.8
		180	25	105.7	81.7
		200	25	105.6	82.3
	26	140	25	105.6	74.7
		160	25	107.3	75.3
		180	25	106.6	83.2
		200	25	106.2	85.2
	52	140	35	106.0	82.0
		140	45	106.5	95.9
		140	55	106.7	90.7

CHAPTER 5: CONCLUSIONS AND RECOMMENDATIONS

5.1 CONCLUSIONS

In this thesis, a continuous process of polymer micronization by rapid depressurization of a polymer/gas solution in an extrusion process is presented. The extrusion process used in this research work was designed to produce particles with minimal change in design of a typical extrusion process and without substantially decreasing the processing rates from normal industrial rates. The sources used to develop this process are the scientific studies published on similar micronization processes and our direct experience of the extrusion foaming process using a twin-screw extruder. Low molecular weight polyethylene (polyethylene wax) and carbon dioxide were chosen for this purpose. Generation of polyethylene wax particles from this extrusion process demonstrated that extrusion micronization technique can be a valid alternative to conventional processes for polymers micro particle production.

The particles collected during experimentation were analysed using various analytical techniques and an investigation on the effect of processing parameters on particle properties and characteristics was performed. The results obtained from Scanning Electron Microscopy and Optical Microscopy measurements indicate that polyethylene wax particles sized in the range of 0.01 to 190 μm were produced. Furthermore, the particle size was found to be a function of nozzle temperature and CO_2 feed rate; the mean particle size increases with an increase in both nozzle temperature and CO_2 feed rate. On the contrary, despite the increase in processing pressure (with increase in polymer feed rate), no significant influence of polymer feed rate on mean particle diameter was observed. Morphology of particles was also found to

be a function of processing parameters. For example, more spherically shaped particles of polyethylene wax were produced at higher nozzle temperature. A decrease in agglomeration with increase in nozzle temperature was also observed. On the contrary, an increase in fibre production and particle agglomeration was observed when the polymer feed rate was increased. Particle deformation also seemed to increase at higher polymer feed rate and CO₂ feed rate.

Based on the size data, particle size distributions were plotted for particles produced at different processing conditions. The distribution plots indicate a considerable effect of nozzle temperature on particle size distributions; particle size distributions broaden as the nozzle temperature increases. However, this phenomenon was only noticed for a considerably high polymer feed rate. At lower feed rate the effect of nozzle temperature was insignificant. In addition, an increase in CO₂ feed rate was found to produce comparatively narrower particle size distribution.

The particles generated during the experiments indicate that particle generation in an extrusion process using supercritical carbon dioxide is achievable. Several advantages of the extrusion micronization process can be noted over conventional methods, which will help promote the applicability of this micronization process in the future [2,6,26,35]:

- High purity of products: produces solvent-free powder without contamination or degradation of the product
- Control over particles produced: particle size, size distribution and morphology of particles can be controlled via the control of processing variable and process equipment

- Versatile process: It has the potential for processing highly viscous, waxy, sticky and thermolabile compounds
- Environmentally acceptable technology: The overall process creates and employs solvents and process aids that, if emitted to the environment, exhibit a lower impact than currently used materials
- Single-step process: allows easier understanding, control and scale-up of the process.

5.2 RECOMMENDATIONS

The application of supercritical fluids, especially supercritical carbon dioxide, for the precipitation of substances has been of great interest to researchers for many years due to the versatile properties of this fluid at supercritical condition. In this work, the production of micronized polymer particles is studied. The experiments completed can form the basis for further work on process understanding and improvement. More specifically, future work should give careful consideration to the role of polymer molecular weight as well as polymer/CO₂ viscosity on particle size and morphology. For that purpose several polymers should be carefully selected with varying molecular weight and polydispersity. The viscosity of the polymer/CO₂ solution can be measured on-line through pressure drop measurements using a converging die, as previously done [76,77]. This additional work can be accomplished through more systematic statistical experimental designs.

The commercialization of a supercritical fluid micronization technology requires predictability and consistency of the characteristics of the product, for which a detailed understanding of the influence of all relevant process variables is necessary. Like any other

supercritical fluid precipitation technology, a common feature of the extrusion micronization process is that it has a large number of process parameters that can affect the performance of the process and characteristic properties of the product. As a result, the effect of other process variables (screw configuration, barrel temperatures) should be studied. In addition, it has been mentioned in many publications that the effect of nozzle size and geometry has a large influence on particle size and morphology. Hence, detailed analysis on the effect of the nozzle geometry and size should be conducted to explore the possibility of producing particles of different sizes and shapes. Finally, particle cooling and collection should be examined carefully in order to minimize particle agglomeration and reduce the production of fibre.

REFERENCES

- [1] Reverchon E, Della Porta G. Supercritical fluids-assisted micronization techniques. Low-impact routes for particle production. *Pure and Applied Chemistry* 2001;73:1293-7.
- [2] Knez Z, Weidner E. Particles formation and particle design using supercritical fluids. *Current Opinion in Solid State and Materials Science* 2003;7:353-61.
- [3] Pasquali I, Bettini R, Giordano F. Solid-state chemistry and particle engineering with supercritical fluids in pharmaceuticals. *European Journal of Pharmaceutical Sciences* 2006;27:299-310.
- [4] Rehman M, Kippax P, York P. Particle engineering for improved dispersion in dry powder inhalers. *Pharmaceutical Technology Europe* 2003;15:34,37-39.
- [5] Kordikowski A, Shekunov T, York P. Polymorph control of sulfathiazole in supercritical CO₂. *Pharm Res* 2001;18:682-8.
- [6] Fages J, Lochard H, Letourneau J-, Sauceau M, Rodier E. Particle generation for pharmaceutical applications using supercritical fluid technology. *Powder Technology* 2004;141:219-26.
- [7] Jung J, Perrut M. Particle design using supercritical fluids: Literature and patent survey. *Journal of Supercritical Fluids* 2001;20:179-219.
- [8] Breitenbach J. Melt extrusion: from process to drug delivery technology. *European Journal of Pharmaceutics and Biopharmaceutics: Official Journal of Arbeitsgemeinschaft Fur Pharmazeutische Verfahrenstechnik e.V* 2002;54:107-17.
- [9] Nalawade SP, Picchioni F, Janssen LPBM. Supercritical carbon dioxide as a green solvent for processing polymer melts: Processing aspects and applications. *Progress in Polymer Science (Oxford)* 2006;31:19-43.

- [10] Nalawade SP, Nieborg VHJ, Picchioni F, Janssen LPBM. Prediction of the viscosity reduction due to dissolved CO₂ of and an elementary approach in the supercritical CO₂ assisted continuous particle production of a polyester resin. *Powder Technol* 2006;170:143-52.
- [11] Nalawade SP, Picchioni F, Janssen LPBM. Batch production of micron size particles from poly(ethylene glycol) using supercritical CO₂ as a processing solvent. *Chemical Engineering Science* 2007;62:1712-20.
- [12] Yoganathan RB, Mammucari R, Foster NR. Dense gas processing of polymers. *Polymer Reviews* 2010;50:144-77.
- [13] Tandya A, Mammucari R, Dehghani F, Foster NR. Dense gas processing of polymeric controlled release formulations. *Int J Pharm* 2007;328:1-11.
- [14] Kemmere MF, Meyer T editors. *Supercritical carbon dioxide in polymer reaction engineering*. Weinheim, Germany: WILEY-VCH Verlag GmbH & Co. KGaA, 2005.
- [15] Nalawade SP, Nieborg VHJ, Picchioni F, Janssen LPBM. Prediction of the viscosity reduction due to dissolved CO₂ of and an elementary approach in the supercritical CO₂ assisted continuous particle production of a polyester resin. *Powder Technol* 2006;170:143-52.
- [16] Hakuta Y, Hayashi H, Arai K. Fine particle formation using supercritical fluids. *Current Opinion in Solid State & Materials Science* 2003;7:341-51.
- [17] Yeo SD, Kiran E. Formation of polymer particles with supercritical fluids: A review. *Journal of Supercritical Fluids* 2005;34:287-308.
- [18] Jung J, Perrut M. Particle design using supercritical fluids: Literature and patent survey. *Journal of Supercritical Fluids* 2001;20:179-219.
- [19] Tom JW, Debenedetti PG. Particle formation with supercritical fluids-a review. *J Aerosol Sci* 1991;22:555-84.

- [20] Brady G.S., Clauser H.R., Vaccari J.A. Material Handbooks. New York, NY: McGraw-Hills Companies, Inc., 2002.
- [21] Ash M., Ash I. Handbook of Green Chemicals. Endicott, NY: Synapse Information Resources Inc., 2004.
- [22] Flick E.W. Handbook of Adhesive Raw Materials. Park Ridge, NJ: Noyes Publication, 1989.
- [23] Freund M., Mozes G. Paraffin Products: Properties, Technologies, Applications. NY: Elsevier Science Publishing Company, Inc., 1982.
- [24] Rosato D.V., Rosato D.V., Rosato M.V. Plastic Product Material and Process Selection Handbook. Kidlington, Oxford, UK: Elsevier Ltd., 2004.
- [25] Pasquali I, Bettini R. Are pharmaceuticals really going supercritical? Int J Pharm 2008;364: 176-87.
- [26] Martín A, Cocero MJ. Micronization processes with supercritical fluids: Fundamentals and mechanisms. Adv Drug Deliv Rev 2008;60:339-50.
- [27] Cooper AI. Polymer synthesis and processing using supercritical carbon dioxide. Journal of Materials Chemistry 2000;10:207-34.
- [28] Kendall JL, Canelas DA, Young JL, DeSimone JM. Polymerizations in Supercritical Carbon Dioxide. Chem Rev 1999;99:543-63.
- [29] Kazarian SG. Polymer processing with supercritical fluids. Polymer Science - Series C 2000;42:78-101.
- [30] Ohshima M. Supercritical CO₂ assisted polymer processing- Current status and future. Polymer Preprints, Japan 2005;54:2420-2.
- [31] Wood CD, Cooper AI, Desimone JM. Green synthesis of polymers using supercritical carbon dioxide. Current Opinion in Solid State and Materials Science 2004;8:325-31.

- [32] Tomasko DL, Li H, Liu D, Han X, Wingert MJ, Lee LJ, Koelling KW. A Review of CO₂ Applications in the Processing of Polymers. *Industrial and Engineering Chemistry Research* 2003;42:6431-56.
- [33] Kikic I, Vecchione F, Alessi P, Cortesi A, Eva F, Elvassore N. Polymer plasticization using supercritical carbon dioxide: Experiment and modeling. *Industrial and Engineering Chemistry Research* 2003;42:3022-9.
- [34] Kwag C, Manke CW, Gulari E. Effects of dissolved gas on viscoelastic scaling and glass transition temperature of polystyrene melts. *Industrial and Engineering Chemistry Research* 2001;40:3048-52.
- [35] Beckman EJ. Supercritical and near-critical CO₂ in green chemical synthesis and processing. *Journal of Supercritical Fluids* 2004;28:121-91.
- [36] Pasquali I, Bettini R. Are pharmaceuticals really going supercritical? *Int J Pharm* 2008;364:176-187.
- [37] Vemavarapu C, Mollan MJ, Lodaya M, Needham TE. Design and process aspects of laboratory scale SCF particle formation systems. *Int J Pharm* 2005;292:1-16.
- [38] Reverchon E. Supercritical antisolvent precipitation of micro- and nano-particles. *Journal of Supercritical Fluids* 1999;15:1-21.
- [39] Jung J, Perrut M. Particle design using supercritical fluids: Literature and patent survey. *Journal of Supercritical Fluids* 2001;20:179-219.
- [40] Matson DW, Fulton JL, Petersen RC, Smith RD. Rapid expansion of supercritical fluid solutions: solute formation of powders, thin films, and fibers. *Industrial and Engineering Chemistry Research* 1987;26:2298-306.
- [41] Phillips EM, Stella VJ. Rapid expansion from supercritical solutions: Application to pharmaceutical processes. *Int J Pharm* 1993;94:1-10.

- [42] Reverchon E. Supercritical antisolvent precipitation of micro- and nano-particles. *Journal of Supercritical Fluids* 1999;15:1-21.
- [43] Reverchon E, Antonacci A. Polymer microparticles production by supercritical assisted atomization. *Journal of Supercritical Fluids* 2007;39:444-52.
- [44] Reverchon E. Supercritical-assisted atomization to produce micro- and/or nanoparticles of controlled size and distribution. *Industrial and Engineering Chemistry Research* 2002;41:2405-11.
- [45] Adami R, Osséo LS, Huopalahti R, Reverchon E. Supercritical AntiSolvent micronization of PVA by semi-continuous and batch processing. *Journal of Supercritical Fluids* 2007;42:288-98.
- [46] Sieversa RE, Huang ETS, Villa JA, Engling G, Brauer PR. Micronization of water-soluble or alcohol-soluble pharmaceuticals and model compounds with a low-temperature Bubble Dryer®. *Journal of Supercritical Fluids* 2003;26:9-16.
- [47] Sievers RE, Quinn BP, Cape SP, Searles JA, Braun CS, Bhagwat P, Rebits LG, McAdams DH, Burger JL, Best JA, Lindsay L, Hernandez MT, Kisich KO, Iacovangelo T, Kristensen D, Chen D. Near-critical fluid micronization of stabilized vaccines, antibiotics and anti-virals. *Journal of Supercritical Fluids* 2007;42:385-91.
- [48] Cape SP, Villa JA, Huang ETS, Yang T-, Carpenter JF, Sievers RE. Preparation of active proteins, vaccines and pharmaceuticals as fine powders using supercritical or near-critical fluids. *Pharm Res* 2008;25:1967-90.
- [49] Alavi S. A. R., Angaji M.T., Gholami Z. Twin-Screw Extruder and Effective Parameters on the HDPE Extrusion Process. 2009:204 - 207.
- [50] Park CB, Suh NP. Rapid polymer/gas solution formation for continuous production of microcellular plastics. *J Manuf Sci Eng Trans ASME* 1996;118:639-45.
- [51] Repka MA. Hot-melt extrusion. *American Pharmaceutical Review* 2009;12:18-27.

- [52] Li YG, Park CB, Li HB, Wang J. Measurement of the PVT property of PP/CO₂ solution. *Fluid Phase Equilib* 2008;270:15-22.
- [53] Hasan MM, Li YG, Li G, Park CB, Chen P. Determination of solubilities of CO₂ in linear and branched polypropylene using a magnetic suspension balance and a PVT apparatus. *J Chem Eng Data* 2010;55:4885-95.
- [54] Kazarian SG, Vincent MF, Bright FV, Liotta CL, Eckert CA. Specific intermolecular interaction of carbon dioxide with polymers. *J Am Chem Soc* 1996;118:1729-36.
- [55] Fried JR, Li W. High-pressure FTIR studies of gas-polymer interactions. *J Appl Polym Sci* 1990;41:1123-31.
- [56] Shah VM, Hardy BJ, Stern SA. Solubility of carbon dioxide, methane, and propane in silicone polymers. Effect of polymer backbone chains. *J Polym Sci Part B* 1993;31:313-7.
- [57] Rindfleisch F, DiNoia TP, McHugh MA. Solubility of polymers and copolymers in supercritical CO₂. *J Phys Chem* 1996;100:15581-7.
- [58] Lei Z, Ohyabu H, Sato Y, Inomata H, Smith Jr. RL. Solubility, swelling degree and crystallinity of carbon dioxide-polypropylene system. *Journal of Supercritical Fluids* 2007;40:452-61.
- [59] Li D-, Liu T, Zhao L, Yuan W-. Solubility and diffusivity of carbon dioxide in solid-state isotactic polypropylene by the pressure - Decay method. *Industrial and Engineering Chemistry Research* 2009;48:7117-24.
- [60] Liao X, Li YG, Park CB, Chen P. Interfacial tension of linear and branched PP in supercritical carbon dioxide. *Journal of Supercritical Fluids* 2010;55:386-94.
- [61] Li G, Wang J, Park CB, Simha R. Measurement of gas solubility in linear/branched PP melts. *J Polym Sci Part B* 2007;45:2497-508.

- [62] Sato Y, Fujiwara K, Takikawa T, Sumarno, Takishima S, Masuoka H. Solubilities and diffusion coefficients of carbon dioxide and nitrogen in polypropylene, high-density polyethylene, and polystyrene under high pressures and temperatures. *Fluid Phase Equilib* 1999;162:261-76.
- [63] Sato Y, Takikawa T, Sorakubo A, Takishima S, Masuoka H, Imaizumi M. Solubility and diffusion coefficient of carbon dioxide in biodegradable polymers. *Industrial and Engineering Chemistry Research* 2000;39:4813-9.
- [64] Areerat S, Funami E, Hayata Y, Nakagawa D, Ohshima M. Measurement and prediction of diffusion coefficients of supercritical CO₂ in molten polymers. *Polym Eng Sci* 2004;44:1915-24.
- [65] Li G, Gunkel F, Wang J, Park CB, Altstädt V. Solubility measurements of N₂ and CO₂ in polypropylene and ethene/octene copolymer. *J Appl Polym Sci* 2007;103:2945-53.
- [66] Li G, Park CB. PP/CO₂ volume swelling from measurement and equations-of-state predictions. *Technical Papers, Regional Technical Conference - Society of Plastics Engineers* 2008;4:2539-45.
- [67] Tammann G, Hesse Z. *Anorg Allegem Chem* 1926;156.
- [68] Johnson KP, Condo PD. Plasticization of polymers with compressed fluid diluents. *Polymeric Materials Science and Engineering, Proceedings of the ACS Division of Polymeric Materials Science and Engineering* 1993;68:291.
- [69] Condo PD, Sanchez IC, Panayiotou CG, Johnston KP. Glass transition behavior including retrograde vitrification of polymers with compressed fluid diluents. *Macromolecules* 1992;25:6119-27.
- [70] Chow TS. Molecular interpretation of the glass transition temperature of polymer-diluent systems. *Macromolecules* 1980;13:362-4.

- [71] Wissinger RG, Paulaitis ME. Glass transitions in polymer/CO₂ mixtures at elevated pressures. *J Polym Sci Part B* 1991;29:631-3.
- [72] Condo PD, Paul DR, Johnston KP. Glass transitions of polymers with compressed fluid diluents: Type II and III behavior. *Macromolecules* 1994;27:365-71.
- [73] Zhang Z, Handa YP. An in situ study of plasticization of polymers by high-pressure gases. *J Polym Sci Part B* 1998;36:977-82.
- [74] Park SS, Park CB, Ladin D, Naguib HE, Tzoganakis C. Development of a dilatometer for measurement of the PVT properties of a polymer/CO₂ solution using a foaming extruder and a gear pump. *J Manuf Sci Eng Trans ASME* 2002;124:86-91.
- [75] Guo Q, Park CB, Xu X, Wang J. Relationship of fractional free volumes derived from the Equations of State (EOS) and the Doolittle equation. *Journal of Cellular Plastics* 2007;43:69-82.
- [76] Lee M, Tzoganakis C, Park CB. Effects of supercritical CO₂ on the viscosity and morphology of polymer blends. *Adv Polym Technol* 2000;19:300-11.
- [77] Lee M, Park CB, Tzoganakis C. Modeling of PS/supercritical CO₂ solution viscosities. Annual Technical Conference - ANTEC, Conference Proceedings 1998;2:1902-6.
- [78] Doolittle AK. Studies in Newtonian Flow. II. The Dependence of the Viscosity of Liquids on Free Space. *J Appl Phys* 1951;22:1471-1475.
- [79] Duvdevani IJ, Klein I. Analysis of Polymer Melt Flow in Capillaries Including Pressure Effects. *SPE Journal* 1967:41-45.
- [80] Royer JR, Gay YJ, Desimone JM, Khan SA. High-pressure rheology of polystyrene melts plasticized with CO₂: Experimental measurement and predictive scaling relationships. *J Polym Sci Part B* 2000;38:3168-80.

- [81] Areerat S, Nagata T, Ohshima M. Measurement and prediction of LDPE/CO₂ solution viscosity. *Polym Eng Sci* 2002;42:2234-45.
- [82] Nobelen M, Hoppe S, Fonteix C, Pla F, Dupire M, Jacques B. Modeling of the rheological behavior of polyethylene/supercritical Formula Not Shown solutions. *Chemical Engineering Science* 2006;61:5334-45.
- [83] Lee M, Tzoganakis C, Park CB. Extrusion of PE/PS blends with supercritical carbon dioxide. *Polym Eng Sci* 1998;38:1112-20.
- [84] Royer JR, Gay YJ, Adam M, DeSimone JM, Khan SA. Polymer melt rheology with high-pressure CO₂ using a novel magnetically levitated sphere rheometer. *Polymer* 2002;43:2375-83.
- [85] Gerhardt LJ, Garg A, Manke CW, Gulari E. Concentration-dependent viscoelastic scaling models for polydimethylsiloxane melts with dissolved carbon dioxide. *J Polym Sci Part B* 1998;36:1911-8.
- [86] Schmitt WJ, Salada MC, Shook GG, Speaker III SM. Finely-divided powders by carrier solution injection into a near or supercritical fluid. *AIChE J* 1995;41:2476-86.
- [87] Gao Y, Kays Mulenda T, Shi Y-, Yuan W-. Fine particles preparation of Red Lake C Pigment by supercritical fluid. *Journal of Supercritical Fluids* 1998;13:369-74.
- [88] Costa MS, Duarte ARC, Cardoso MM, Duarte CMM. Supercritical antisolvent precipitation of PHBV microparticles. *Int J Pharm* 2007;328:72-7.
- [89] Chen K, Zhang X, Pan J, Zhang W, Yin W. Gas antisolvent precipitation of Ginkgo ginkgolides with supercritical CO₂. *Powder Technol* 2005;152:127-32.
- [90] Yeo S-, Lim G-, DeBenedetti PG, Bernstein H. Formation of microparticulate protein powders using a supercritical fluid antisolvent. *Biotechnol Bioeng* 1993;41:341-6.

- [91] Reverchon E. Supercritical antisolvent precipitation of micro- and nano-particles. *Journal of Supercritical Fluids* 1999;15:1-21.
- [92] Park CB, Baldwin DF, Suh NP. Effect of the pressure drop rate on cell nucleation in continuous processing of microcellular polymers. *Polym Eng Sci* 1995;35:432-40.
- [93] Mansour A, Chigier N. Air-blast atomization of non-Newtonian liquids. *J Non Newtonian Fluid Mech* 1995;58:161-94.
- [94] Palakodaty S, York P, Pritchard J. Supercritical fluid processing of materials from aqueous solutions: The application of SEDS to lactose as a model substance. *Pharm Res* 1998;15:1835-43.
- [95] Nalawade SP, Picchioni F, Janssen LPBM, Patil VE, Keurentjes JTF, Staudt R. Solubilities of sub- and supercritical carbon dioxide in polyester resins. *Polym Eng Sci* 2006;46:643-9.
- [96] Allen T. *Powder Sampling and Particle Size Determination*. Oxford, UK: Elsevier B.V., 2003.
- [97] Weidner E, Steiner R, Knez Z. Powder generation from polyethyleneglycols with compressible fluids. *Process Technology Proceedings* 1996;12:223-8.
- [98] Dragoo AL, Robbins CR, Hsu SM. A critical assessment of requirements for ceramic powder characterization. *Adv.Ceram.* 1987;21:711-20.

Appendix A: Formulas for Mean Particle Size Calculation

Table 0.1: Definition of Mean Particle Diameters

Name	Symbol	Formula
Number, Length or Mean Diameter	x_{NL}	$\Sigma x dN / \Sigma dN$
Number, Volume or Volume Mean Diameter	x_{NV}	$\left(\Sigma x^2 dN / \Sigma dN \right)^{1/3}$
Surface, Volume or Sauter Mean Diameter	x_{SV}	$\Sigma x^2 dN / \Sigma x^3 dN$

**Appendix B: Data for Particle Size Calculation
(Optical Microscope Results)**

Table 0.2: Diameters of Polyethylene Wax Particles Produced at a Constant Polymer Feed Rate of 13 g/min and Different Nozzle Temperatures Measured via an Optical Microscope (Screw Speed=50 rpm, CO₂ Feed Rate =25 ml/min)

140°C				160°C				180°C		200°C			
1.3	3.1	4.7	9.2	0.9	3.7	5.5	12.9	1	5.4	0.7	2.7	4.7	8.5
1.4	3.1	4.7	9.2	0.9	3.7	5.5	13	1.5	5.6	0.8	2.7	4.8	8.6
1.4	3.1	4.8	9.6	1	3.7	5.5	13.5	1.7	5.8	0.8	2.7	4.8	8.6
1.5	3.2	4.9	9.7	1	3.8	5.5	13.6	2	6.1	0.9	2.7	4.8	8.8
1.6	3.3	5	10.4	1.1	3.8	5.5	13.9	2.2	6.4	0.9	2.8	5	9
1.7	3.3	5.2	10.6	1.2	3.8	5.6	14.1	2.4	6.8	0.9	2.9	5.1	9
1.7	3.4	5.2	10.7	1.3	3.9	5.6	14.2	2.7	6.8	1	3	5.2	9.2
1.8	3.5	5.2	11.3	1.3	4.1	5.7	14.4	2.8	7.1	1	3.1	5.4	9.3
1.8	3.6	5.3	11.4	1.5	4.1	5.7	16.9	2.9	7.3	1	3.1	5.4	9.4
1.9	3.6	5.4	12	1.5	4.1	5.7	17.5	3.2	8.2	1.2	3.2	5.5	10.1
2	3.6	5.6	12.6	1.6	4.2	5.9	19.1	3.2	8.6	1.5	3.3	5.5	10.2
2	3.6	5.9	12.9	1.7	4.2	6.1	19.3	3.3	8.6	1.7	3.3	5.7	10.8
2	3.6	6.3	13.5	1.7	4.3	6.4		3.3	8.7	1.7	3.4	5.8	10.9
2.1	3.7	6.4	17.1	1.7	4.3	6.5		3.4	8.8	1.8	3.4	5.9	11.8
2.2	3.7	6.6	39.6	1.7	4.4	6.8		3.6	8.9	1.9	3.5	6	11.9
2.2	3.7	6.7		2.1	4.4	6.9		3.6	9.6	1.9	3.5	6.1	13.4
2.3	3.7	6.9		2.2	4.5	7.3		3.6	9.7	2	3.6	6.1	15.9
2.3	3.8	7		2.2	4.6	7.5		3.6	10.2	2	3.7	6.2	17.8
2.4	3.9	7		2.4	4.7	7.6		3.6	10.5	2	3.8	6.3	17.8
2.4	3.9	7.2		2.4	4.7	7.8		3.7	11	2.1	3.9	6.3	18.3
2.4	3.9	7.2		2.4	4.7	7.8		3.8	11.3	2.1	4	6.3	19.2
2.5	4	7.2		2.9	4.8	8.2		4.2	11.4	2.2	4	6.4	19.5
2.5	4.1	7.3		2.9	4.9	8.6		4.3	11.7	2.2	4	6.6	20.5
2.5	4.2	7.3		2.9	5	8.8		4.4	12.1	2.2	4	6.8	25.9
2.5	4.3	7.3		3	5	9.1		4.5	13.1	2.2	4.1	6.9	29.6
2.7	4.3	7.5		3.1	5.1	9.2		4.5	13.3	2.2	4.2	6.9	35.3
2.7	4.4	7.6		3.1	5.1	9.3		4.7	13.9	2.3	4.3	7	36.8
2.8	4.5	7.6		3.2	5.2	9.7		4.8	21.1	2.3	4.3	7.1	49.6
2.8	4.5	7.7		3.2	5.2	10.1		4.8		2.4	4.5	7.1	
2.8	4.5	8.2		3.2	5.3	11.5		5		2.5	4.5	7.2	
2.9	4.6	8.7		3.3	5.3	11.5		5.1		2.5	4.5	7.3	
3	4.6	8.7		3.5	5.3	11.8		5.2		2.5	4.5	8	
3.1	4.6	8.8		3.6	5.4	12.2		5.3		2.6	4.6	8.1	

Table 0.3: Diameters of Polyethylene Wax Particles Produced at a Constant Polymer Feed Rate of 26 g/min and Different Nozzle Temperatures Measured via an Optical Microscope (Screw Speed=50 rpm, CO₂ Feed Rate =25 ml/min)

140°C				160°C				180°C		200°C
0.8	2.9	4.7	11.7	0.3	3	4.9	7.8	1.8	7.8	1.8
0.8	2.9	4.9	12.4	1.1	3	4.9	7.9	2.9	7.9	2
0.9	3	4.9	12.9	1.2	3.1	4.9	7.9	3.2	7.9	2.3
1	3.1	5	14	1.3	3.3	5	7.9	3.3	8.2	2.6
1.1	3.1	5.3	14	1.4	3.4	5	8	3.6	8.2	3.2
1.1	3.1	5.5	17.9	1.5	3.4	5.1	8.3	3.8	8.6	3.8
1.2	3.1	5.6	19.1	1.6	3.5	5.2	8.5	3.8	8.7	4
1.3	3.2	5.7	27.6	1.7	3.5	5.2	8.7	4.2	8.8	4.4
1.5	3.2	5.8	28.3	1.7	3.6	5.2	8.9	4.3	9	7
1.6	3.2	5.9	36.5	1.7	3.6	5.2	9.4	4.4	9.1	7.4
1.6	3.2	6		1.7	3.7	5.2	9.6	4.4	9.1	7.5
1.6	3.2	6.1		1.7	3.8	5.3	9.9	4.5	9.4	8.2
1.7	3.3	6.1		1.8	3.9	5.3	10	4.5	10.3	8.4
1.7	3.4	6.1		1.9	4.1	5.4	10.6	4.5	10.6	8.6
1.7	3.4	6.3		1.9	4.1	5.4	10.8	4.6	10.6	9
1.8	3.4	6.3		1.9	4.1	5.5	11	5.1	10.9	9.2
1.9	3.5	6.4		2	4.2	5.5	11	5.4	11	10.4
2	3.6	6.5		2.2	4.2	5.5	11.4	5.5	11.1	12
2	3.6	7		2.3	4.2	5.5	11.6	5.5	12.1	13.2
2	3.6	7.1		2.4	4.3	5.6	12.2	5.5	12.2	13.4
2	3.6	7.3		2.4	4.3	5.6	12.3	5.5	12.3	14
2.1	3.6	7.4		2.4	4.3	5.8	12.3	5.5	12.6	14.6
2.2	3.7	7.7		2.5	4.3	5.9	12.5	6.1	13	15.9
2.3	3.7	7.7		2.5	4.3	6	12.7	6.1	13.2	18.3
2.3	3.7	7.8		2.5	4.4	6	14.4	6.1	13.8	23
2.4	3.8	7.8		2.6	4.4	6.2	15.7	6.2	14.4	25.3
2.4	3.8	8.2		2.6	4.4	6.3	17.6	6.2	14.9	
2.5	3.8	8.2		2.6	4.4	6.3	23.4	6.3	15.2	
2.5	3.9	8.2		2.6	4.5	6.4	26.8	6.5	15.4	
2.5	3.9	8.2		2.6	4.5	6.4		7	15.5	
2.6	4.1	8.4		2.7	4.6	6.6		7.2	20.7	
2.7	4.2	8.5		2.7	4.6	6.7		7.2	21.2	
2.7	4.3	8.6		2.8	4.6	6.7		7.3	21.8	
2.7	4.3	8.8		2.9	4.7	6.8		7.7	21.9	
2.7	4.3	9.6		2.9	4.8	6.9		7.8	24.1	
2.7	4.4	9.7		2.9	4.8	7.2		7.8	25	
2.7	4.6	10.8		2.9	4.8	7.6		7.8	27.8	
2.8	4.7	11.3		3	4.9	7.8		7.8	37.9	

Table 0.4: Diameters of Polyethylene Wax Particles Produced at Different CO₂ Feed Rate Obtained via Optical Microscopic Measurements (Screw Speed=50 rpm, Polymer Feed Rate =52 g/min, Nozzle Temperature= 140°C)

15 ml/min		35 ml/min	45 ml/min		55 ml/min	
1.1	4.5	1.6	2.3	16.2	0.3	13.2
1.5	4.6	2	2.7	18.6	1.5	13.4
1.5	5.9	2.5	3.1	18.9	2.1	14
1.7	6.1	3.8	3.6	18.9	2.3	14
1.8	6.1	4.7	3.7	19	2.6	14.3
2.5	6.7	5	4.4	22.8	2.7	16.1
2.9	7.3	5.8	4.4	23.1	2.8	17.2
3.3	8.8	5.9	4.6	26	2.8	17.3
3.9	8.9	6.2	5.7	27.3	2.9	17.5
4	9	6.7	5.7	28.3	3	18
4.4	9.1	7	5.8	30.2	3.2	18.3
4.7	9.1	7.8	6	33.6	3.4	23.4
5.5	9.6	7.9	6	36	3.4	29.6
5.8	11.5	8	6.1	36.7	3.7	58
6	15.1	8.4	6.2	38	3.8	
6.2	25.6	8.8	6.3	47.3	3.9	
7.6	29.9	8.9	6.6	48.4	4.1	
8	33.7	10.3	6.6	52.7	4.2	
8.5		10.4	7.2	54.9	4.8	
10.7		11.1	7.3	59.3	5.1	
12		11.2	7.3	59.8	5.2	
12.6		12.4	7.5	116.5	5.3	
13.3		12.9	8.1	118.8	5.5	
13.5		14.8	8.9		6	
16.3		16.3	9.1		6	
18.3		18.2	9.2		6.4	
19		18.4	9.4		8.4	
20.5		20.5	9.9		8.5	
1.5		22.6	10.5		8.8	
1.7		29.4	10.5		9.1	
1.8			11.1		9.2	
2.6			11.6		10.3	
3.3			12.4		10.5	
3.4			12.5		10.7	
3.9			13.9		10.8	
4			14.3		11.5	
4			14.4		11.5	
4.3			14.9		12.9	

Appendix C: Data for Particle Size Distribution Plots

Table 0.5: Frequency and Normalized Frequency of Particle Diameters of Polyethylene Wax Particles Produced at 15 g/min Polymer Feed Rate (Screw Speed=50 rpm, CO₂ Feed Rate =25 ml/min)

Range	Middle of Range	140°C		160°C		180°C		200°C	
		Freq.	Norm. Freq.	Freq.	Norm. Freq.	Freq.	Norm. Freq.	Freq.	Norm. Freq.
0	0	0	0.00	0	0.00	0	0.00	0	0.00
0 to 2	1	10	8.77	15	13.51	3	4.92	16	12.60
2 to 4	3	44	38.60	25	22.52	18	29.51	37	29.13
4 to 6	5	24	21.05	37	33.33	15	24.59	27	21.26
6 to 8	7	17	14.91	10	9.01	6	9.84	17	13.39
8 to 10	9	8	7.02	7	6.31	8	13.11	11	8.66
10 to 12	11	5	4.39	4	3.60	6	9.84	6	4.72
12 to 14	13	4	3.51	6	5.41	4	6.56	1	0.79
14 to 16	15	0	0.00	3	2.70	0	0.00	1	0.79
16 to 18	17	1	0.88	2	1.80	0	0.00	2	1.57
18 to 20	19	0	0.00	2	1.80	0	0.00	3	2.36
20 to 22	21		0.00		0.00	1	1.64	1	0.79
22 to 24	23		0.00		0.00		0.00	0	0.00
24 to 26	25		0.00		0.00		0.00	1	0.79
26 to 28	27		0.00		0.00		0.00	0	0.00
28 to 30	29		0.00		0.00		0.00	1	0.79
30 to 32	31		0.00		0.00		0.00		0.00
32 to 34	33		0.00		0.00		0.00		0.00
34 to 36	35		0.00		0.00		0.00	2	1.57
36 to 38	37		0.00		0.00		0.00		0.00
38 to 40	39	1	0.88		0.00		0.00		0.00
40 to 42	41		0.00		0.00		0.00		0.00
42 to 44	43		0.00		0.00		0.00		0.00
44 to 46	45		0.00		0.00		0.00		0.00
46 to 48	47		0.00		0.00		0.00		0.00
48 to 50	49		0.00		0.00		0.00	1	0.79
Total Number of Particles		114		111		61		127	

Table 0.6: Frequency and Normalized Frequency of Particle Diameters of Polyethylene Wax Particles Produced at 26 g/min Polymer Feed Rate (Screw Speed=50 rpm, CO₂ Feed Rate =25 ml/min)

Range	Middle of Range	140°C		160°C		180°C		200°C	
		Freq.	Norm. Freq.	Freq.	Norm. Freq.	Freq.	Norm. Freq.	Freq.	Norm. Freq.
0	0	0	0.00	0	0.00	0	0.00	0	0.00
0 to 2	1	17	13.71	16	11.19	1	1.32	1	4.17
2 to 4	3	51	41.13	35	24.48	6	7.89	5	20.83
4 to 6	5	18	14.52	48	33.57	15	19.74	2	8.33
6 to 8	7	16	12.90	19	13.29	19	25.00	3	12.50
8 to 10	9	10	8.06	8	5.59	9	11.84	5	20.83
10 to 12	11	3	2.42	7	4.90	6	7.89	2	8.33
12 to 14	13	2	1.61	5	3.50	7	9.21	2	8.33
14 to 16	15	2	1.61	2	1.40	5	6.58	3	12.50
16 to 18	17	1	0.81	1	0.70	0	0.00	0	0.00
18 to 20	19	1	0.81	0	0.00	0	0.00	1	4.17
20 to 22	21	0	0.00	0	0.00	4	5.26	0	0.00
22 to 24	23		0.00	1	0.70	0	0.00		0.00
24 to 26	25		0.00		0.00	2	2.63		0.00
26 to 28	27	1	0.81	1	0.70	1	1.32		0.00
28 to 30	29	1	0.81		0.00		0.00		0.00
30 to 32	31		0.00		0.00		0.00		0.00
32 to 34	33		0.00		0.00		0.00		0.00
34 to 36	35		0.00		0.00		0.00		0.00
36 to 38	37	1	0.81		0.00	1	1.32		0.00
38 to 40	39		0.00		0.00		0.00		0.00
40 to 42	41		0.00		0.00		0.00		0.00
42 to 44	43		0.00		0.00		0.00		0.00
44 to 46	45		0.00		0.00		0.00		0.00
46 to 48	47		0.00		0.00		0.00		0.00
48 to 50	49		0.00		0.00		0.00		0.00
Total Number of Particles		124		143		76		24	

Table 0.7: Frequency and Normalized Frequency of Particle Diameters of Polyethylene Wax Particles Produced at Different CO₂ Feed Rate (Screw Speed=50 rpm, Polymer Feed Rate =52 g/min, Nozzle Temperature = 140°C)

Range	Middle of Range	15 ml/min		35 ml/min		45 ml/min		55 ml/min	
		Freq.	Norm. Freq.	Freq.	Norm. Freq.	Freq.	Norm. Freq.	Freq.	Norm. Freq.
0	0	0	0.00	0	0.00	0	0.00	0	0.00
0 to 2	1	6	10.53	1	3.33	0	0.00	2	3.92
2 to 4	3	10	17.54	3	10.00	5	9.09	14	27.45
4 to 6	5	12	21.05	4	13.33	6	10.91	7	13.73
6 to 8	7	7	12.28	5	16.67	11	20.00	3	5.88
8 to 10	9	8	14.04	4	13.33	6	10.91	5	9.80
10 to 12	11	2	3.51	4	13.33	4	7.27	6	11.76
12 to 14	13	4	7.02	2	6.67	3	5.45	3	5.88
14 to 16	15	1	1.75	1	3.33	3	5.45	3	5.88
16 to 18	17	1	1.75	1	3.33	1	1.82	4	7.84
18 to 20	19	2	3.51	2	6.67	4	7.27	2	3.92
20 to 22	21	1	1.75	1	3.33		0.00		0.00
22 to 24	23		0.00	1	3.33	2	3.64	1	1.96
24 to 26	25	1	1.75		0.00		0.00		0.00
26 to 28	27		0.00		0.00	2	3.64		0.00
28 to 30	29	1	1.75	1	3.33	2	3.64	1	1.96
30 to 32	31		0.00		0.00		0.00		0.00
32 to 34	33	1	1.75		0.00	1	1.82		0.00
34 to 36	35		0.00		0.00		0.00		0.00
36 to 38	37		0.00		0.00	2	3.64		0.00
38 to 40	39		0.00		0.00	1	1.82		0.00
40 to 42	41		0.00		0.00		0.00		0.00
42 to 44	43		0.00		0.00		0.00		0.00
44 to 46	45		0.00		0.00		0.00		0.00
46 to 48	47		0.00		0.00	2	3.64		0.00
48 to 50	49		0.00		0.00		0.00		0.00
Total Number of Particles		57		30		55		51	

Appendix D: Viscosity Data for PE Wax and Micronized PE Wax

Table 0.8: Shear Viscosity of Unprocessed Polyethylene Wax Pallets Measured via a Capillary Rheometer using a die with L/D ratio of 50/20 at 90°C and 110°C

		Shear Viscosity (Pa.s)							
Ram Rate (°/min)	Shear Rate (1/sec)	90°C				100°C			
		Run 1	Run 2	Run 3	Avg.	Run 1	Run 2	Run3	Avg.
0.2	30.16	2488.6	2720.2	2648.2	2619.0	838.97	810.66	802.24	817.29
0.4	60.32	1557	1648.2	1571.1	1592.1	518.57	512.13	490.26	506.99
0.6	90.48	1108.3	1184.7	1195.8	1162.9	378.31	371.45	362.01	370.59
0.8	120.64	892.37	811.3	967	890.22	297.89	297.89	280.51	292.10
1.2	180.96	651.96	597.49	700.43	649.96	209.31	204.17	202.02	205.17
2.2	331.76	384.39	388.6	436.1	403.03	130.31	125.63	127.51	127.82
3.2	482.56	300.3	313.01	329.25	314.19	100.53	95.703	95.703	97.31
6.2	934.97	181.3	187.78	200.07	189.72		58.942		58.94
9	1357.2	118.9	140.74	142.74	134.13				

Table 0.9: Shear Viscosity of Unprocessed Polyethylene Wax Pallets Measured via a Capillary Rheometer using a die with L/D ratio of 20/50 at 110° C

		Shear Viscosity (Pa.s)				
Ram Rate (°/min)	Shear Rate (1/sec)	110°C				
		Run 1	Run 2	Run3	Run 4	Average
0.01	23.563	15.812	9.2235	13.176	13.176	12.85
0.02	47.125	10.541	8.5647	9.8823	9.2235	9.55
0.04	94.251	5.2706	5.9294	6.5882	6.5882	6.09
0.1	235.63	3.2612	4.48	4.48	4.6118	4.21
0.4	942.51	2.8988	2.9976	3.1623	3.0306	3.02
0.6	1413.8	2.8329	2.7231	2.7012	2.6353	2.72
0.8	1885	2.6847	2.5529	2.5035	2.3558	2.52
1	2356.3	2.3586	2.3849	2.3059	2.1873	2.31
2	4712.5	1.9831	2.016	1.9435	1.8974	1.96

Table 0.10: Shear Viscosity of Polyethylene Wax Particles (Produced at a Polymer Feed Rate 26 g/min, CO₂ Feed Rate 45 ml/min, Nozzle Temperature 180°C and Screw Speed 50 rpm) Measured via a Capillary Rheometer Using a Die with L/D Ratio of 50/20 at 90°C and 100°C

		Shear Viscosity (Pa.s)							
Ram Rate	Shear Rate	90°C				100°C			
(°/min)	(1/sec)	Run 1	Run 2	Run 3	Avg.	Run 1	Run 2	Run 3	Avg.
0.2	30.16					1196.7	1163.2	1178.7	1179.53
0.4	60.32			2725.4	2725.4	633.09	738.6	759.19	710.29
0.6	90.48	1890.2	1890.7	1929.3	1903.4	472.67	569.61	584.19	542.16
0.8	120.64	1445	1447	1530.6	1474.2	410.48	450.37	449.08	436.64
1.2	180.96	1074	1086.9	1117.3	1092.7	268.08	320.4	306.68	298.39
2.2	331.76	664.2	695.09	670.99	676.8	203.54	184.12	194.18	193.95
3.2	482.56	483.5	477.87	487.36	482.9		144.12	146.53	145.33
6.2	934.97	291.06	285.5	278.19	284.9		91.734	91.319	91.53
9	1357.2	212.4	211.54	211.49	211.8		71.315		71.32

Table 0.11: Shear Viscosity of Polyethylene Wax Particles (Produced at a Polymer Feed Rate 26 g/min, CO₂ Feed Rate 45 ml/min, Nozzle Temperature 180° C and Screw Speed 50 rpm) Measured via a Capillary Rheometer Using a Die with L/D Ratio of 20/50 at 110°C

		Shear Viscosity (Pa.s)			
Ram Rate	Shear Rate	110°C			
(°/min)	(1/sec)	Run 1	Run 2	Run 3	Average
0.01	23.563	52.706	54.023	54.023	53.58
0.02	47.125	31.623	31.623	30.65	31.30
0.04	94.251	18.776	19.106	18.447	18.78
0.1	235.63	11.464	12.122	11.595	11.73
0.4	942.51	5.6659	5.7318	5.7647	5.72
0.6	1413.8	4.8094	4.3922	4.7655	4.66
0.8	1885	3.7388	3.7059	3.7223	3.72
1	2356.3	3.1427	3.4522	3.3995	3.33
2	4712.5	2.576	2.7341	2.6616	2.66

Appendix E: Optical Microscope Images

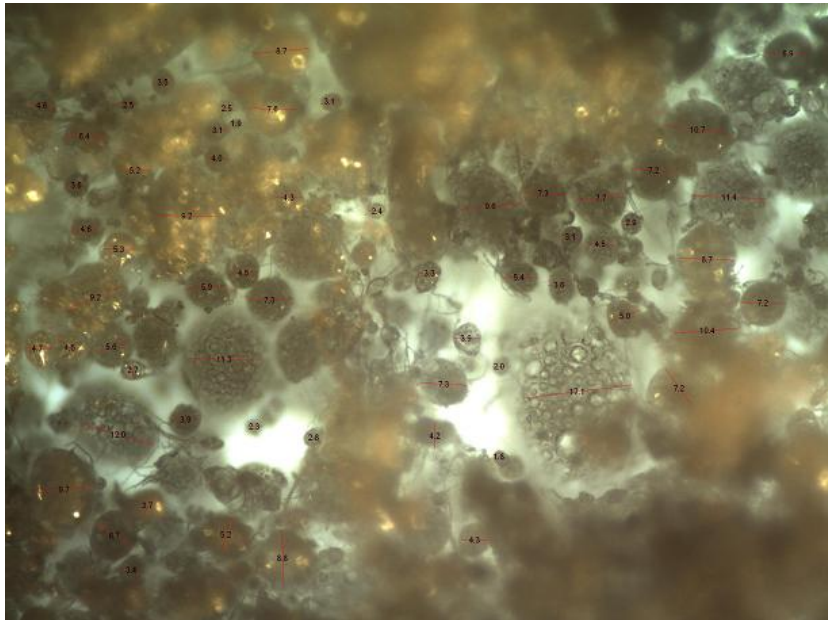


Figure 0.1: Optical Microscope Image of Particles Produced at Polymer Feed Rate =13 g/min and Nozzle Temperature =140 °C (CO₂ Feed Rate = 25 ml/min, Screw Speed = 50 rpm)

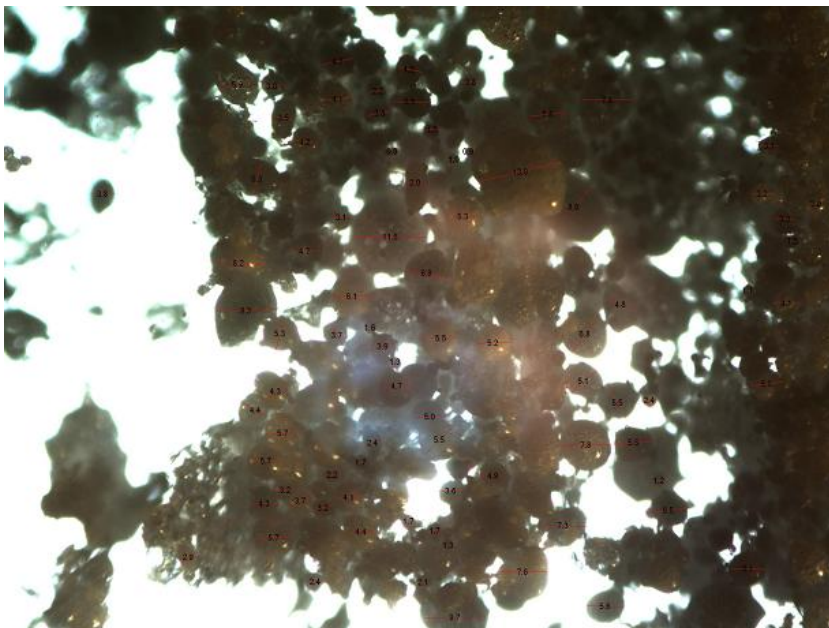


Figure 0.2: Optical Microscope Image of Particles Produced at Polymer Feed Rate =13 g/min and Nozzle Temperature =160 °C (CO₂ Feed Rate = 25 ml/min, Screw Speed = 50 rpm)

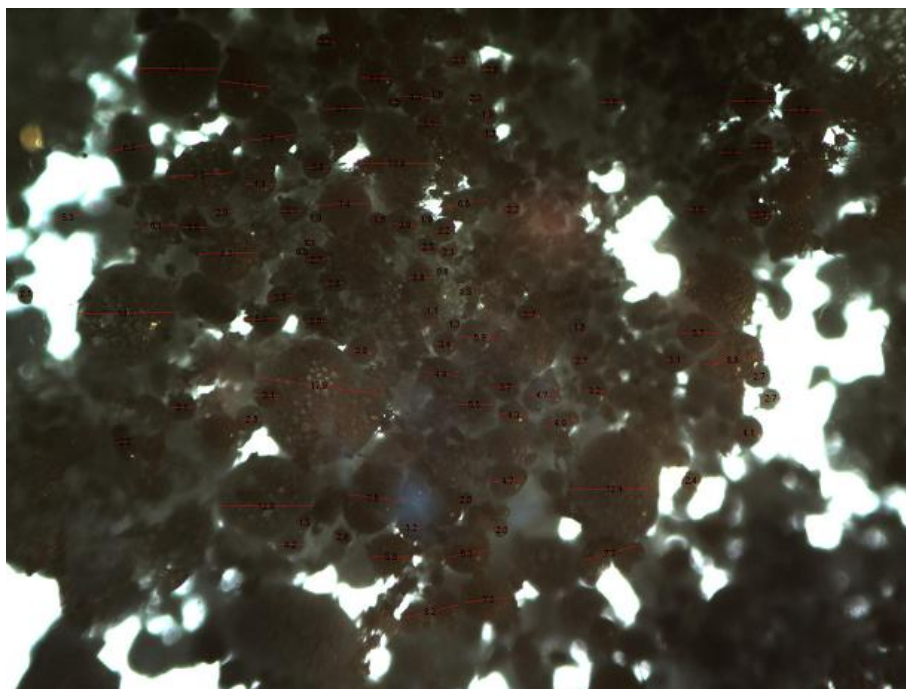


Figure 0.5: Optical Microscope Image of Particles Produced at Polymer Feed Rate =26 g/min and Nozzle Temperature =140 °C (CO₂ Feed Rate = 25 ml/min, Screw Speed = 50 rpm)

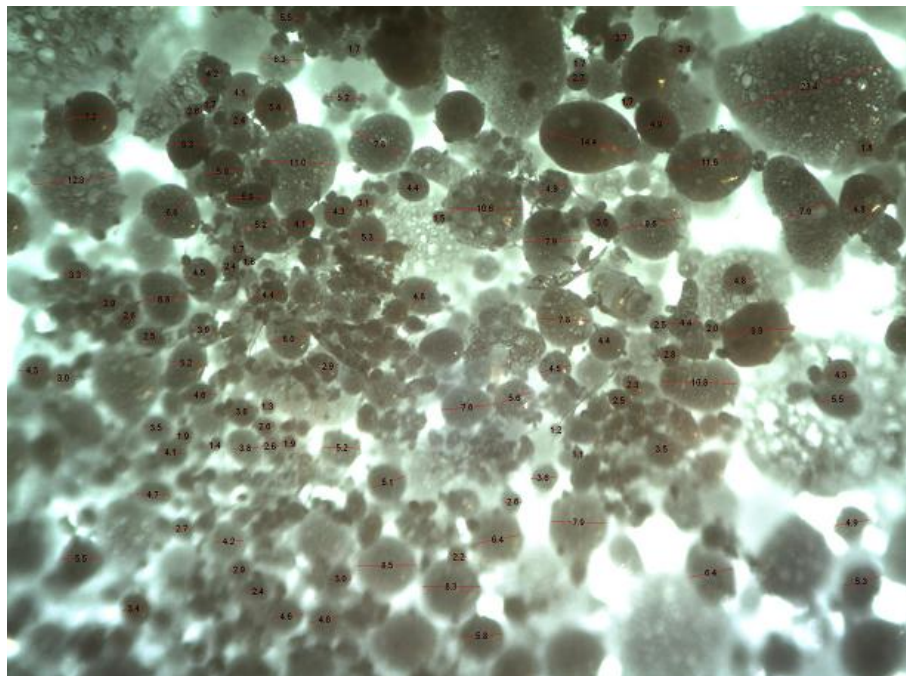


Figure 0.6: Optical Microscope Image of Particles Produced at Polymer Feed Rate =26 g/min and Nozzle Temperature =160 °C (CO₂ Feed Rate = 25 ml/min, Screw Speed = 50 rpm)

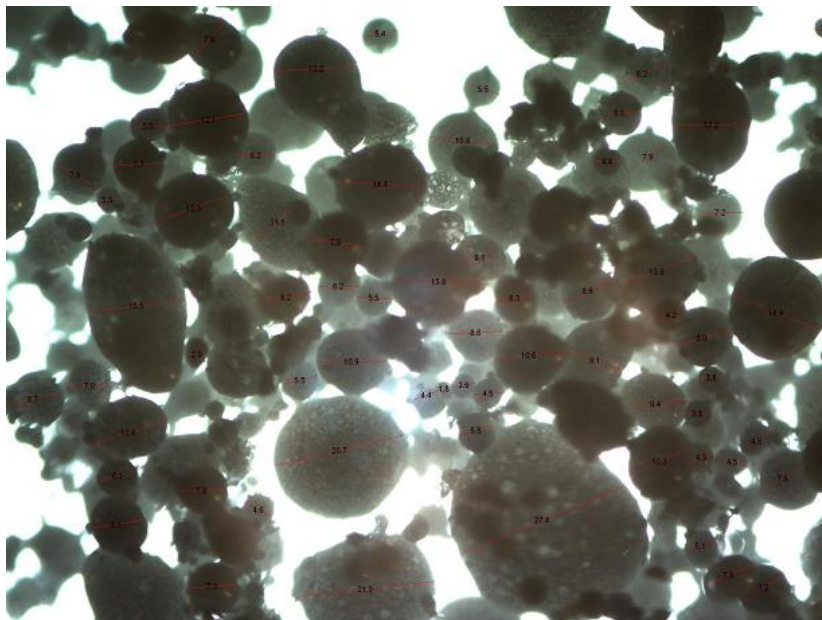


Figure 0.7: Optical Microscope Image of Particles Produced at Polymer Feed Rate =26 g/min and Nozzle Temperature =180 °C (CO₂ Feed Rate = 25 ml/min, Screw Speed = 50 rpm)

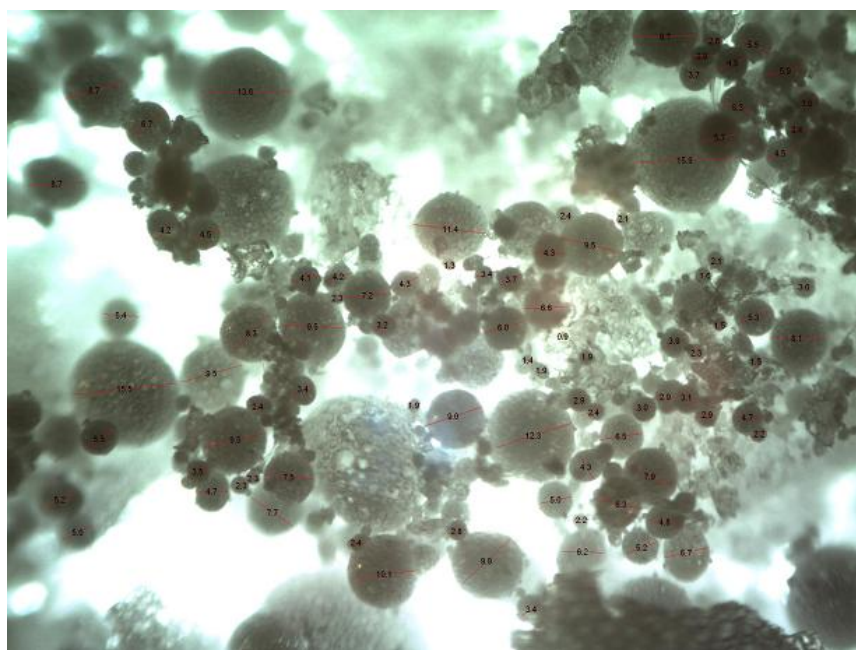


Figure 0.8: Optical Microscope Image of Particles Produced at Polymer Feed Rate =26 g/min and Nozzle Temperature =200 °C (CO₂ Feed Rate = 25 ml/min, Screw Speed = 50 rpm)

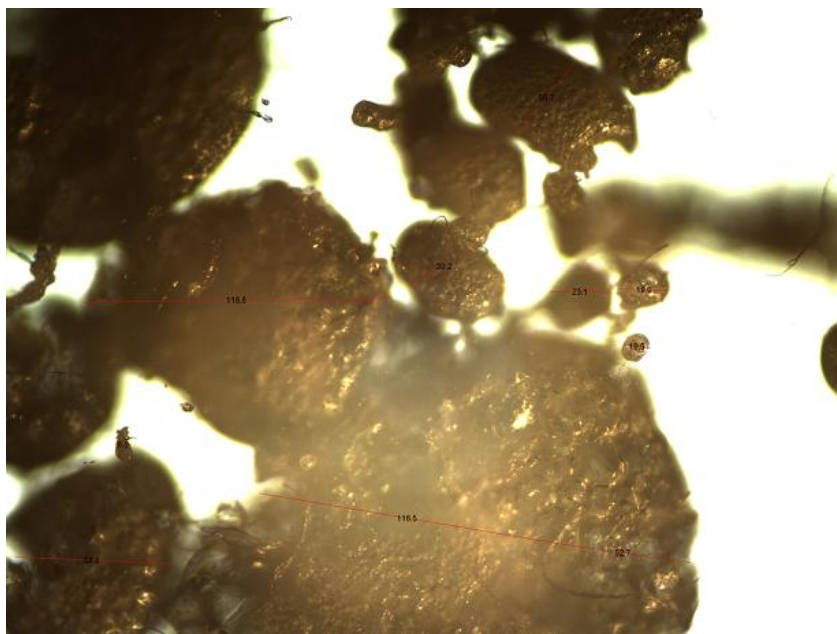


Figure 0.9: Optical Microscope Image of Particles Produced at CO₂ Feed Rate of 35 ml/min
(Polymer Feed Rate =52 g/min, Nozzle Temperature =140 °C, Screw Speed = 50 rpm)

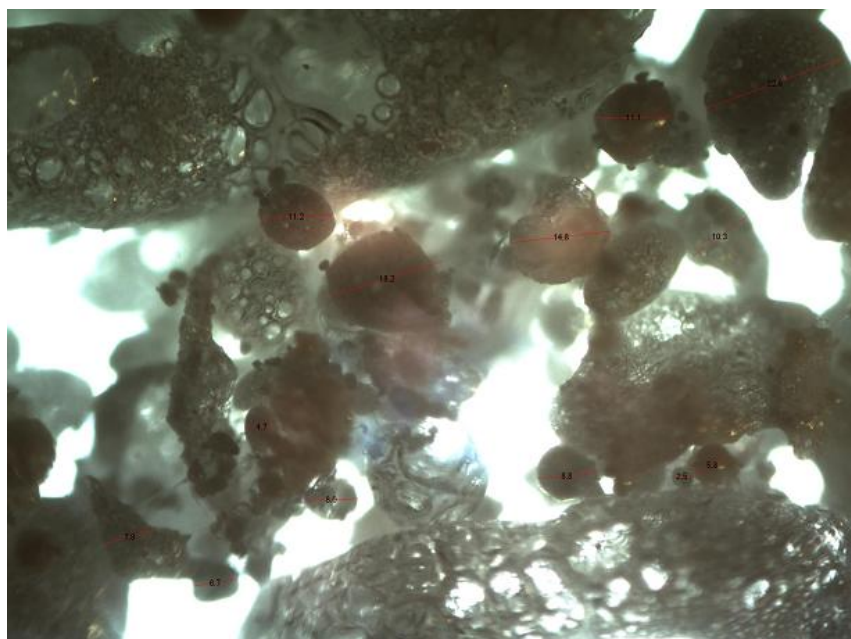
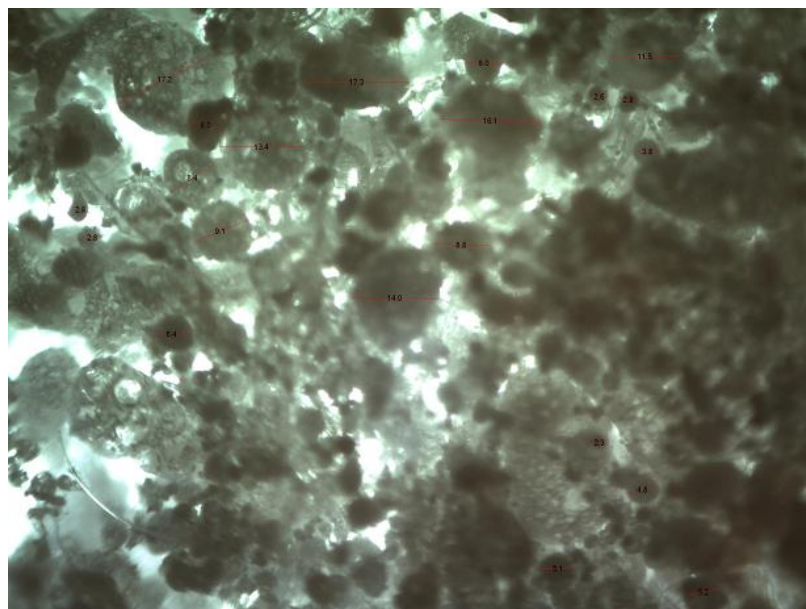


Figure 0.10: Optical Microscope Image of Particles Produced at CO₂ Feed Rate of 45 ml/min
(Polymer Feed Rate= 52 g/min, Nozzle Temperature =140 °C, Screw Speed = 50 rpm)



**Figure 0.11: Optical Microscope Image of Particles Produced at CO₂ Feed Rate of 55 ml/min
(Polymer Feed Rate= 52 g/min, Nozzle Temperature =140 °C, Screw Speed = 50 rpm)**

Appendix F: SEM Images

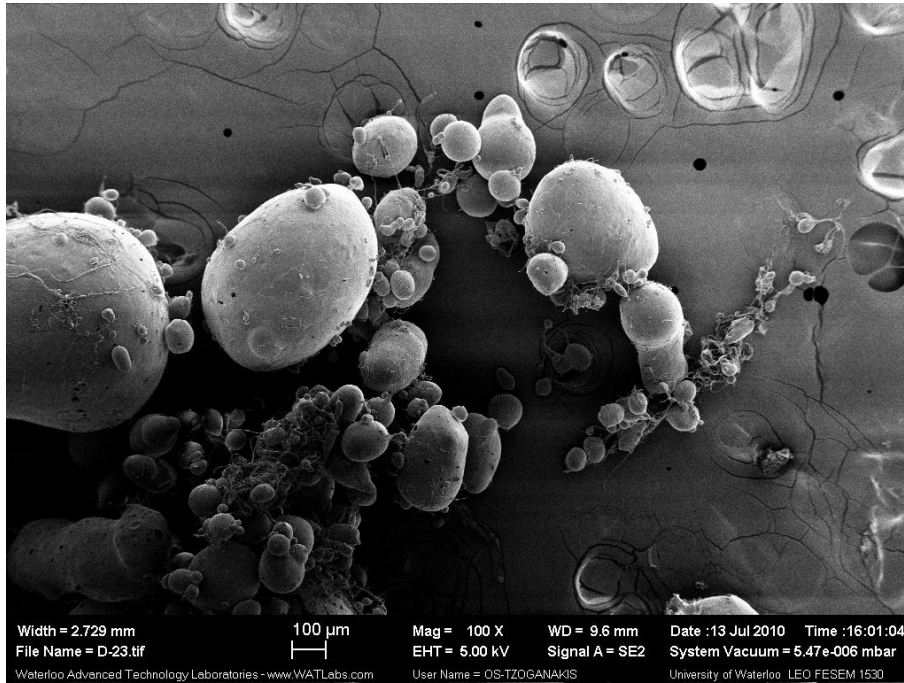


Figure 0.12: SEM Images of Particles Produced at Polymer Feed Rate= 13 g/min, CO₂ Feed Rate =25 ml/min, Screw Speed =50 rpm, and Nozzle Temperature= 140°C

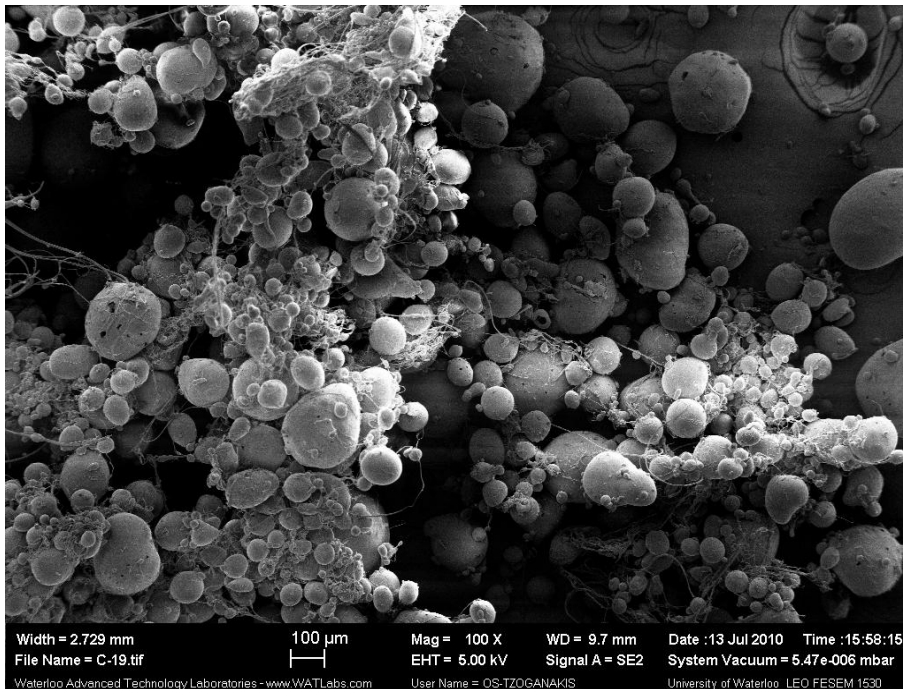


Figure 0.13: SEM Images of Particles Produced at Polymer Feed Rate= 13 g/min, CO₂ Feed Rate= 25 ml/min, Screw Speed =50 rpm, and Nozzle Temperature =160°C

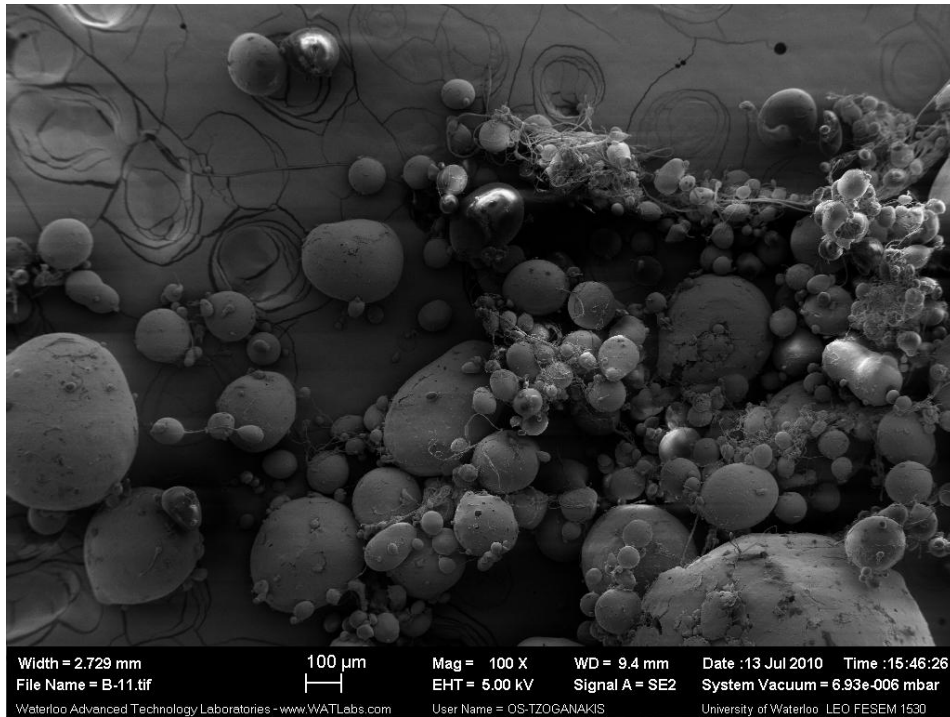


Figure 0.14: SEM Images of Particles Produced at Polymer Feed Rate= 13 g/min, CO₂ Feed Rate =25 ml/min, Screw Speed =50 rpm, and Nozzle Temperature =180°C

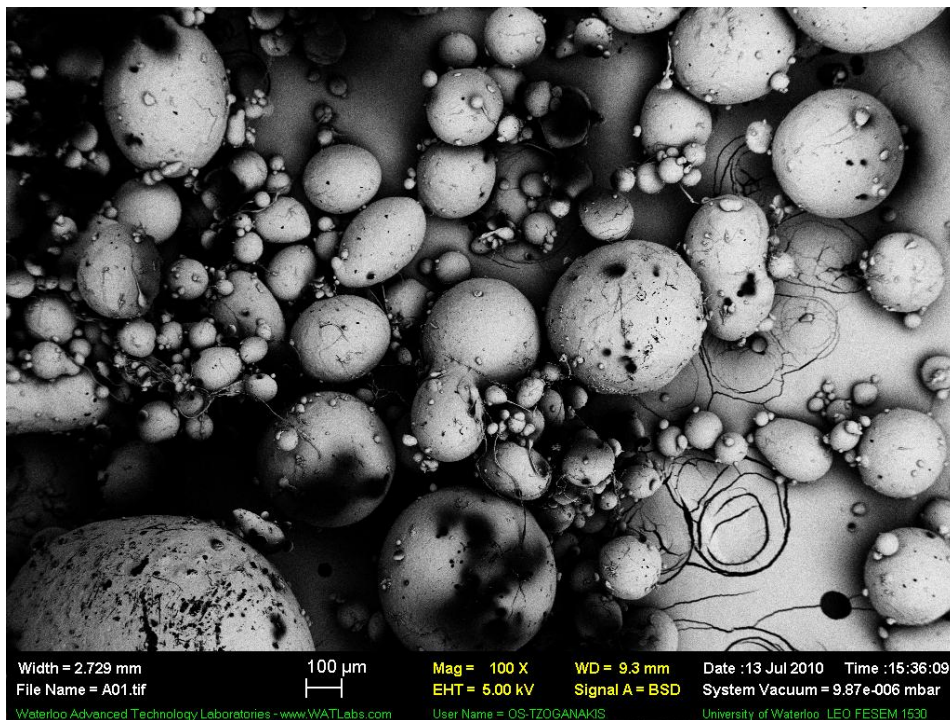


Figure 0.15: SEM Images of Particles Produced at Polymer Feed Rate= 13 g/min, CO₂ Feed Rate =25 ml/min, Screw Speed =50 rpm, and Nozzle Temperature =200°C

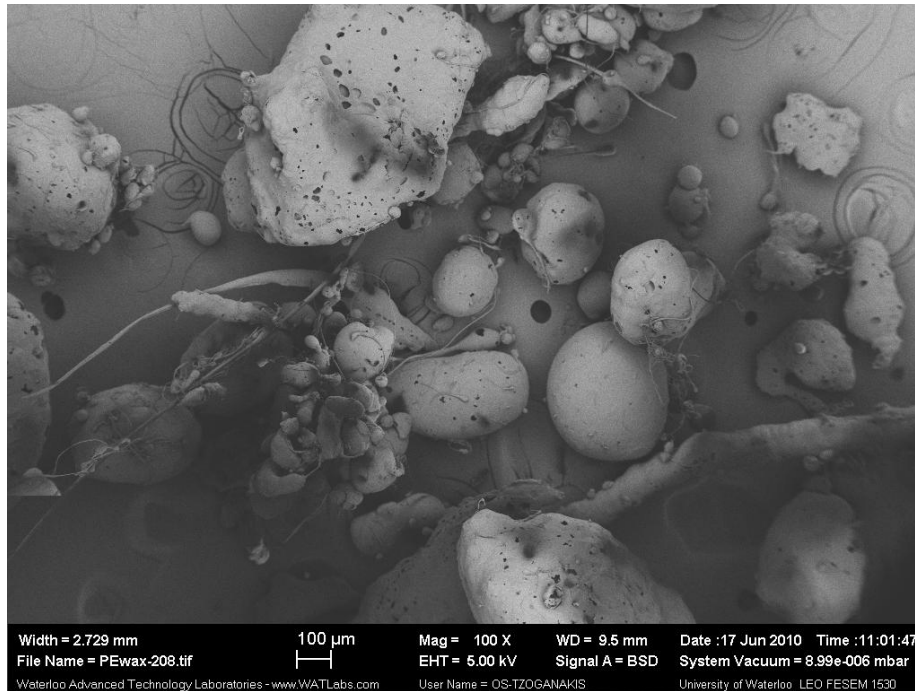


Figure 0.16: SEM Images of Particles Produced at Polymer Feed Rate= 26 g/min, CO₂ Feed Rate =25 ml/min, Screw Speed =50 rpm, and Nozzle Temperature =140°C

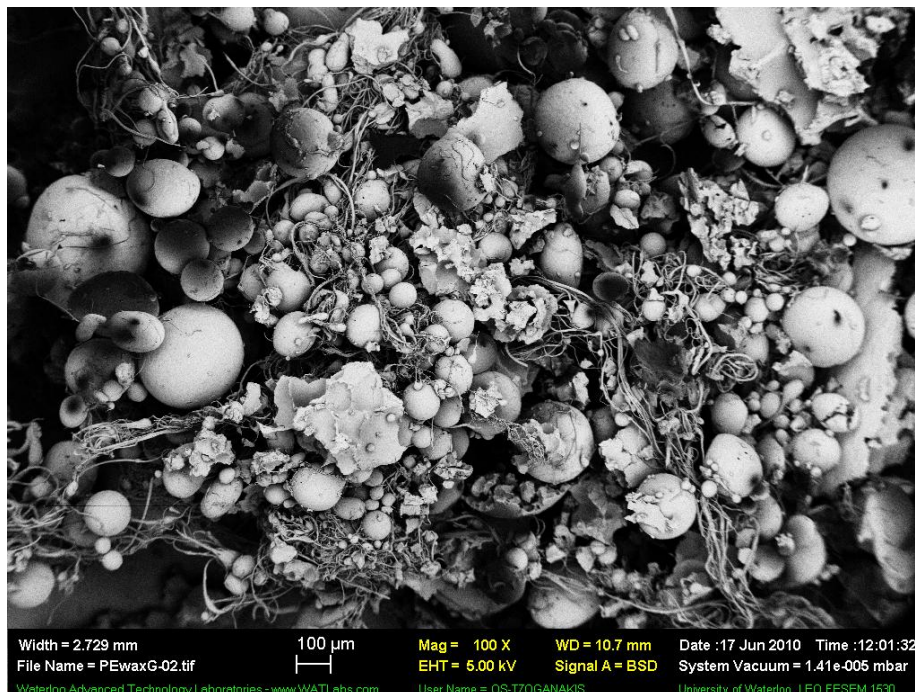


Figure 0.17: SEM Images of Particles Produced at Polymer Feed Rate= 26 g/min, CO₂ Feed Rate =25 ml/min, Screw Speed =50 rpm, and Nozzle Temperature =160°C



Figure 0.18: SEM Images of Particles Produced at Polymer Feed Rate= 26 g/min, CO₂ Feed Rate =25 ml/min, Screw Speed =50 rpm, and Nozzle Temperature =180°C

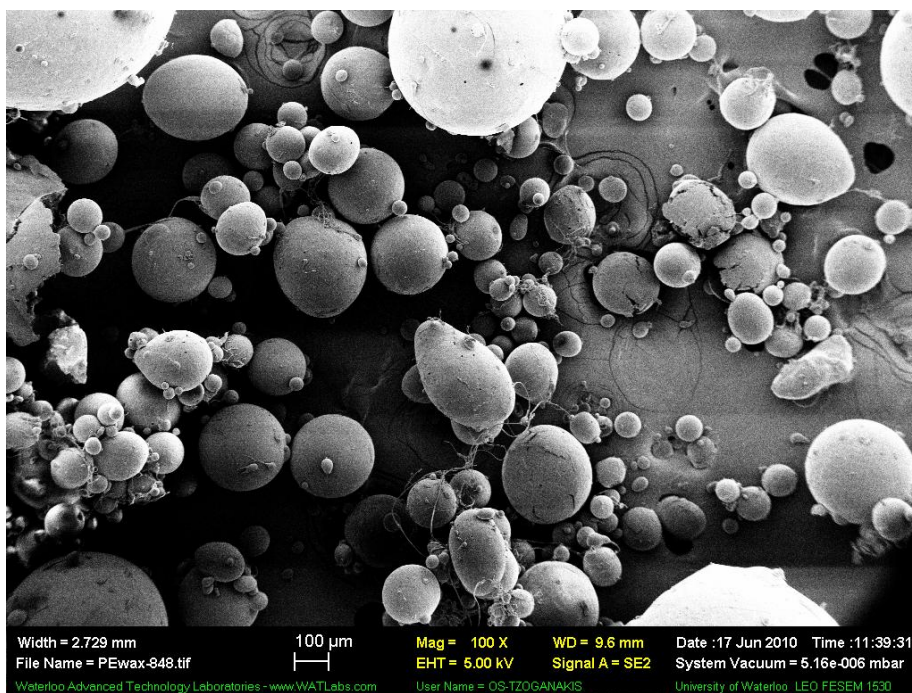


Figure 0.19: SEM Images of Particles Produced at Polymer Feed Rate =26 g/min, CO₂ Feed Rate =25 ml/min, Screw Speed =50 rpm, and Nozzle Temperature =200°C

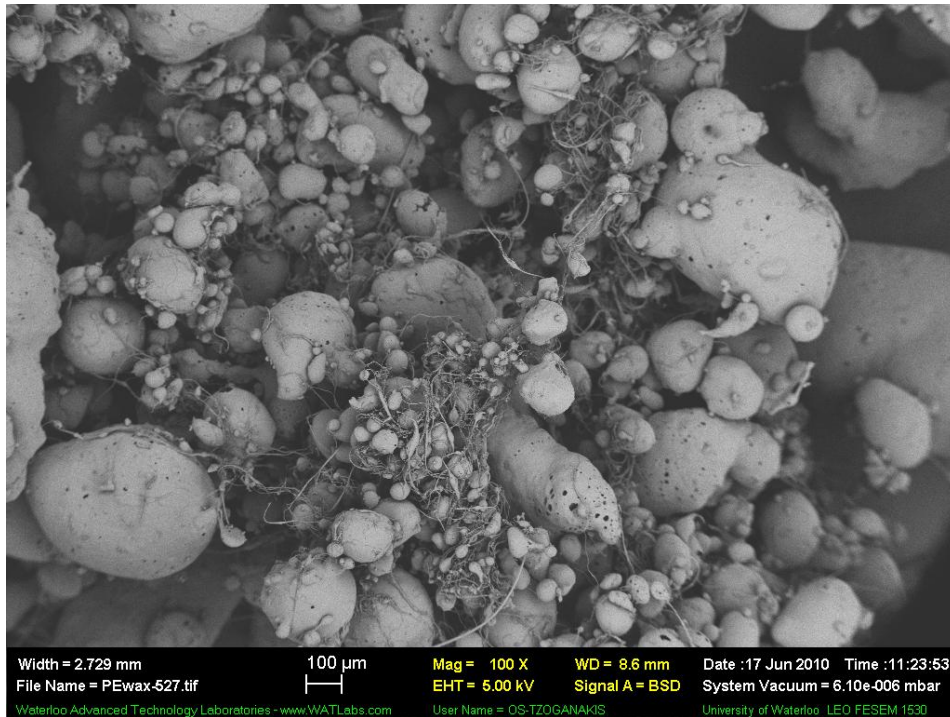


Figure 0.20: SEM Images of Particles Produced at Polymer Feed Rate =52 g/min, CO₂ Feed Rate =35 ml/min, Screw Speed =50 rpm, and Nozzle Temperature =200°C

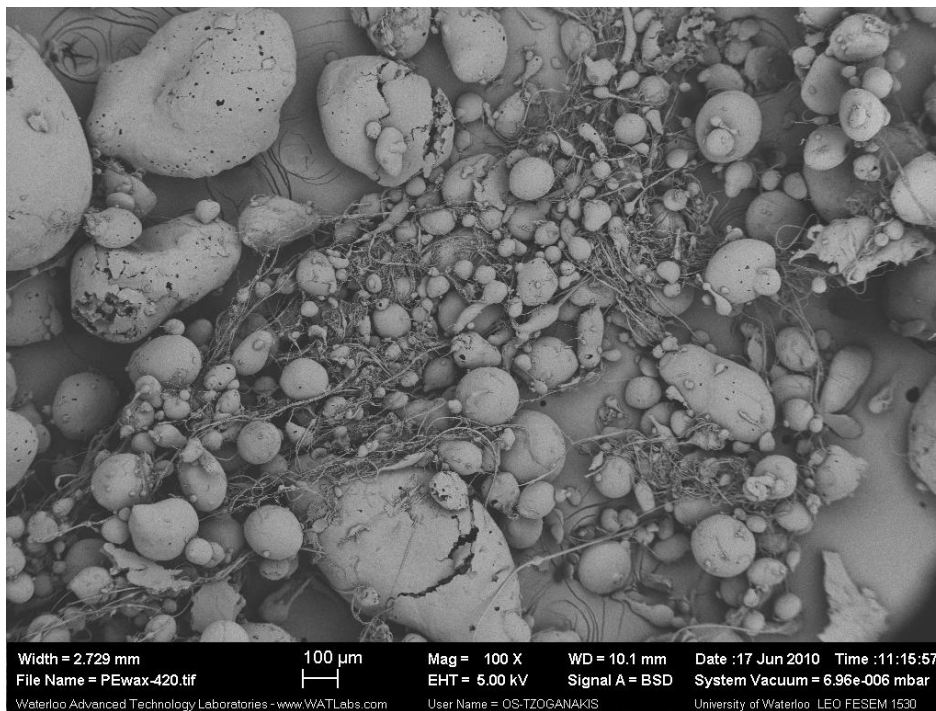


Figure 0.211: SEM Images of Particles Produced at Polymer Feed Rate =52 g/min, CO₂ Feed Rate =45 ml/min, Screw Speed =50 rpm, and Nozzle Temperature =200°

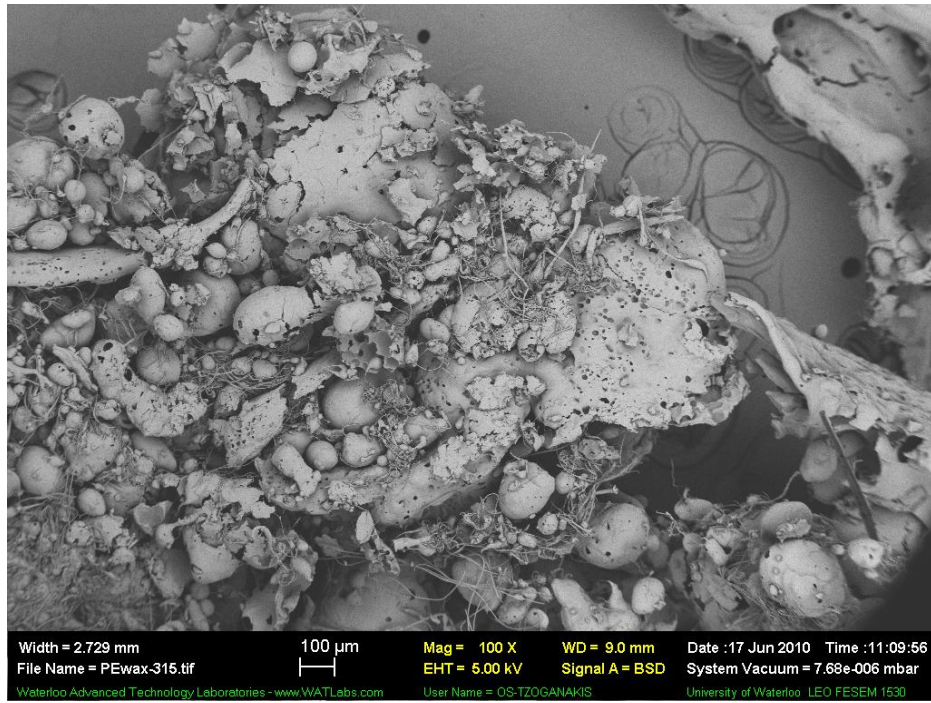
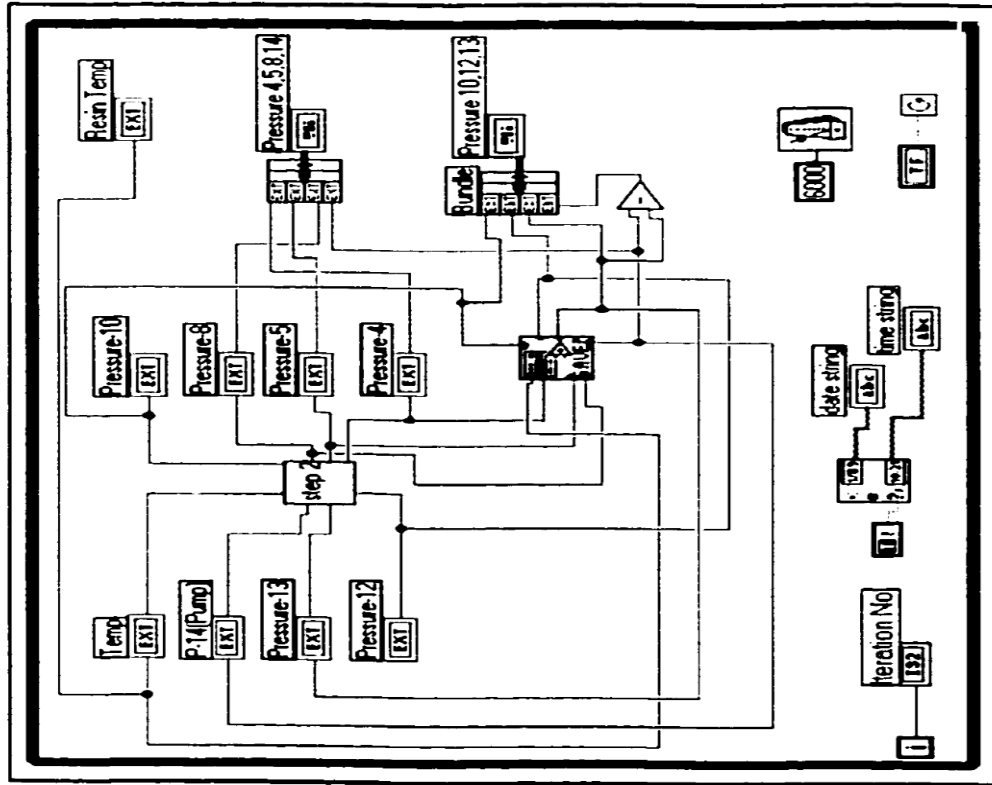


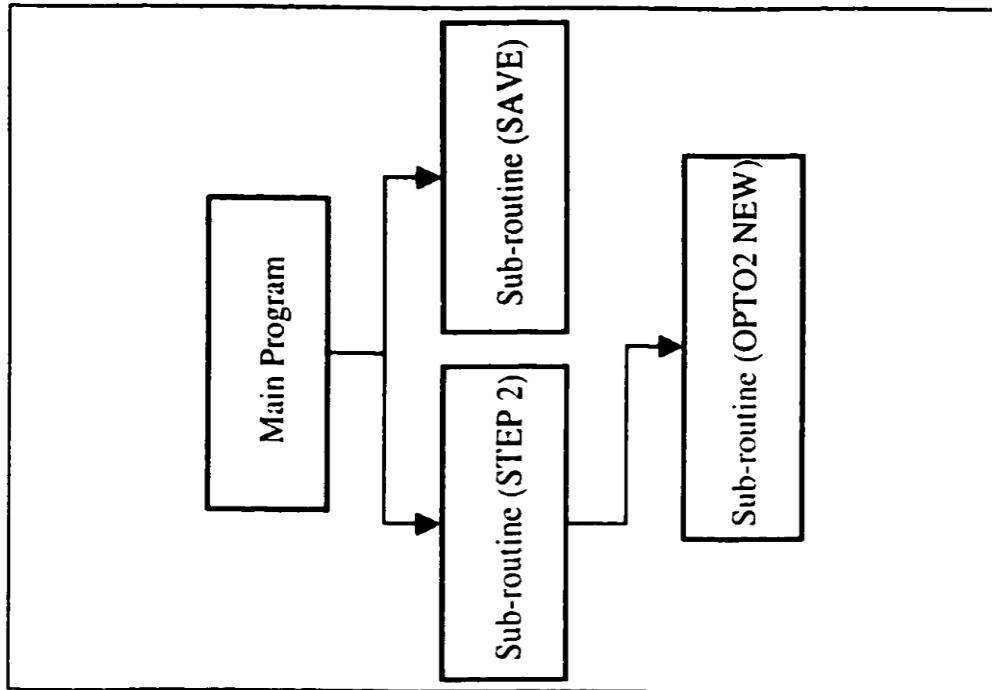
Figure 0.22: SEM Images of Particles Produced at Polymer Feed Rate =52 g/min, CO₂ Feed Rate =55 ml/min, Screw Speed =50 rpm, and Nozzle Temperature =200°

Appendix G: LABVIEW Program for Data Acquisition

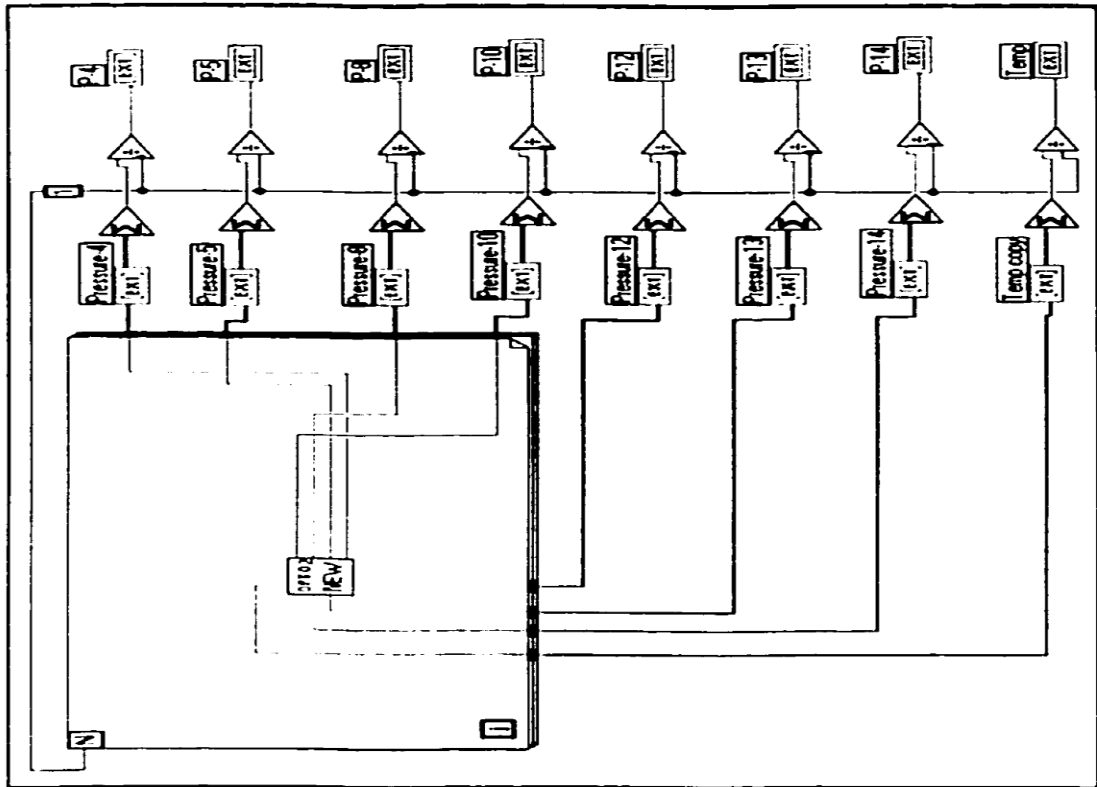
2. Main Program



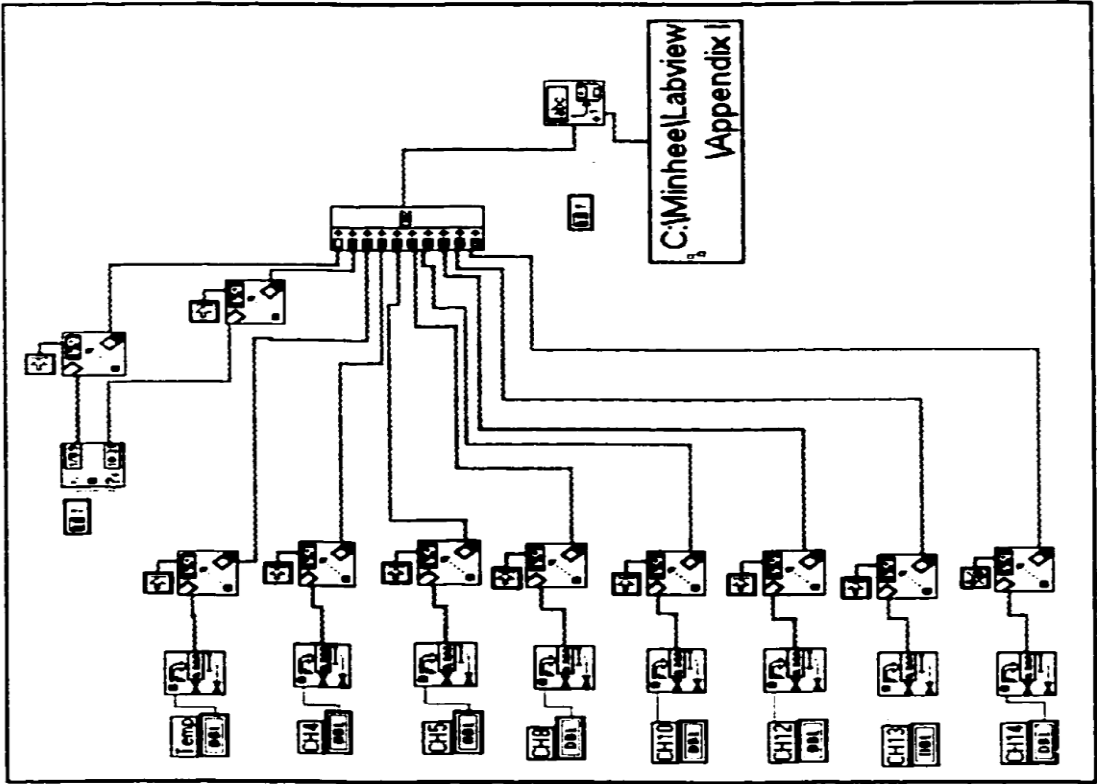
1. Flow Chart



3. Sub-routine (STEP 2.VI)



4. Sub-routine (SAVE.VI)



5. Sub-routine (OPTO2 NEW.VI)

